WIND TUNNEL GUST SIMULATION

by

Ray M. Umbarger

WIND TUNNEL GUST SIMULATION

by

Ray M. Umbarger

December 1970

PRINCETON UNIVERSITY

DEPARTMENT OF
AEROSPACE AND MECHANICAL SCIENCES

136570

WIND TUNNEL GUST SIMULATION

by

Ray M. Umbarger

December 1970

Submitted in partial fulfillment
of the requirements for the degree
of Master of Science in Engineering
from Princeton University, 1970.

LIBRARY
NAVAL POSTGRADUATE SCHOOL
MONTEREY, CALIF. 93940

ACKNOWLEDGEMENT

Grateful acknowledgement is made of the knowledge and assistance afforded me by Professor H. C. Curtiss, Jr. and Mr. William F. Putman of the Dynamic Model Track of Princeton University. Also the technical advice and help of Mr. E. L. Griffith and Mr. John P. Kukon was of immeasurable worth.

Thanks also goes to Mrs. Ingrid Loeffler for her patience in the typing of this report.

This thesis carries No. 964-T in the records of the Department of Aerospace and Mechanical Sciences.

TABLE OF CONTENTS

	PAGE
SUMMARY AND INTRODUCTION	iii
LIST OF SYMBOLS	v
DESCRIPTION OF TEST EQUIPMENT	1
EXPERIMENTAL PROCEDURES	9
EXPERIMENTAL RESULTS:	
A. Static:	
1) Discussion	11
2) Data	14
B. Dynamic:	
1) Discussion	27
2) Data	
C. Numerical Example	36
PROPOSED MODEL	40
CONCLUSIONS	50
BIBLIOGRAPHY	52

APPENDICES:

APPENDIX I	- Theoretical Discussion of Jet Augmented Flap	55
APPENDIX II	- Two Dimensional Smoke Tunnel Experimentation	79
APPENDIX III	- Frequency Scaling	87
APPENDIX IV	- Analytical Approach to Vane Dynamics	89

SUMMARY AND INTRODUCTION

This report presents the results of experimentation with a single jet-augmented flapped airfoil for generating gusts of high reduced frequency for the range

$$0 < K < 1.5$$

in a wind tunnel. The experimental data from a single jet flap in conjunction with the theoretical assumption of superposition, are used to postulate combinations of trailing vortices from an assumed array of multiple jet flaps for the production of an oscillating cross-sectionally-uniform gust. The objective of this report is to study and understand the effects of different parameters such as flap deflection angle, flap frequency, dynamic pressure, and the position at which the induced velocity is measured, on the uniformity of the generated turbulence across the wind tunnel test section and finally to combine these system variables to produce sufficiently uniform gusts.

Three areas of work were the main points of concentration:

1.) Experimental testing in both the static and dynamic cases with a single jet flap or vortex generator in the wind tunnel.
2.) Superimposing the results of the experimental data into an array of four generators in an attempt to produce a uniform cross-sectional gust.
3.) Comparison of the gust model designed using the experimental data and superposition with the model using a theoretical analysis of a single trailing vortex and superposition.

The testing was accomplished in the Princeton University 4' X 5' wind tunnel with jet augmentation of a simple plain flapped airfoil. The jet augmentation increased greatly the magnitude of induced velocity generated, and the use of a flapped airfoil decreased the size and inertia of the moving components.

The experimental results consist of measured values of induced velocity due to a single half span vortex generator. Both static and dynamic data were taken. In the static case, the magnitude of induced velocity was dependent on certain variables such as flap deflection angle sensor vane position in the test section and free stream velocity. Statically, many combinations of parameters were observed and recorded. Thus, the partial derivative of induced velocity with respect to each parameter was separately observed. For the dynamic data, induced velocity was dependent on Strouhal Number. Bi-directional as well as uni-directional gusts were generated and were compared. An analysis of the effects of high frequency cancellation and vortex filament movement illustrated a similarity in peak to peak magnitude in both types of generated turbulence.

The second area of study was the use of the experimental data in the hypothesis of an array of generators that would produce the desired uniform gust model. Superposition was used to pattern the symmetrical array of trailing vortex filaments into this desired model.

Finally, a similar array was developed from a trailing vortex filament in an inviscid flow field. This theoretical model was compared to the model using the experimental data and superposition previously designed. They were in close agreement.

LIST OF SYMBOLS

A_j	Slot Area; $A_j = bh$; (ft^2)
AR	Aspect Ratio of jet augmented airfoil
b	Span of the vortex generator (ft)
$\bar{c}$	Average chord of gust generator (ft)
C_D	Drag component of the sensor vanes
C_{D_q}	Same as $\frac{\partial C_D}{\partial q}$
$C_{D_{MIN}}$	Minimum drag coefficient
C_f	Chord length of the flap (ft)
C_L	Total lift coefficient of the vortex generator
C_μ	Blowing coefficient of the vortex generator; $\dot{m}_j V_j / qS$
D_F, D_A	Drag on the fore and aft airfoils of the sensors, respectively (lb)
DYNAMIC	Time variation with flap deflection.
h	Perpendicular distance of a point in space to a vortex core which is inducing a flow at that point (ft)
h_j	Width of the slot (inches)
h_s	Streamline deflection distance in 2-D smoke tunnel testing - (inches)
I	Moment of inertia or the vane potentiometer system (slug-ft)
K	Reduced frequency - nondimensional frequency of flap oscillation

$K_{A/C}$	Full scale reduced frequency
K_{MOD}	Model reduced frequency
$l_{A/C}$	Significant distance of full aircraft used in computing reduced frequency (ft)
LATERAL	Induced velocity perpendicular to the generator chord (direction)
l_f, l_A	Moment arms of the fore and aft airfoils of the sensors, respectively (lb)
l_{MOD}	Significant distance of model used in computing reduced frequency (ft)
$\dot{m}_j$	Mass flow rate of jet air through the blowing slot; $\dot{m}_j = \rho A_j V_j$
P	Point in test section to be observed
P_1	Pressure at upper boundary of the jet sheet (lb/ft^2)
P_2	Pressure at lower boundary of the jet sheet (lb/ft^2)
q	Dynamic pressure of the test section (lb/ft^2)
R	Radius of curvative of the jet sheet (ft)
Re	Reynold's Number; $\frac{\rho V_\infty l}{\mu}$
S	Area of the vortex generator airfoil (ft^2)
STATIC	Constant maximum flap position.
S_V	Area of the airfoils on the sensing vanes (ft^2)
V_j	Jet ejection velocity; always considered sonic in the present study (ft/sec)
VERTICAL	Induced velocity parallel to the generator span (Z direction)
V_∞	Free stream wind tunnel velocity (ft/sec)
w_p	Induced velocity at point P (ft/sec)
$\lvert w_p \rvert$	Magnitude of w_p (ft/sec)

X	Streamwise distance from the leading edge of the test section (ft)
Y	Distance from the left wall of the test section looking downstream (feet)
Z	Vertical distance from the base of the test section looking downstream (feet)
α_e	Effective angle of attack (deg) - angle measured from the zero lift line
α_i	Induced angle of attack at the vortex generator (degrees)
$\alpha_{i\,CORE}$	Angle at which the shed vortex core will trail off behind the flap (Degrees)
$\alpha_{i\,\infty}$	Induced angle in the wake at infinity (degrees)
α_{STALL}	Stall angle of attack (degrees)
γ_1	2-D circulation at upper boundary of jet sheet (ft^2/sec)
γ_2	2-D circulation at lower boundary of jet sheet (ft^2/sec)
γ_j	2-D circulation caused by emitted jet sheet (ft^2/sec)
Γ	Circulation about the shed vortex core (ft^3/sec)
Γ_c	Total circulation causing pressure lift (ft^3/sec)
Γ_j	Total circulation causing momentum lift (ft^3/sec)
$\frac{\partial(\,)}{\partial(\,)}$	Derivative holding all other variables constant
δ_F	Magnitude of flap deflection either positively or negatively (degrees)
δ_{VANE}	Sensor position in streamwise (X) direction as well as in the cross-sectional plane (Y-Z)
ϵ_∞	Same as $\alpha_{i\,\infty}$
ζ	Non-dimensional damping coefficient of sensor vanes

θ	Angle of incidence of the relative wind to the airfoil surfaces of the vane sensors (radians)
θ_A, θ_B	Angle involved in the determination of the influence of a semi-infinite vortex of a point in space (degrees)
$\lambda_{A/C}$	Wave length of the full scale gust to be simulated (ft)
λ_{MOD}	Wave length of the model gust (ft)
ρ	Density of air; constant (lb/ft^3)
τ	Torque produced by the aerodynamic loading on the airfoils of the sensors (ft-lb)
$\omega_{A/C}$	Full scale gust frequency (hz)
ω_f	Flap frequency of oscillation (hz)
ω_{MOD}	Model gust frequency (hz)
ω_n	Natural frequency of vane sensors (rad/sec)

DESCRIPTION

Gust simulation in the 4 X 5 foot Princeton University wind tunnel was conducted using a blown flap gust generator. No attempt was made to improve the design of the gust generator based on experimental observations. However, changes were made in the sensors during the trial runs to improve the data output and to increase experimental accuracy. The individual parts will be discussed separately including the changes in the sensor construction during this trial run period.

Wind Tunnel

The tunnel test section (Figure 1), nominally four feet by five feet, is forty-two inches high and fifty-nine inches wide. This Princeton facility has the least tunnel turbulence of all the wind tunnels at the Forrestal Campus. Its dynamic pressure is variable over a range of tunnel velocities up to approximately 100 mph. The maximum tunnel free stream velocity used in the experiments was 100 ft/sec which is below the upper limit where tunnel turbulence tends to be amplified. The test section has a streamwise length of 80 inches, thus allowing surveys at three positions, two, six and ten chord lengths downstream from the jet flap model.

Inherent in any wind tunnel is its turbulence caused by wall surface irregularities and friction (shear) stresses. This turbulence has its own characteristics of frequency and amplitude which must be filtered out of the final data in an attempt at some degree of accuracy. The frequency of the turbulence was recorded in the initial trial runs as 40-50 Hz, which was well above the testing range of the experiment and was easily distinguishable and filtered. The magnitude of the turbulence varied between one and two degrees of free stream deflection in a steady state condition, and was filtered out of the data presented.

JET FLAP VORTEX GENERATION

The jet flap was designed specifically to increase the lift capability of a particular airfoil section. Since the C_L is increased, the circulation also increases and hence the strength of the trailing vortex far exceeds that of a simply flapped airfoil.

To create a sinusoidal gust the airfoil section was chosen as a NACA 0012 symmetric airfoil. The flap, (Figure 2) was taken to be a .45c flap for reasons discussed in APPENDIX II. Blowing over both sides of the flap was necessary to insure a symmetrical gust profile.

This trailing vortex generator was a half span model mounted to the tunnel floor plate to facilitate oscillating the flap. Mechanically, the flap is oscillated by means of a connecting rod attached to a driven fly wheel as in Figure 3. The wheel has different radial attachments for the connecting rod. By increasing the radial position the actual flap deflection can be increased both positively and negatively.

The drive wheel is powered by an electric motor through a 10 to 1 ratio reduction gear box with a right angle power transmission. The motor was rated for maximum power output for 27 volts with 69 amperes of current. Throughout the entire range of tests the voltage never increased over 27 volts with 10 amperes; therefore, the maximum power output was never approached. All powered components are controlled from a central console as shown in Figure 4.

Blowing over the flap was accomplished by the introduction of a .015 in. width slot over the full twelve inch semi-span of the airfoil. A large plenum chamber was designed into the flap construction to feed air to this slot. The Schramm Compressor was able to produce a plenum chamber pressure of approximately 30 psi, enough to choke the slot and give spanwise uniformity to the jet sheet. Line loss was almost 50 psi from the output of the compressor to the point of induction into the plenum chamber.

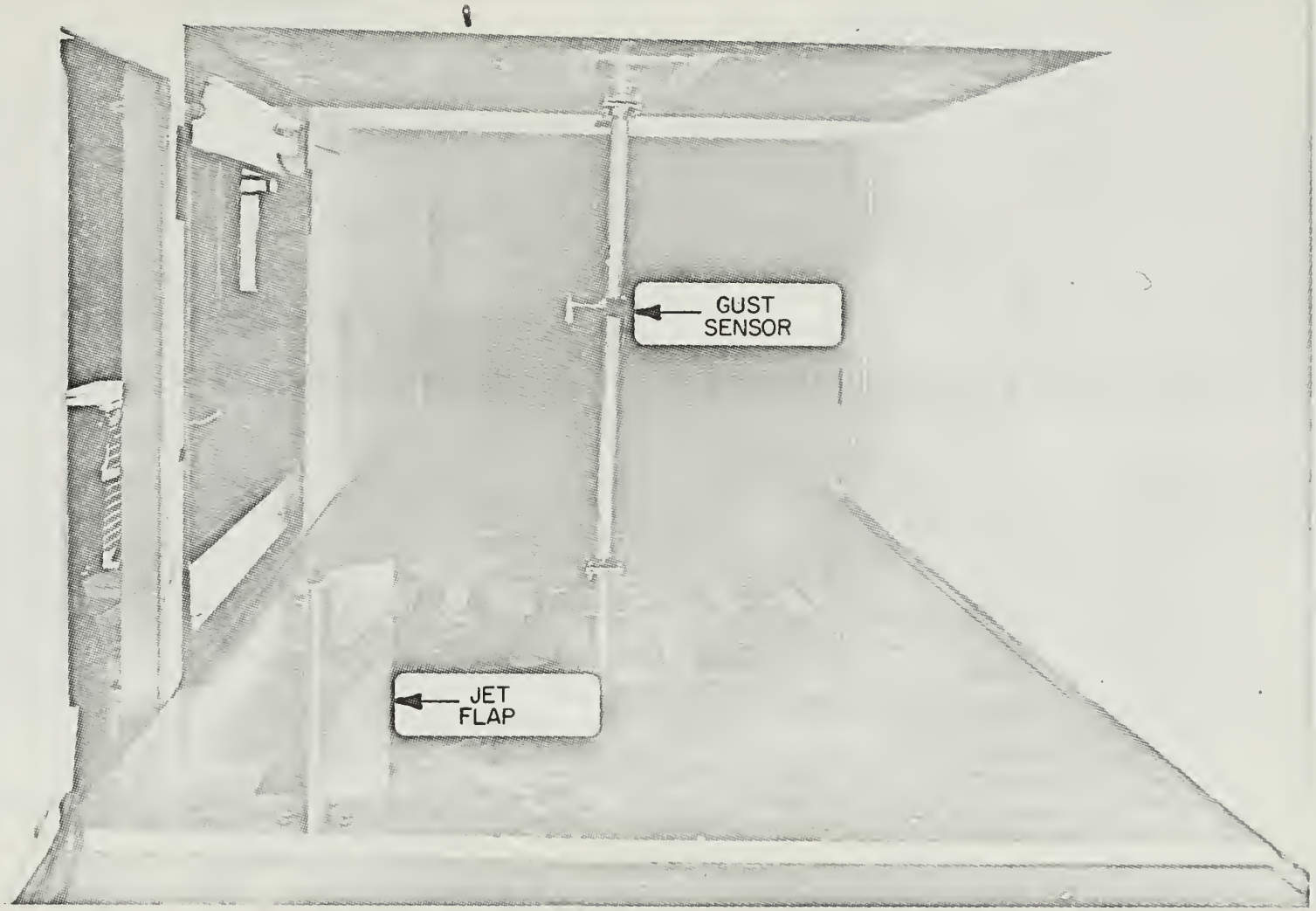

FIGURE I. DOWNSTREAM VIEW OF TEST SECTION.

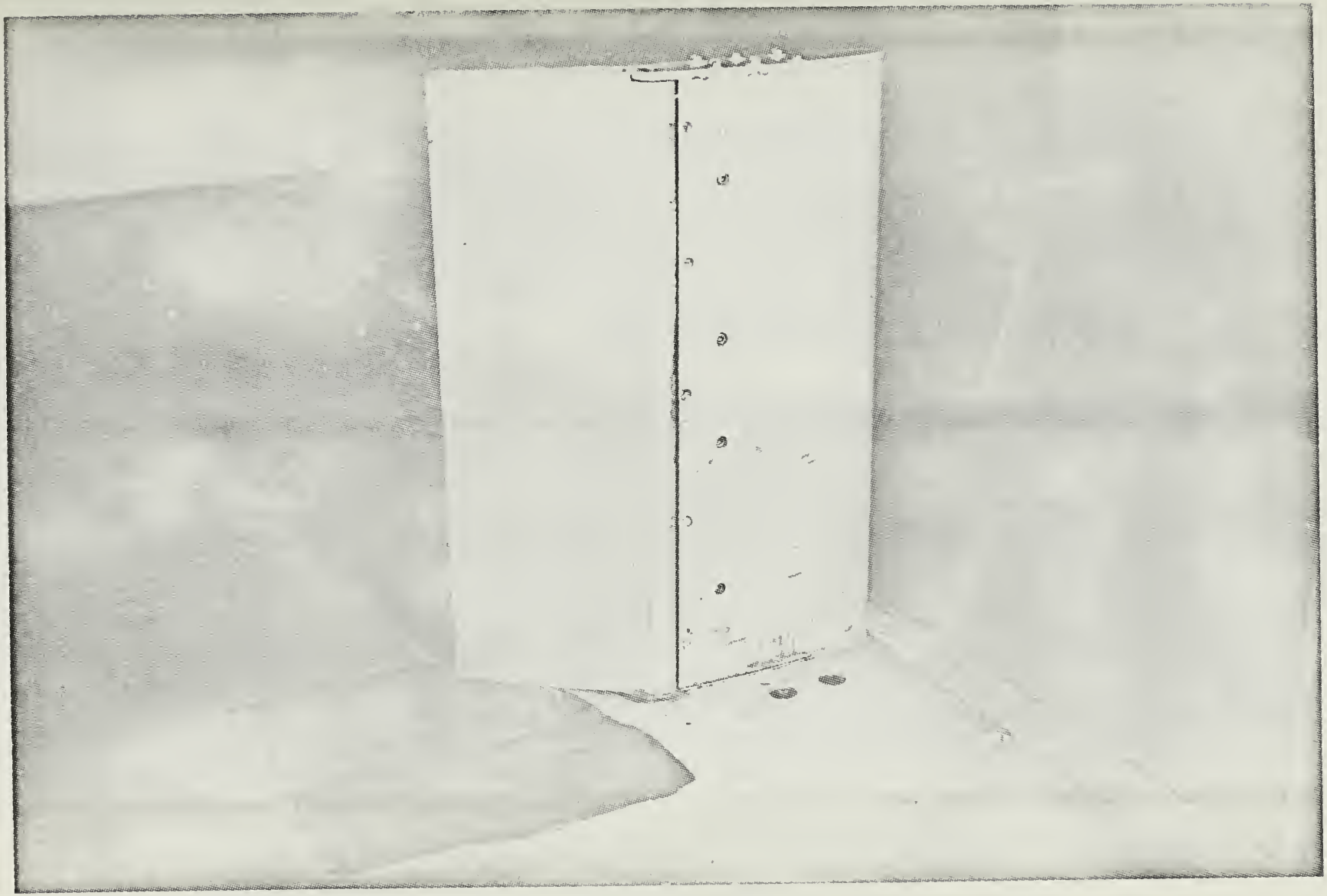

FIGURE 2. JET AUGMENTED FLAP; VORTEX GENERATOR.

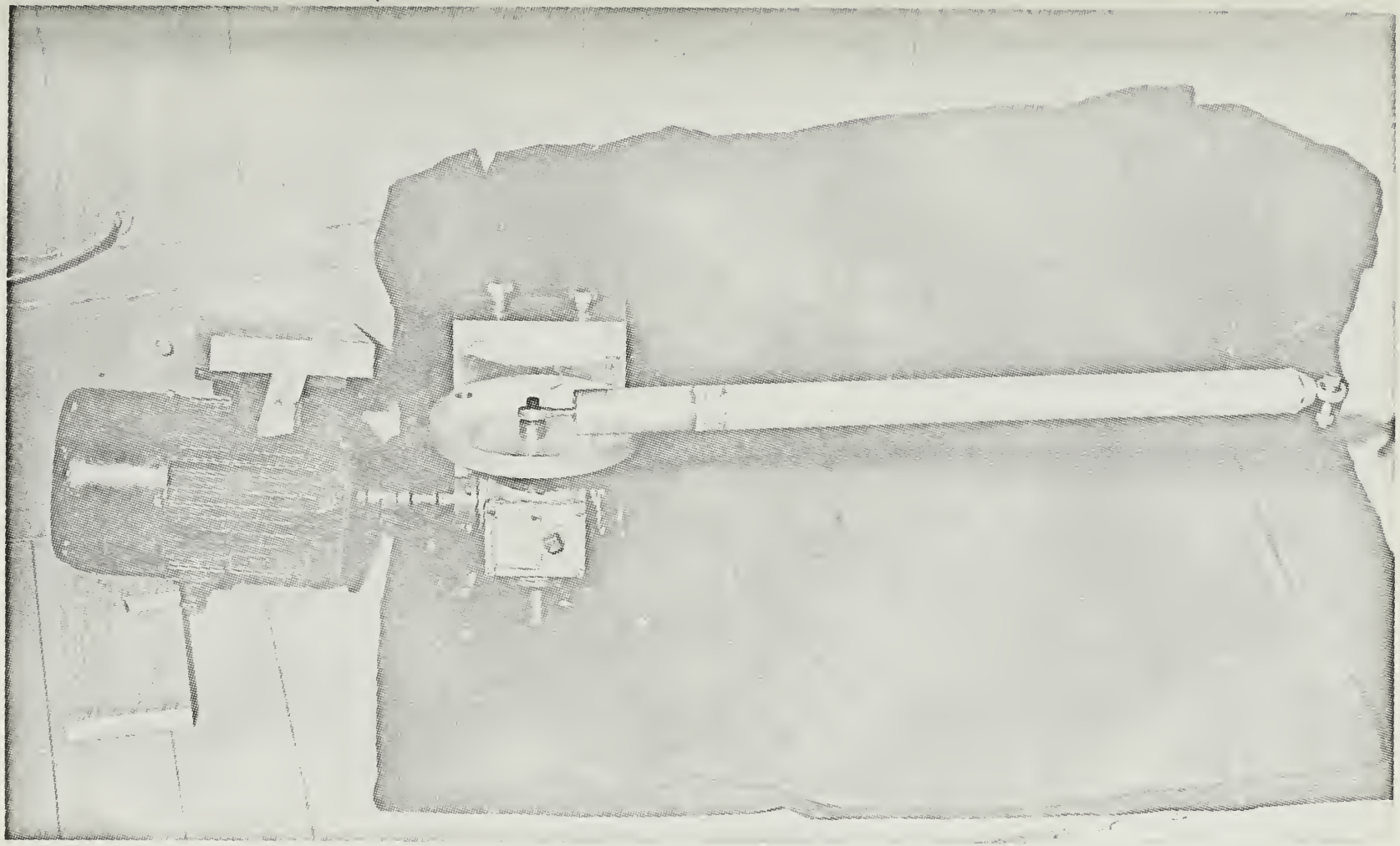

FIGURE 3. DRIVE MECHANISM FOR JET FLAP; ELECTRIC D.C. MOTOR, GEAR BOX, DRIVING WHEEL, AND CONNECTING ARM.

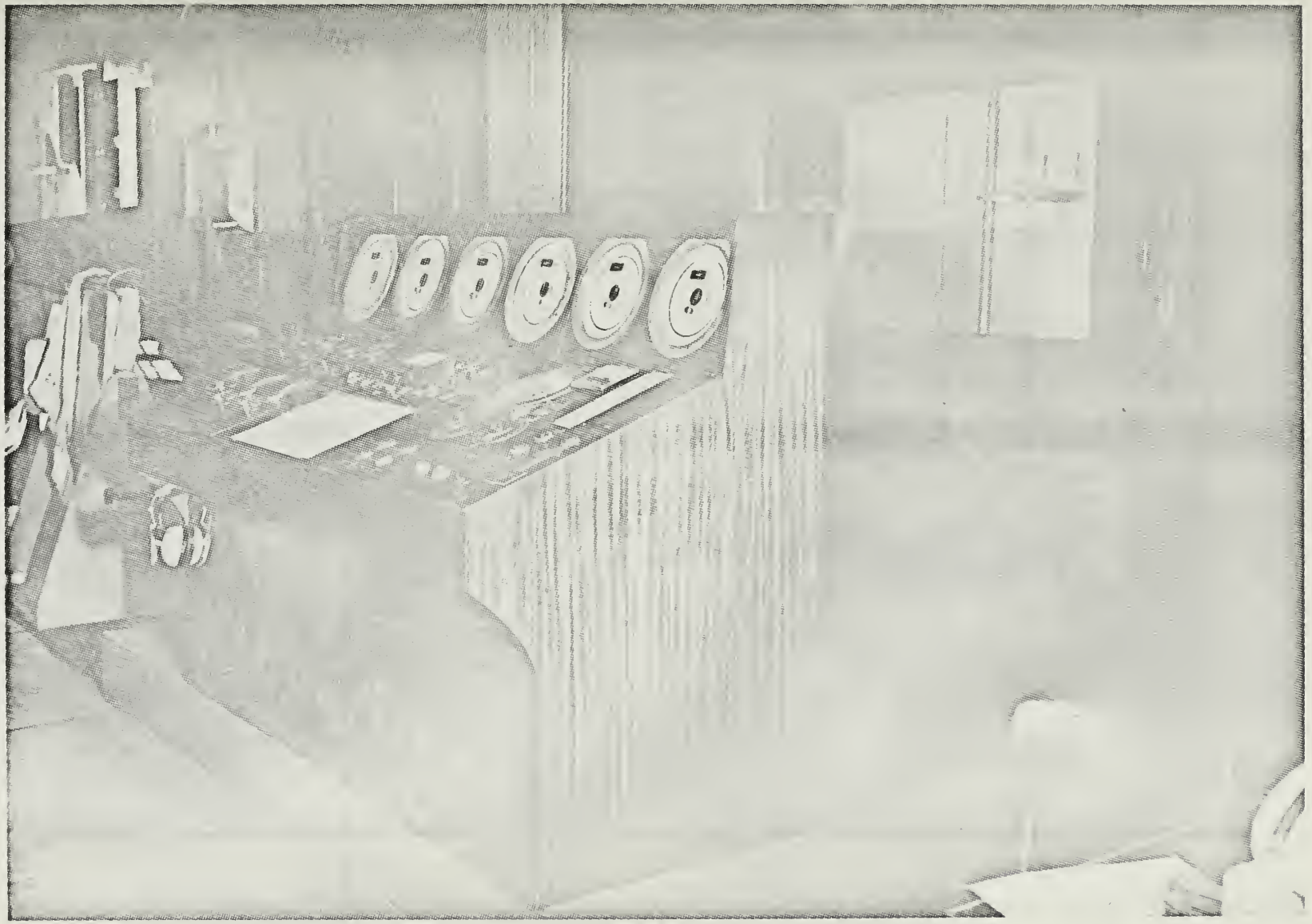

FIGURE 4. CONTROL CONSOLE AND WIND TUNNEL.

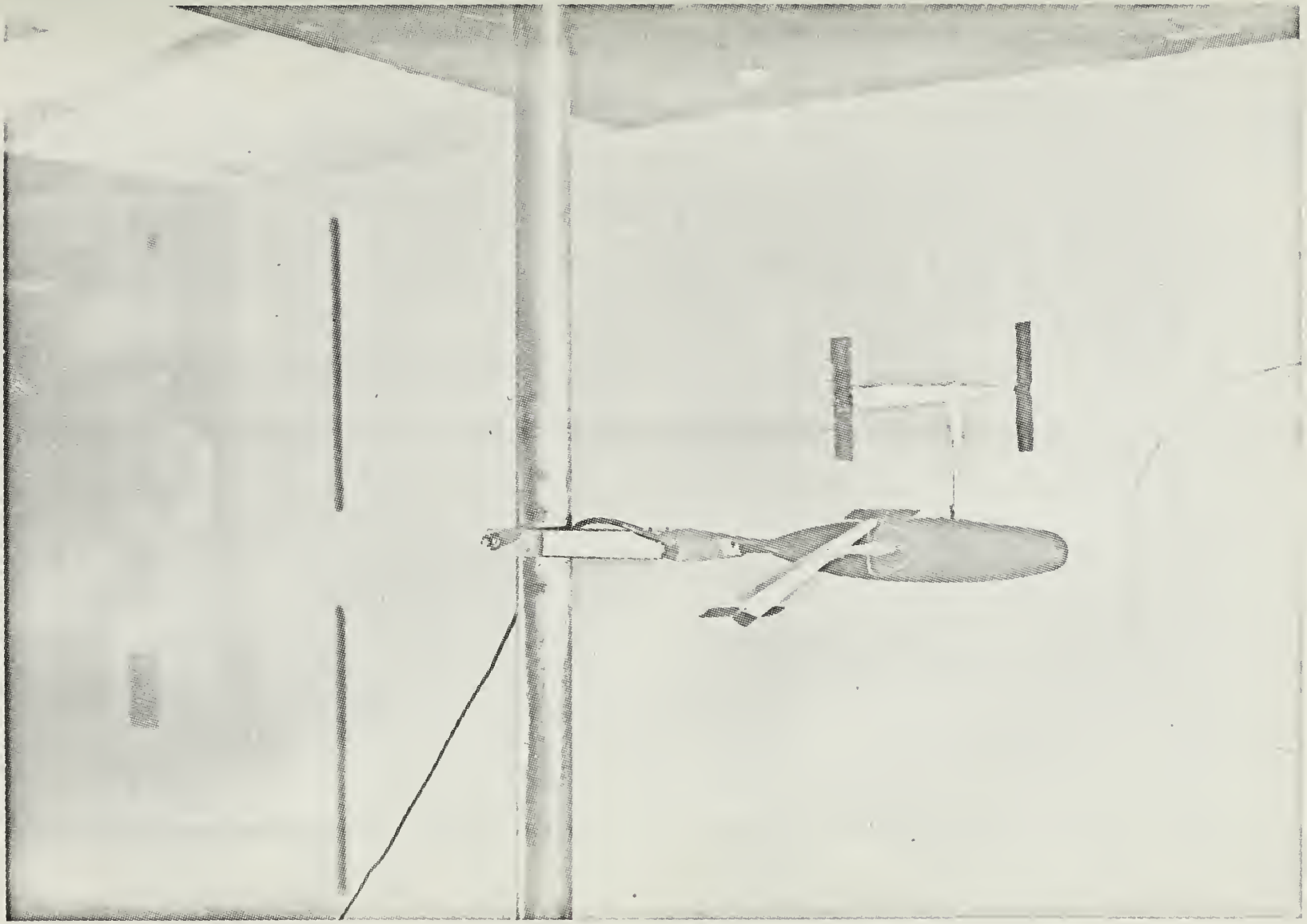

FIGURE 5. GUST SENSOR.

INSTRUMENTATION

Air stream following vanes mounted on low inertia potenticmeters in Figure 5 were used to measure the steady state and time varying response of the free stream air to the sinusoidal oscillation of the jet flap airfoil upstream. The dynamics of the vanes and their design characteristics are discussed in Appendix IV. Adequate speed of response and no overshoot in time response are two desirable characteristics of the vanes. After many different types of vanes were designed and tested, the vanes shown in Figure 5 were used. They have low aspect ratio conical bodies with laterally-protruding wings at leading and trailing edges. By inducing an impulse perpendicular to the free stream in a steady state condition it was observed that with an aft moment arm of 3 inches and a forward arm of 1.5 inches, the vanes are critically damped at all tunnel velocities. This is advantageous for accuracy in data recording. The natural frequency was in the vicinity of 30-35 Hz which is well beyond the range of experimentally-induced frequencies.

The probe shows the configuration of the potentiometers and vanes in the free stream. One potentiometer is mounted laterally placing its vane in position to record any vertical component of deflection in the stream. The vertically mounted pot and vane will record the horizontal component of disturbance. By vectorially adding these components we arrive at the velocity vector induced at that point. If we assume that this velocity vector is perpendicular to a radius to the vortex core then this represents a good method for experimentally locating the vortex core position laterally in the tunnel.

Electrically excited by a 15 volts source the potentiometers were attached to a Sanborn heated stylus recorder and a Brush pen recorder. With maximum frequency capability of 60 cps and 100 cps, the Sanborn and Brush recorders, respectively, could easily accommodate even the high tunnel turbulence frequencies. Calibration was accomplished by mechanically varying the vanes through a known angular distance. Brush and Sanborn

recorders had 1 mm displacement on the recorders equal to 1.5 degrees of vane deflection for the former and 1.3 degrees for the latter.

EXPERIMENTAL PROCEDURES

The experimental testing was accomplished over a period of six weeks. A number of assumptions had to be made to simplify reduction of the data. Incompressible flow and constant temperature were assumed. With a number of variable parameters, the most efficient means of surveying cross sectional areas of the tunnel was devised.

The variable parameters consist of the following:

1.) Tunnel dynamic pressure which alone varied the C_μ value.
2.) Blown flap deflection, δ_f.
3.) Frequency of flap deflection, ω_f.
4.) Position at which the induced velocity is measured in test section, S_{VANE}.

The technique consisted of the following steps:

First fix the following:

1.) The specific δ_f value.
2.) A specific vane position in the tunnel, S_{VANE}.
3.) The initial tunnel dynamic pressure, q.
4.) The initial flap frequency, ω_f.

The range of these parameters is very important in gust simulation. The various combinations can change the magnitude, direction, and span-wise distortion of particular gusts.

For the present discussion the following magnitudes of the parameters were employed.

The initial condition consisted of

(1) $\delta_F = \pm 30^\circ$
(2) $V_\infty = 100$ ft/sec
(3) $\omega_f = 0$

First, a static case was run for each new V_∞ and δ_F. The blown flap was manually cranked, slowly, through a single cycle. This created a good static trace. Then the flap was oscillated through a range of 1 hz, 2 hz, 4 hz, 8 hz, and 16 hz, with the run time of 10 to 15 seconds. Next the V_∞ was lowered to 75 ft/sec and the static and dynamic cases were run again. Finally, the V_∞ was fixed at 50 ft/sec and the process was repeated. The V_∞ and δ_F changes were made for all δ_{max} in a specific cross section of tunnel at x = 2.0c downstream from the model. After this cross section was surveyed, the vanes were moved to the x = 6.0c downstream section and finally, the x = 10.0c downstream section. The δ_f magnitude was then changed to accommodate a variation of $\pm 45^\circ$. After the entire tunnel was surveyed again at $\delta_F = \pm 45^\circ$, the δ_f was changed to $\pm 60^\circ$ for the third and final run through the tunnel. During the $\delta_f = \pm 30^\circ$ survey, approximately eleven to thirteen evenly spaced points were surveyed in each cross section. For the $\delta_f = \pm 45^\circ$ and $\pm 60^\circ$, only four of the centrally located points in each section were observed. This reduction in survey points does not decrease the accuracy of the experiments. Induced velocity magnitude variations are still discernible and comparisons with different parameter regimes can still be made.

A few runs were made without blowing augmentation for comparison with the augmented generator. And finally, data were taken with the connecting arm shortened, to oscillate the flap unidirectionally from $\delta_F = 0^\circ$ to $\delta_F = 60^\circ$ for dynamic observations discussed later.

DISCUSSION OF EXPERIMENTAL RESULTS

STATIC:

In the static case the experimental trends were correlated with the theory. In Figure 8 a typical central position of δ_{TAPE} was chosen and observed. Diffusion of the vortices downstream is negligible from a theoretical as well as experimental point of view. Westmore (Reference 29) relates a variation of w_p with downstream distance as follows:

$$w_p = \frac{\Gamma_0}{2\pi r}\left\{1 - \exp\left[-\frac{r^2}{(42b^2 + 1.2\bar{c}\frac{\Gamma_0 x}{V_\infty})(10^{-4})}\right]\right\}$$

By substitution it is observed that, with the tunnel "q's" in the present discussion and the short length of streamwise distance, diffusion downstream is negligible. Even with the additional turbulence introduced by the tunnel walls, no dissipation can be observed over this distance. In fact, as is observable in Figure 7, there is a strengthening in Γ as the probe is translated downstream. This is most likely due to the decrease in h and increase in $\cos\theta_n$ for positions farther downstream when $\delta_F = +$, (Figure 19).

Having assumed that all of the vorticity is wrapped up in a single trailing vortex, the profile of downwash (Reference 18) is as follows:

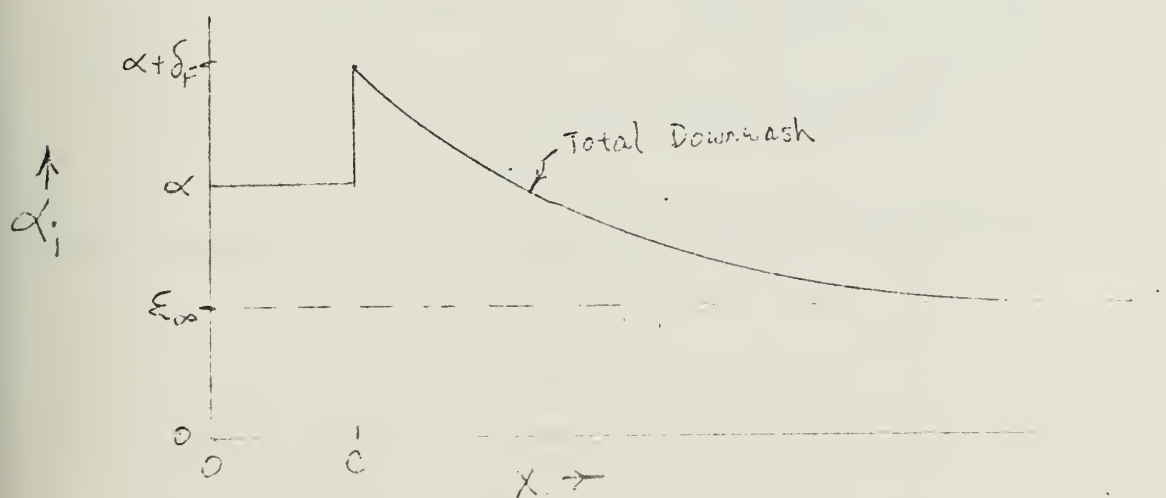

Figure 6

Although this graph is induced angle of attack with distance X, it gives a good indication of the actual variation with distance of the vorticity as a combination of circulation and jet sheet components to the total value. This, therefore, is a good representation of the strength of the trailing vortices. Here then we can see that as X increases it is obvious that at some central position, $|\omega_p|$ will be greater than at an even farther δ_{VANE} downstream. Observing the actual tendencies in Figure 7 we see that this hypothesis holds true in all cases. In the x = 2.0c position, the large value of h and small cos Θ_n magnitude, due to core position, will overcome this initial Γ at x = c+; hence, the value of ω_p will peak at x = 6.0c downstream. This discussion represents the static case with the flap deflected positively, (toward the centerline of the tunnel). It also introduces the interference tendency far downstream due to wall effects that are not noticeable near the flap.

When the flap is directed in a minus direction, (toward the closer tunnel wall), h will increase with x as will cos Θ_n . Thus, their effects tend to cancel in the generation of ω_p. Again Γ will vary as in Figure 6. Theoretically, the general trend for $|\omega_p|$ should be decreasing in value with downstream distance. This is normally true (Figure 19).

In the set of Figures 8 to 16, the entire cross-section is viewed. Both magnitude and direction of the ω_p vectors make the position of the core in the static condition easily located. The solid vectors are for $+\delta_f$ and the hatched vectors for $-\delta_f$. Magnitude and direction differences between the hatched and solid vectors illustrate the movement of the equivalent vortex core position across the tunnel.

In any cross-section, δ_{VANE} movement obviously decreases ω_p with increasing h proving experimentally that

$$\omega_p \sim \frac{1}{r}$$

Velocity and C_μ changes alone can be observed by comparing Figures 8, 9, and 10. These are typical arrays of cross-sectional induced velocity vectors with varying free stream velocity, V_∞. Thus, as is evident from these figures,

$$\frac{\partial w_p}{\partial V_\infty} \equiv +$$

The general trend is toward an increased w_p for an increase in V_∞; however, the partial derivative value is not strong. Hence, this variation is somewhat erratic. Experimentally, (Figures 17 and 18), this solution agrees with the theoretical evaluation in Appendix I.

Flap deflection changes, $\Delta\delta_F$, have the most obvious affects on of all the parameters. As can be seen in Appendix I,

(1) $\Gamma \sim \delta_F$

(2) $h \sim \frac{1}{f(\delta_F)}$

(3) $\cos\theta_n \sim g(\delta_F)$

All three add a positive increment to the partial derivative such that

$$\frac{\partial w_p}{\partial \delta_F} \equiv +$$

A comparison, in progression, of Figures 8, 11 and 14 will give a typical view of the change in magnitude of the induced velocity as a function of δ_F. Figure 20 gives a typical graphical picture of this progression. It can be observed that the $|w_p|(\delta_F)$ seems to be of the order of an increasing power function. It appears then that in fact the partials

$$\frac{\partial h}{\partial \delta_F} \text{ and } \frac{\partial \cos\theta_n}{\partial \delta_F}$$ have

greater influence at higher values of δ_F.

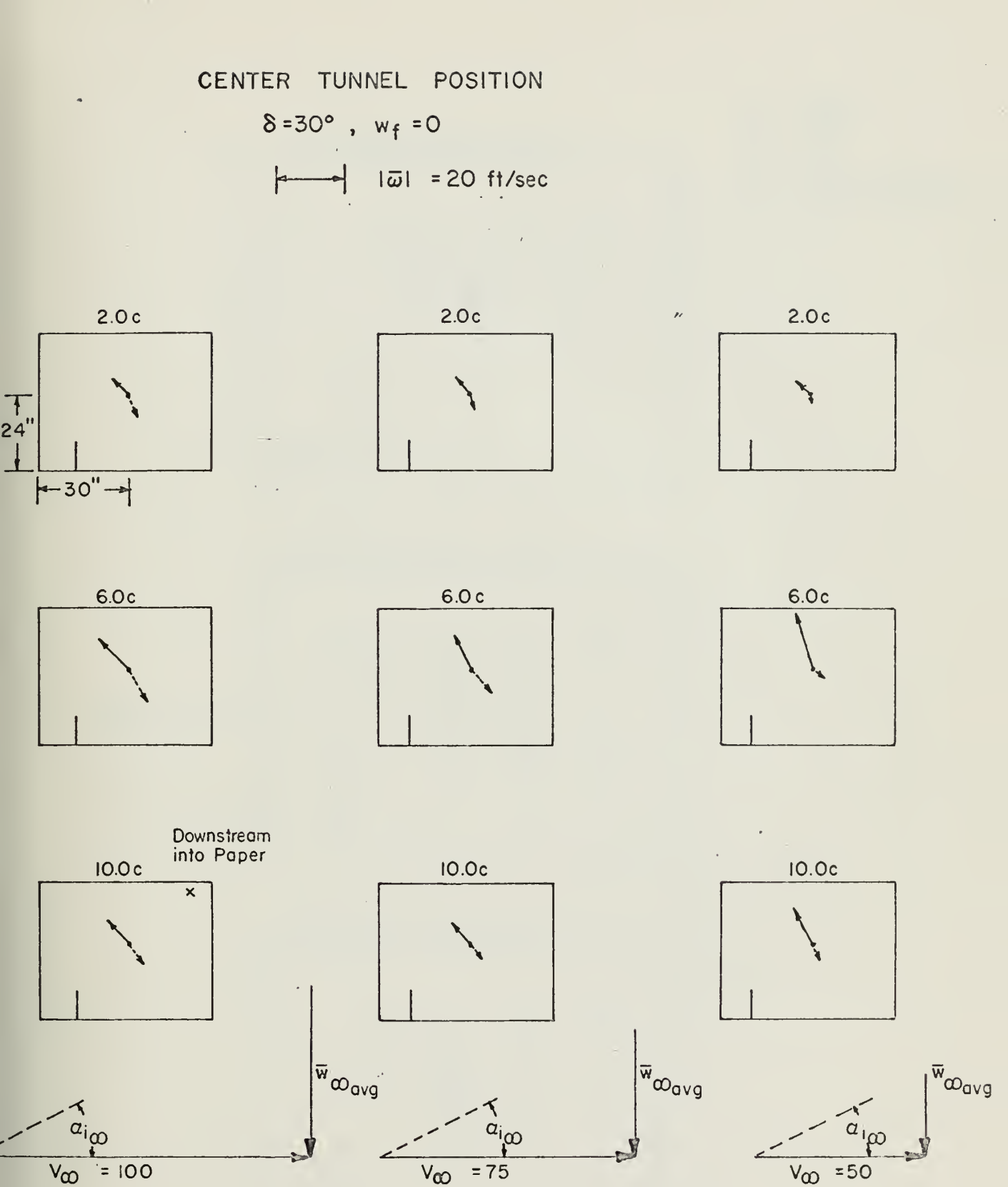

FIGURE 7. COMPARISON OF THE MAGNITUDE OF INDUCED VELOCITY AT A CENTRAL POSITION AT VARYING DOWNSTREAM POSITIONS WITH THE THEORETICAL INDUCED VELOCITY AT X=∞ IN THE WAKE OF THE JET FLAP.

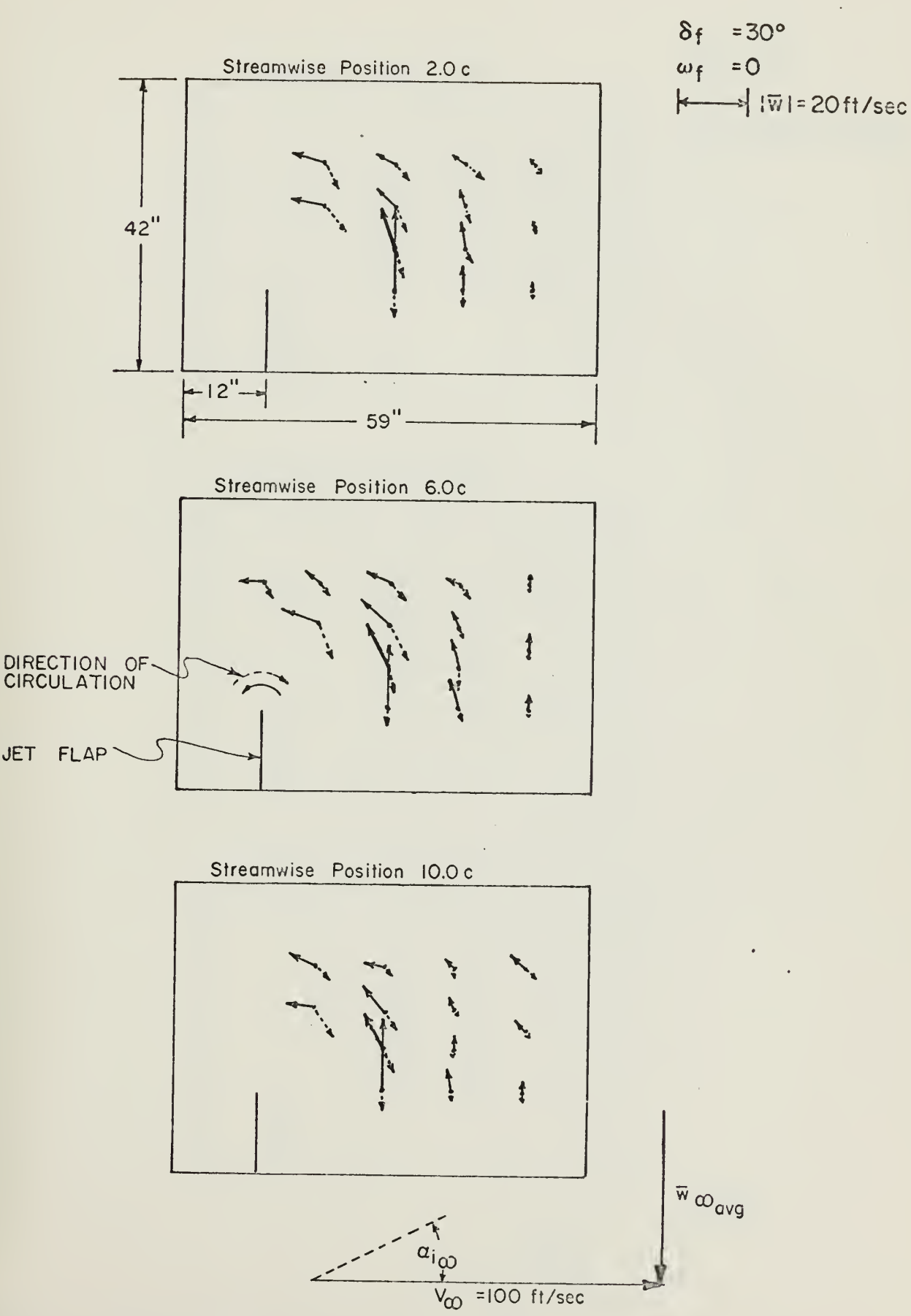

FIGURE 8. COMPARISON OF CROSS-SECTION SURVEYS OF INDUCED VELOCITY WITH ($w_{\infty_{avg}}$) AT X=∞ IN THE WAKE OF THE JET FLAP

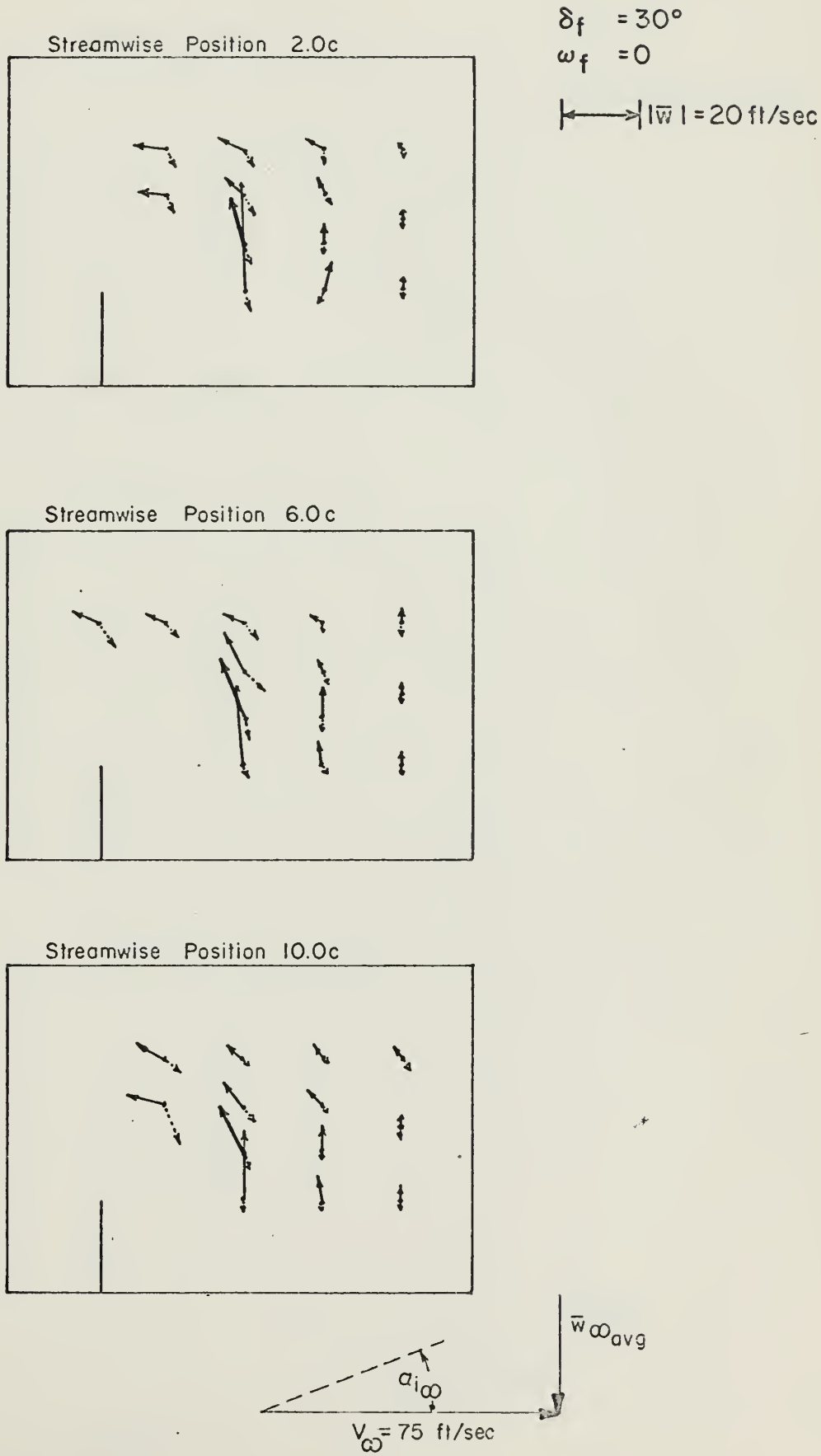
δ_f = 30°
ω_f = 0
$|\bar{w}|$ = 20 ft/sec
Streamwise Position 2.0c
Streamwise Position 6.0c
Streamwise Position 10.0c
$\bar{w}_{\infty_{avg}}$
α_{i_∞}
V_∞ = 75 ft/sec

FIGURE 9.

$\delta_f = 30°$

$\omega_f = 0$

$|\bar{w}| = 20$ ft/sec

Streamwise Position 2.0c

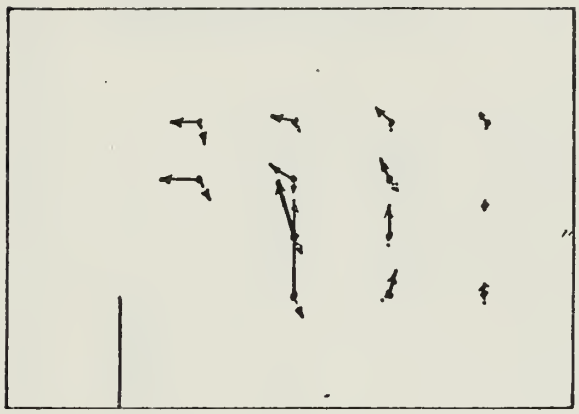

Streamwise Position 6.0c

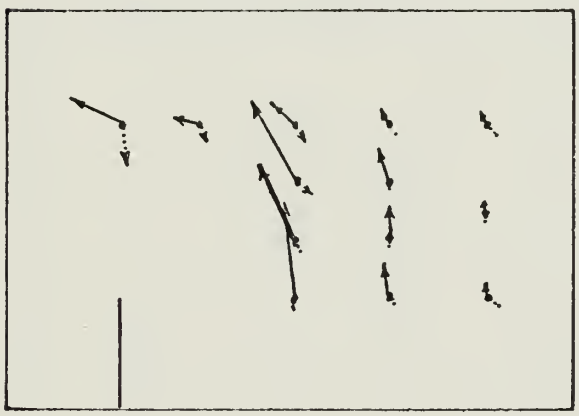

Streamwise Position 10.0c

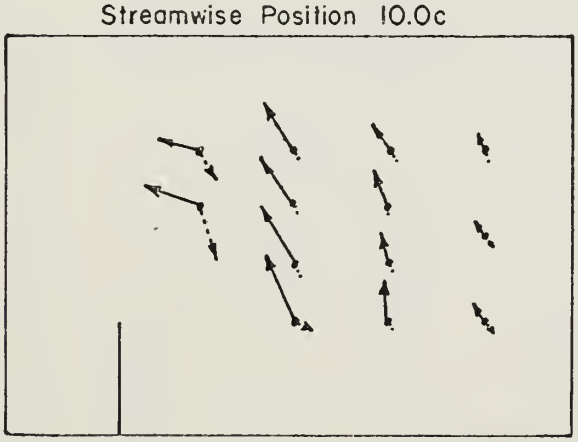

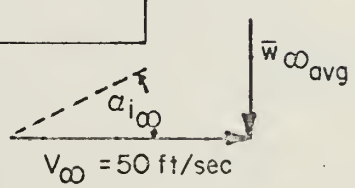

FIGURE 10.

$\delta_f = 45°$

$\omega_f = 0$

$|\bar{w}| = 20$ ft/sec

Streamwise Position 2.0c

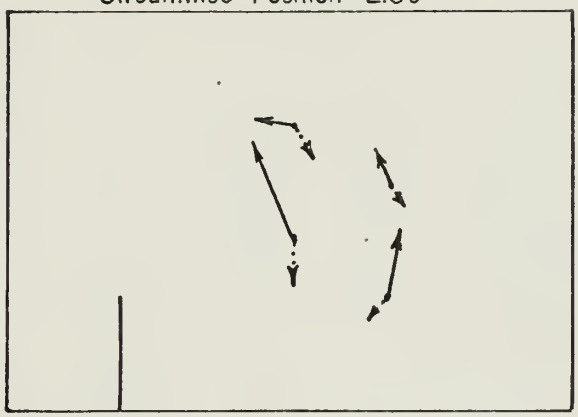

Streamwise Position 6.0c

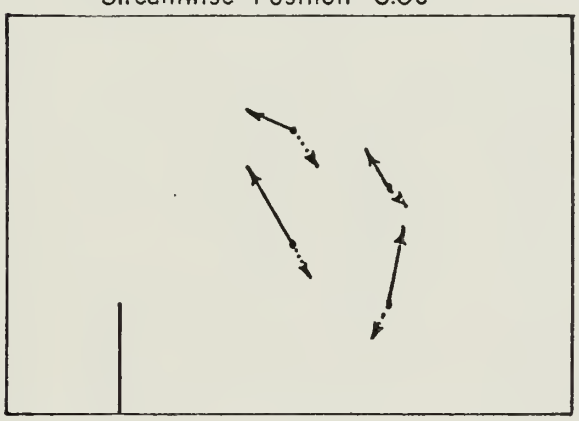

Streamwise Position 10.0c

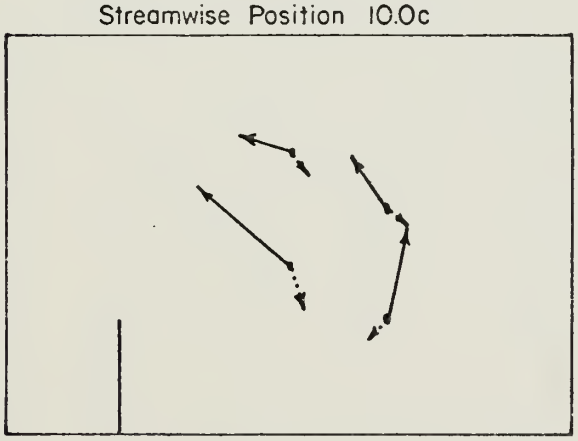

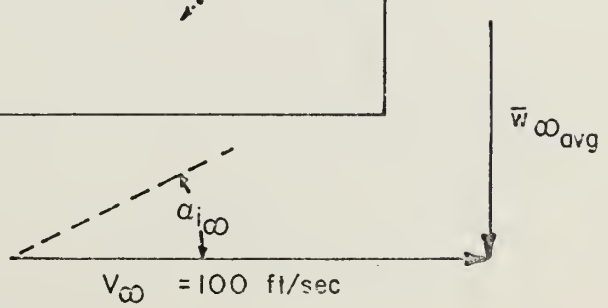

FIGURE 11.

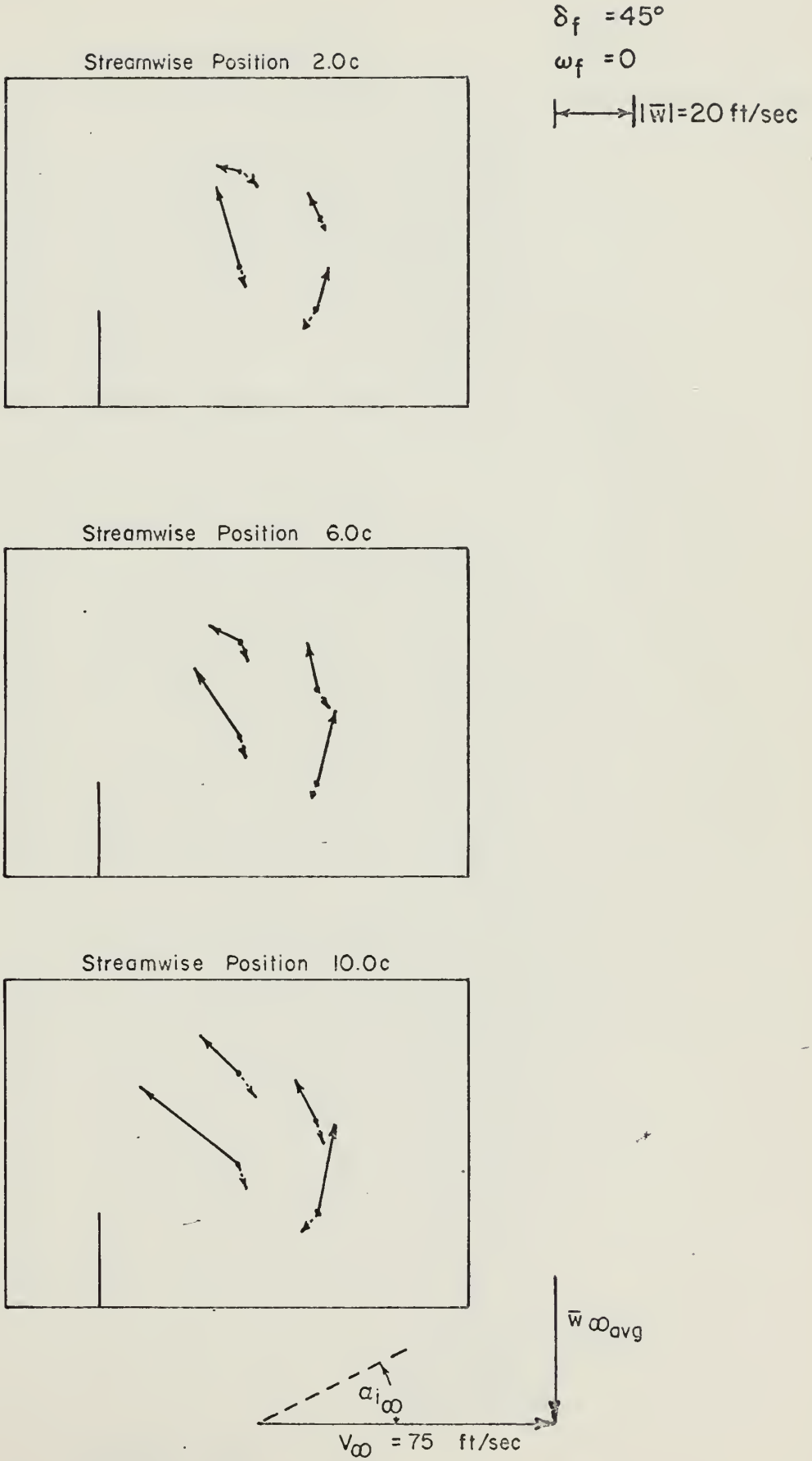
δ_f =45°
ω_f =0
|$\bar{w}$|=20 ft/sec
Streamwise Position 2.0c
Streamwise Position 6.0c
Streamwise Position 10.0c
$\bar{w}_{\infty_{avg}}$
α_{i_∞}
V_∞ = 75 ft/sec

FIGURE 12.

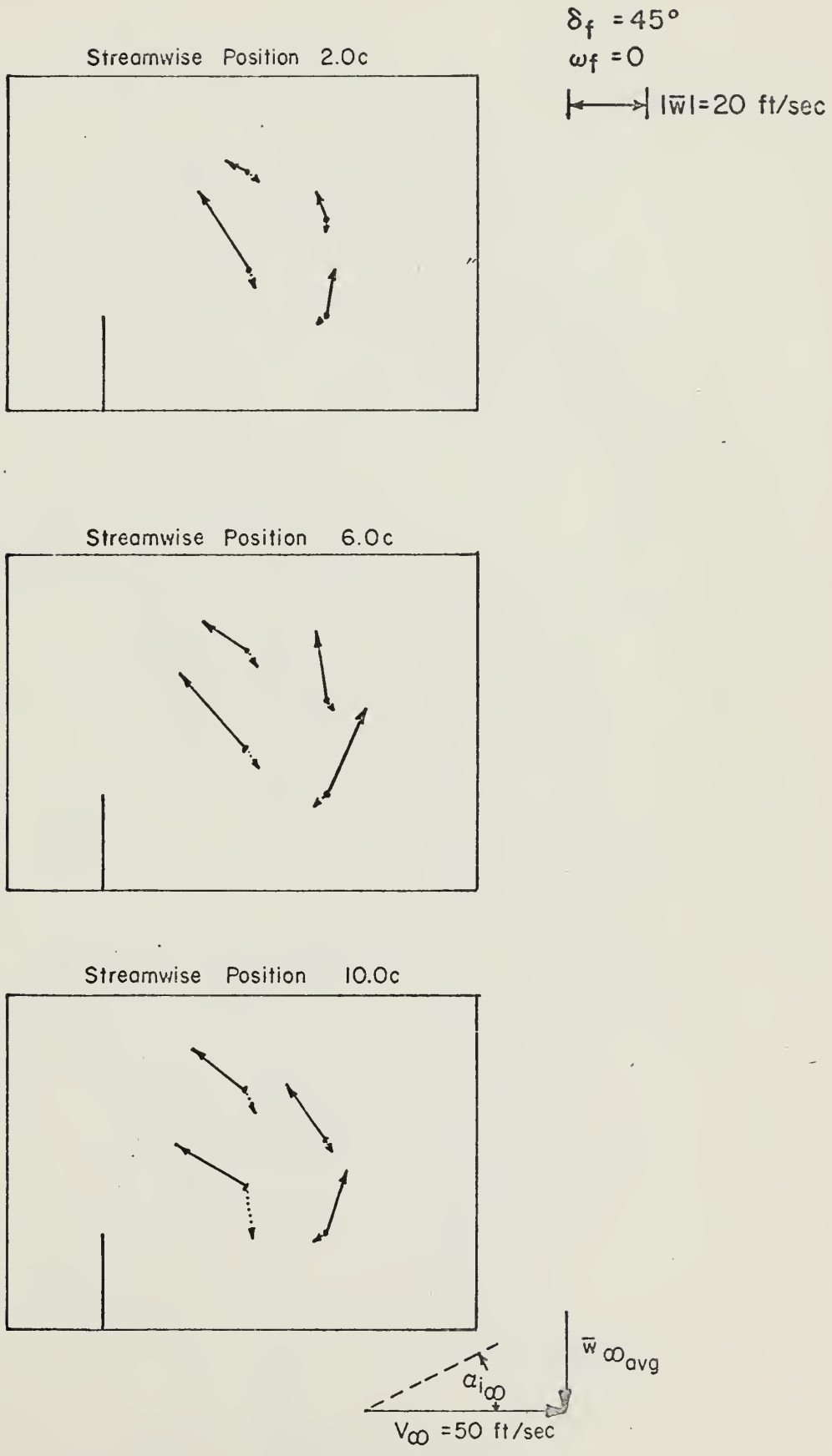
$\delta_f = 45°$
$\omega_f = 0$
$|\bar{w}| = 20$ ft/sec
Streamwise Position 2.0c
Streamwise Position 6.0c
Streamwise Position 10.0c
$\bar{w}_{\infty_{avg}}$
α_{i_∞}
$V_\infty = 50$ ft/sec

FIGURE 13.

$\delta_f = 60°$

$\omega_f = 0$

$|\bar{w}| = 20$ ft/sec

Streamwise Position 2.0c

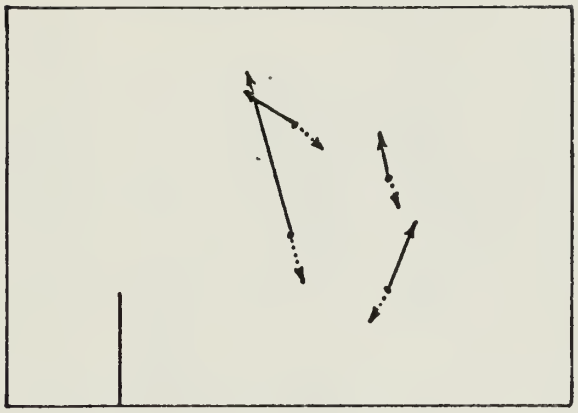

Streamwise Position 6.0c

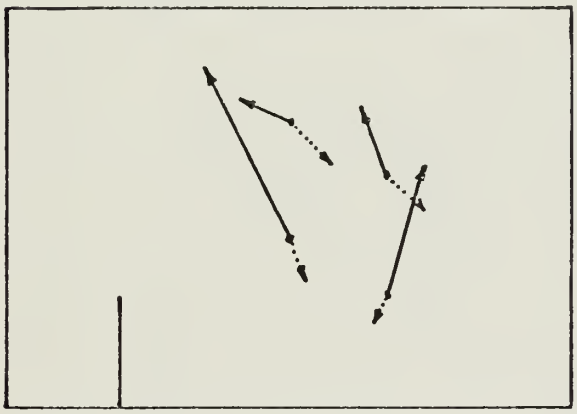

Streamwise Position 10.0 c

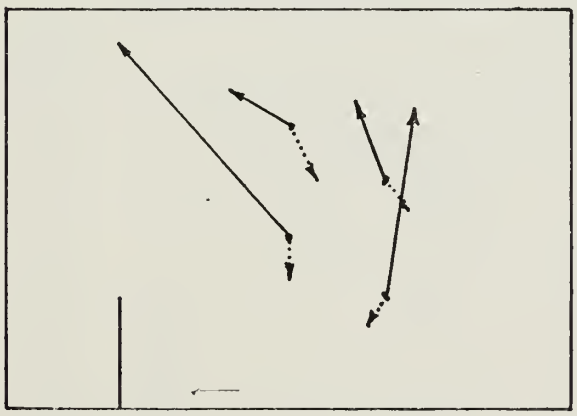

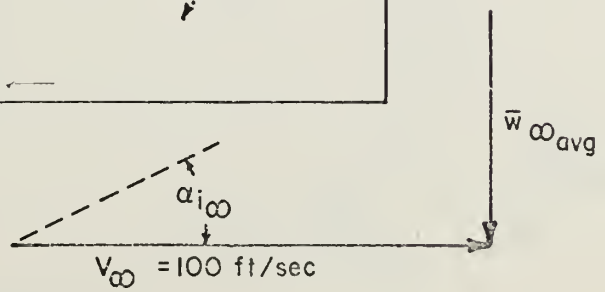

FIGURE 14.

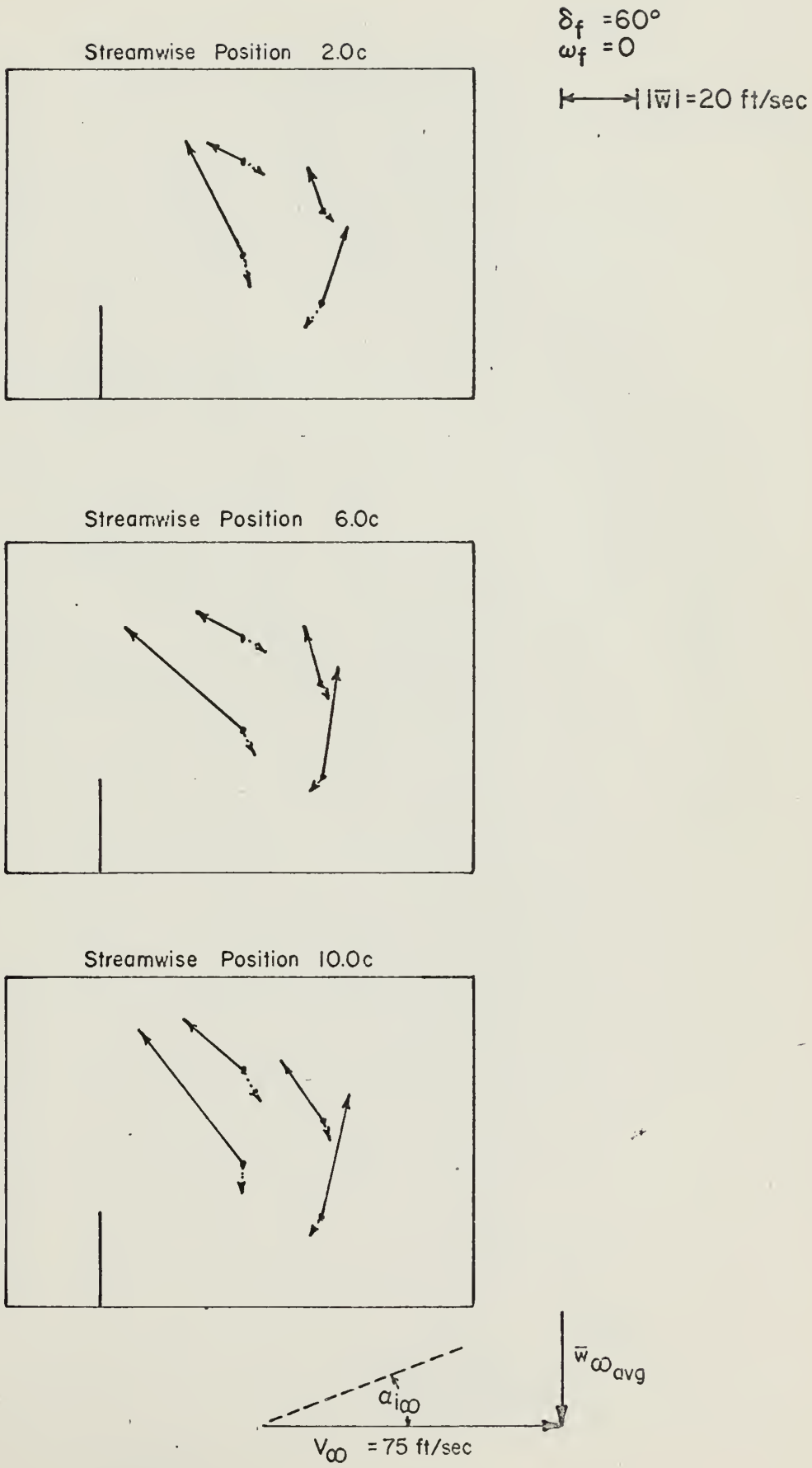
δ_f =60°
ω_f =0
|w̄|=20 ft/sec
Streamwise Position 2.0c
Streamwise Position 6.0c
Streamwise Position 10.0c
$\bar{w}_{\infty_{avg}}$
α_{i_∞}
V_∞ =75 ft/sec

FIGURE 15.

$\delta_f = 60°$

$\omega_f = 0$

$|\bar{w}| = 20$ ft/sec

Streamwise Position 2.0 c

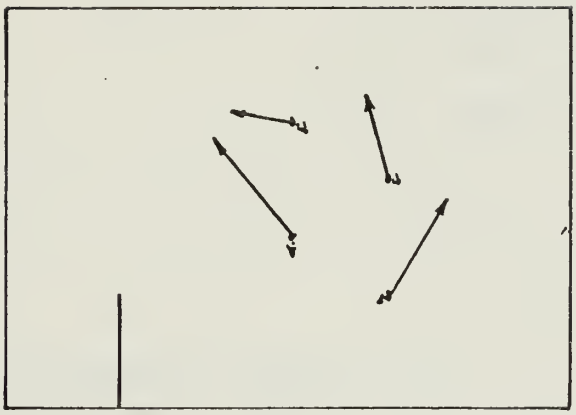

Streamwise Position 6.0 c

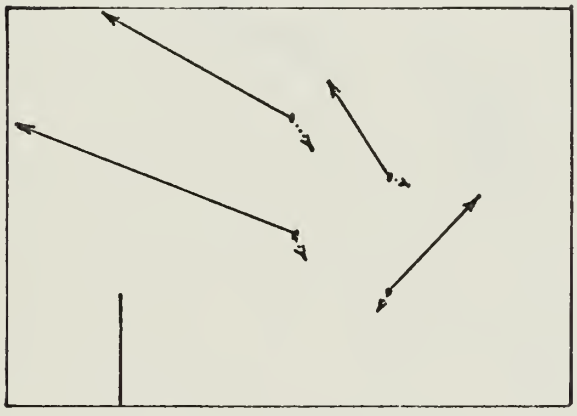

Streamwise Position 10.0c

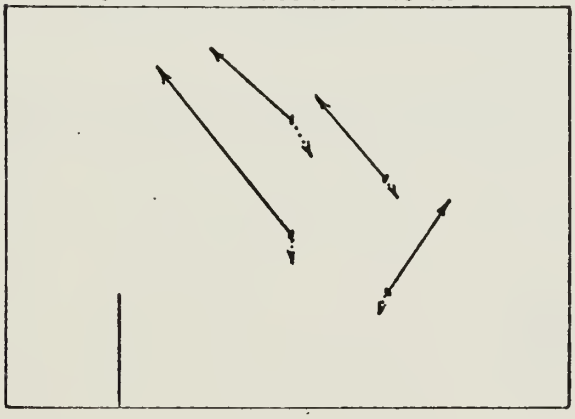

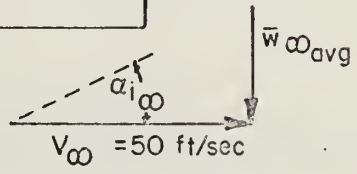

FIGURE 16.

$\delta_f = 0 \rightarrow +60°$
$\omega_f = 0$

——— $V_\infty = 100$ ft/sec
--------- $V_\infty = 75$ ft/sec
— — $V_\infty = 50$ ft/sec

STREAMWISE POSITION 2.0c

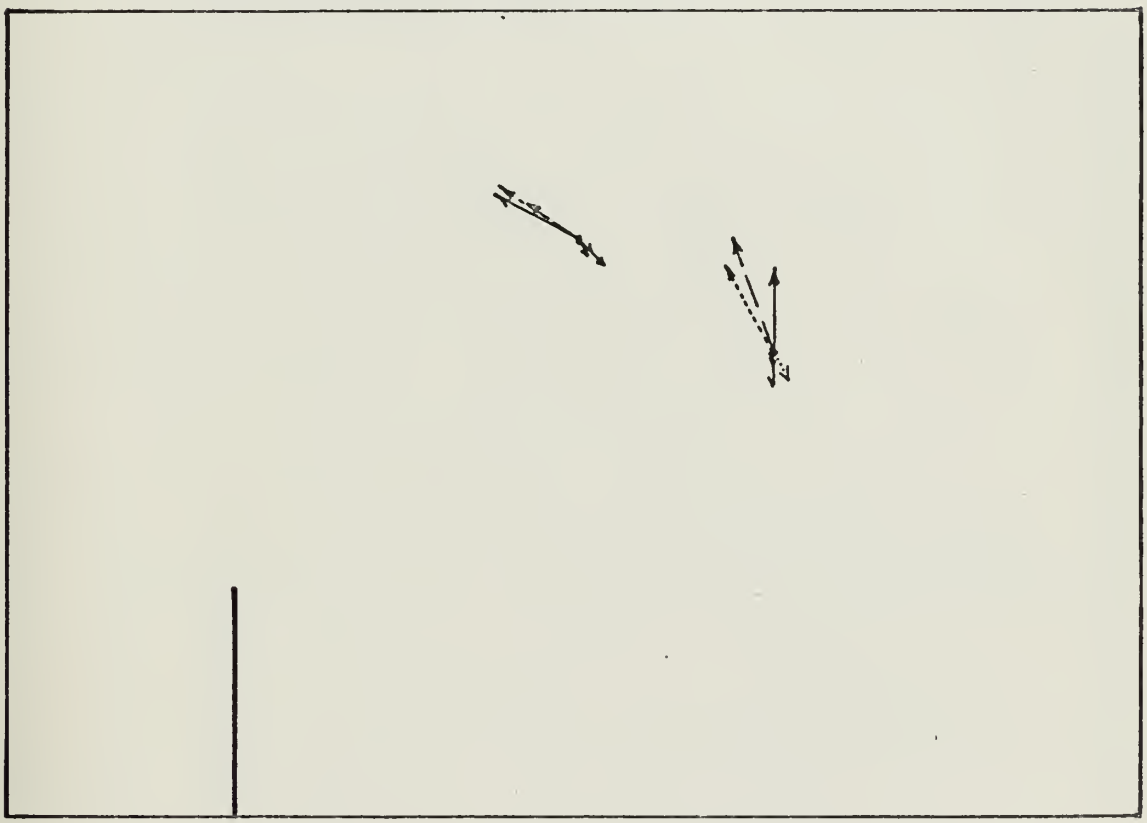

$|\bar{w}| = 20$ ft/sec

FIGURE 17. VARIATION OF INDUCED VELOCITY AT PARTICULAR POSITIONS FOR VARIABLE FREE-STREAM TUNNEL VELOCITY.

$\delta_f = 0 \rightarrow +60°$

$\omega_f = 0$

——— $V_\infty = 100$ ft/sec

------- $V_\infty = 75$ ft/sec

— — $V_\infty = 50$ ft/sec

STREAMWISE POSITION 6.0c

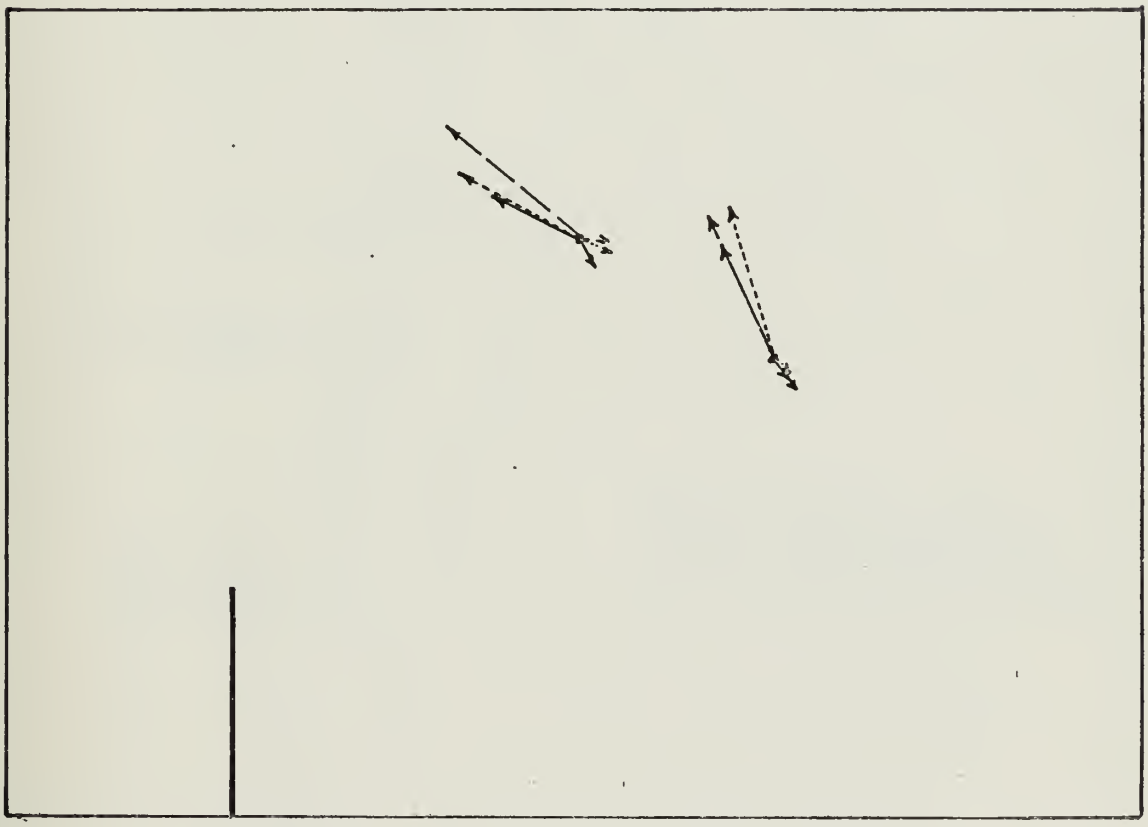

$|\bar{w}| = 20$ ft/sec

FIGURE 18.

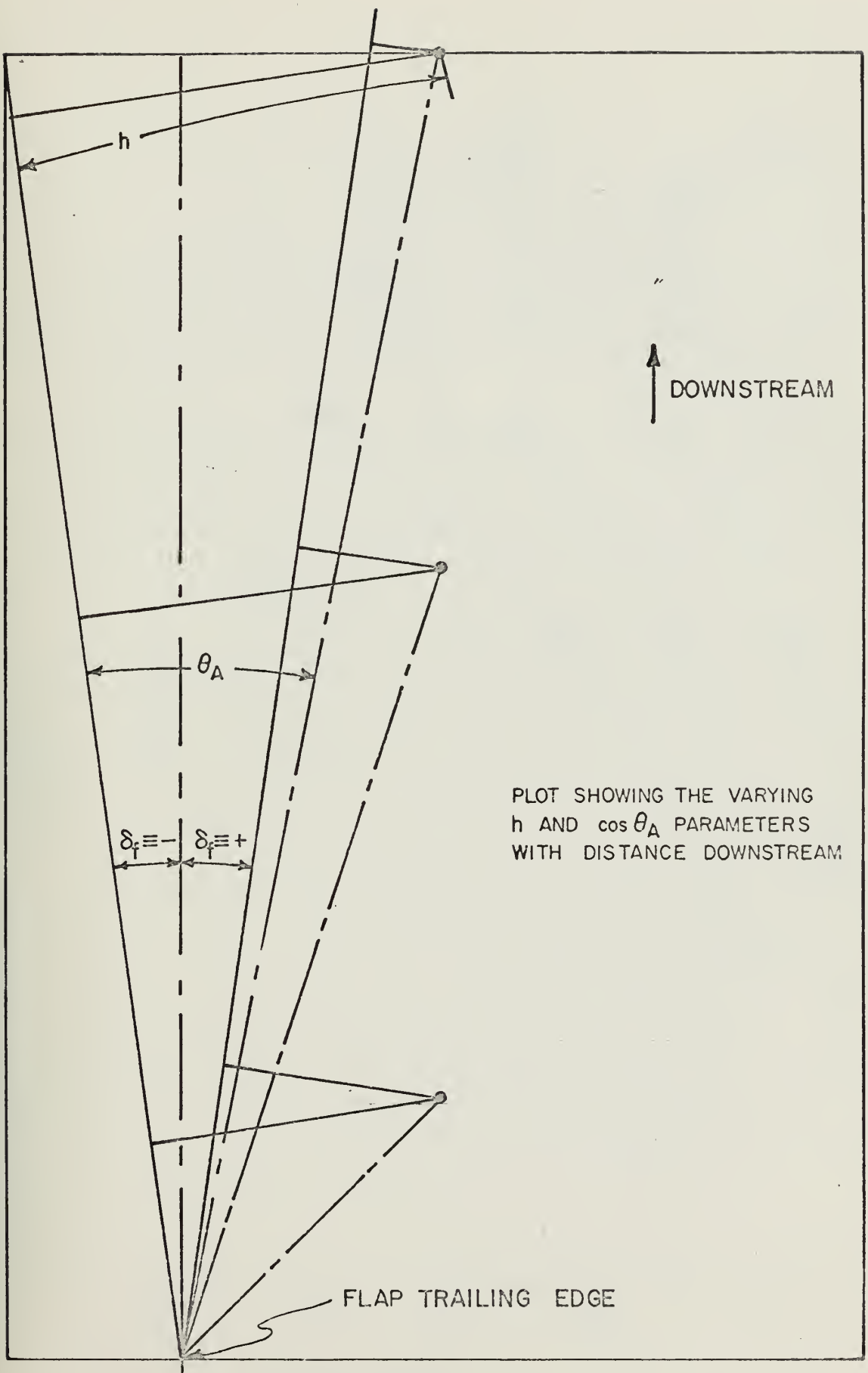
h
DOWNSTREAM
θ_A
$\delta_f \equiv -$
$\delta_f \equiv +$
PLOT SHOWING THE VARYING
h AND cos θ_A PARAMETERS
WITH DISTANCE DOWNSTREAM
FLAP TRAILING EDGE

FIGURE 19.

PLOT OF INDUCED VELOCITY MAGNITUDE AT STREAMWISE POSITION 6.0c DOWNSTREAM AS A FUNCTION OF δ_f.

$V_\infty \equiv$ CONSTANT
$\omega_f = 0$

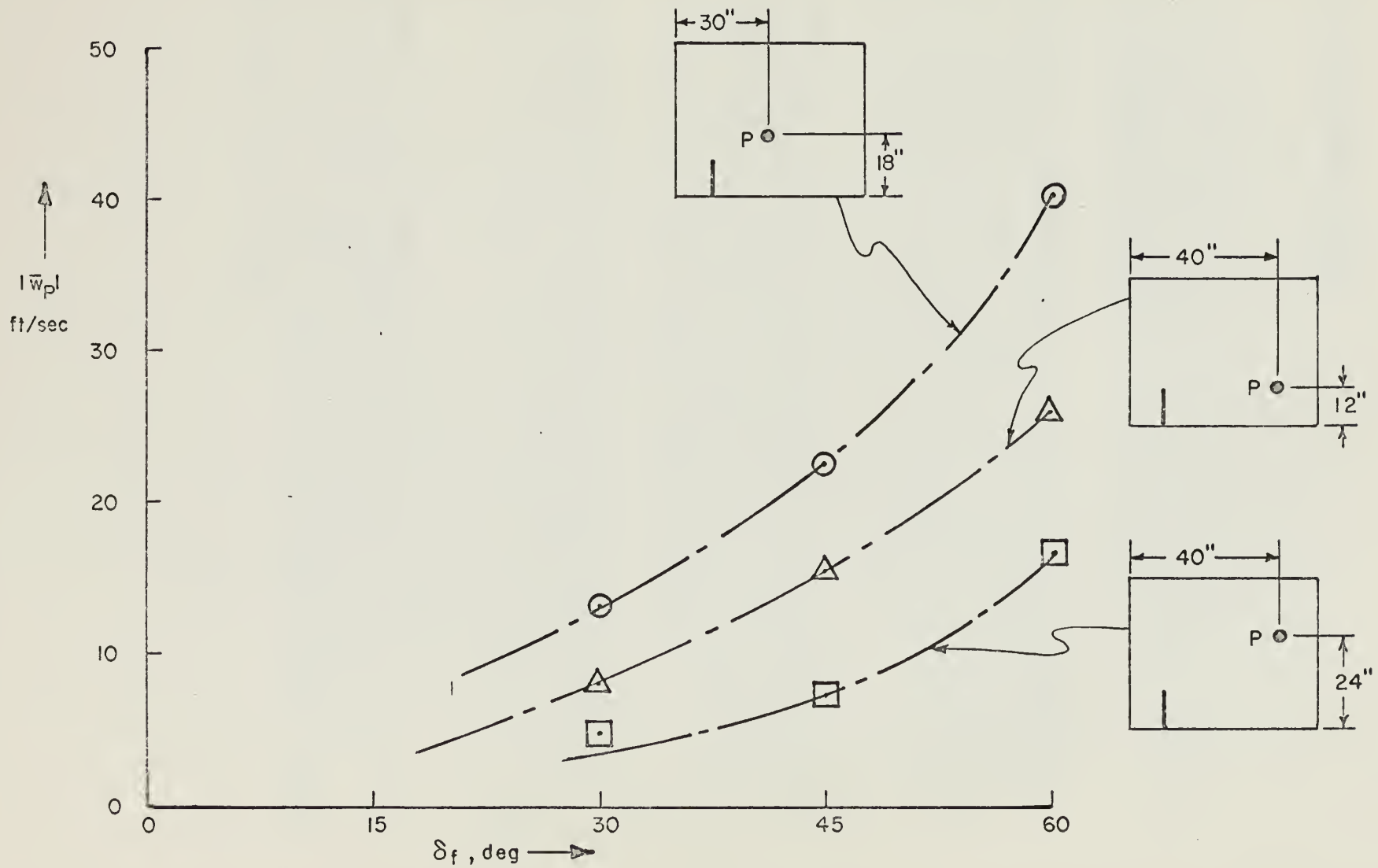

FIGURE 20.

DISCUSSION OF EXPERIMENTAL RESULTS

DYNAMIC:

The dynamic experimental data for the majority of cases agree with the theoretical trends discussed in Appendix I. In all regimes, the decrease in induced velocity amplitude with high frequency is evident.

Induced angle of attack holding all the variables but ω_T constant, was recorded as a function of reduced frequency (Strouhal Number), K. As can be seen from Figures 22 and 23, magnitude peaks in ω_p arise at intermediate values of K for those sectional positions investigated. As K is increased these data tend to show the same decreasing trend as Figure 21.

The rapid decay of magnitude of induced velocity as a function of K in Figures 21 - 23 at high frequency shows strikingly the dynamic interference affect of high frequency oscillation of the airstream. Some of the high frequency data, however, does show a reduction trend about a biased value of ω_p; this is due to the vortex filament movement downstream.

In the augmented case, as is stated in the theory of Appendix I, at high K, the magnitude of ω_p, for the sinusoidal symmetrically-oscillating flap does level off to a constant value in the range $0 < \omega_p|_{\omega_f = \infty} < \frac{1}{2}\omega_{p_{STATIC}}$

In Figures 21 - 23, a comparison was made of the induced flow generated without blowing augmentation. It is obvious that the trends of peaking with intermediate values of K and decay with high values of K occur here, too. But as before, the use of blowing creates a great increase in magnitude even at high K values.

Experimental results (Figures 24 - 27) indicate unidirectional flap oscillation decreases the cancellation of the harmonic components which appear in the symmetrical case. However, the theory proposes that this high frequency cancellation should be exactly the same as that for the symmetrical deflection. The theory and experiment disagree at this point since the $|\omega_p|$ does not diminish symmetrically around the mean value.

Vortex filament motion as described in Appendix I will only change the value of the bias such that at $\omega_f = \infty$, the $|\omega_p|$ when the filament is assumed motionless, is less than $|\omega_p|$ when the filament is in motion. This fact is still of less importance than the previous disagreement between the calculated and the experimental cancellation.

Although further experimentation at higher K is necessary to verify the experimental decay of ω_p with K, it would seem impossible to create a gust by means of an oscillating jet flap and trailing vortex system for Strouhal Numbers much in excess of 2.5.

STREAMWISE POSITION 6.0 c, SECTIONAL POSITION 30" x 18"

$\delta_f = \pm 60°$

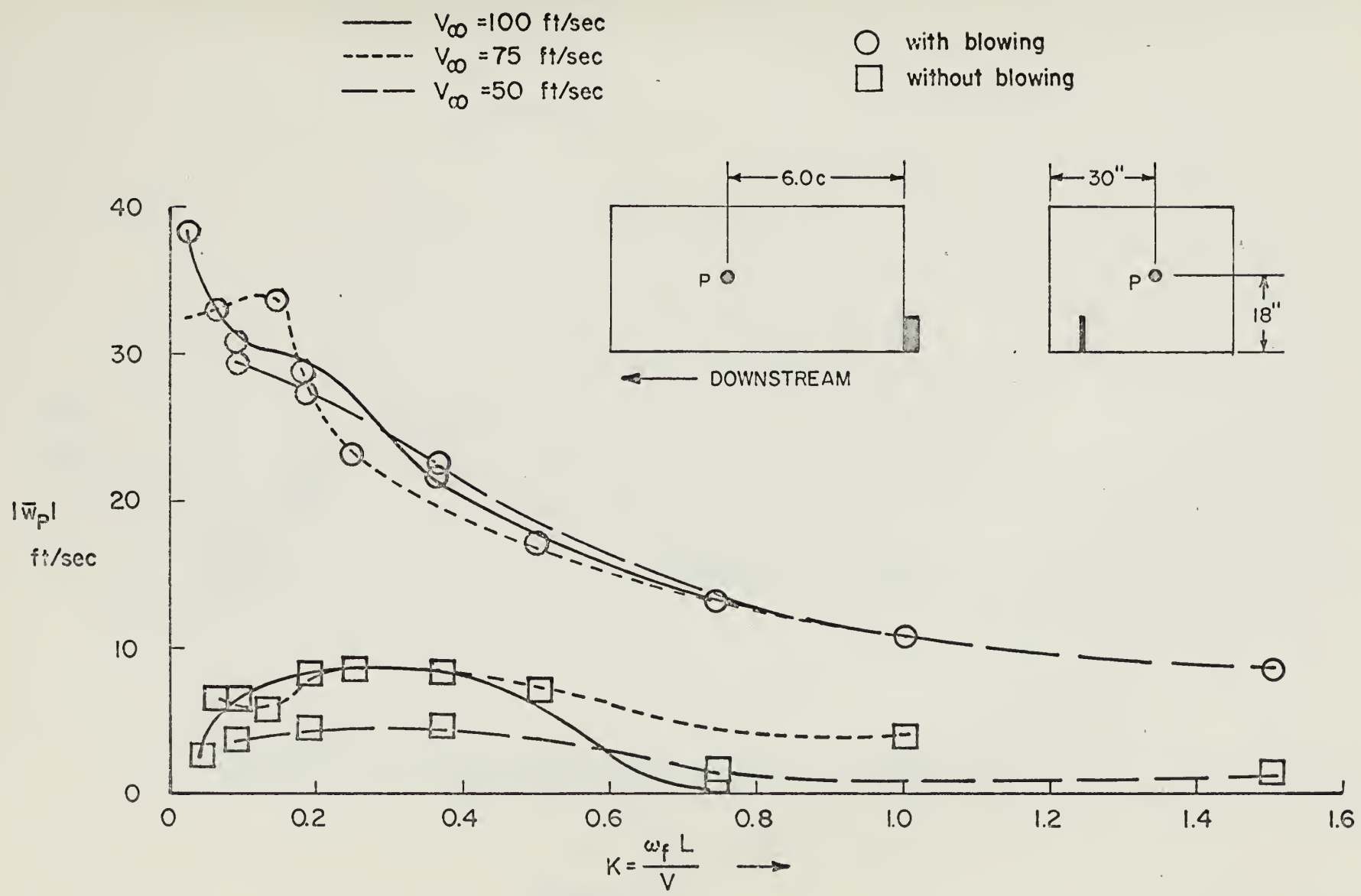

FIGURE 21.

STREAMWISE POSITION 6.0c, SECTIONAL POSITION 40" x 24"

$\delta_f = \pm 60°$

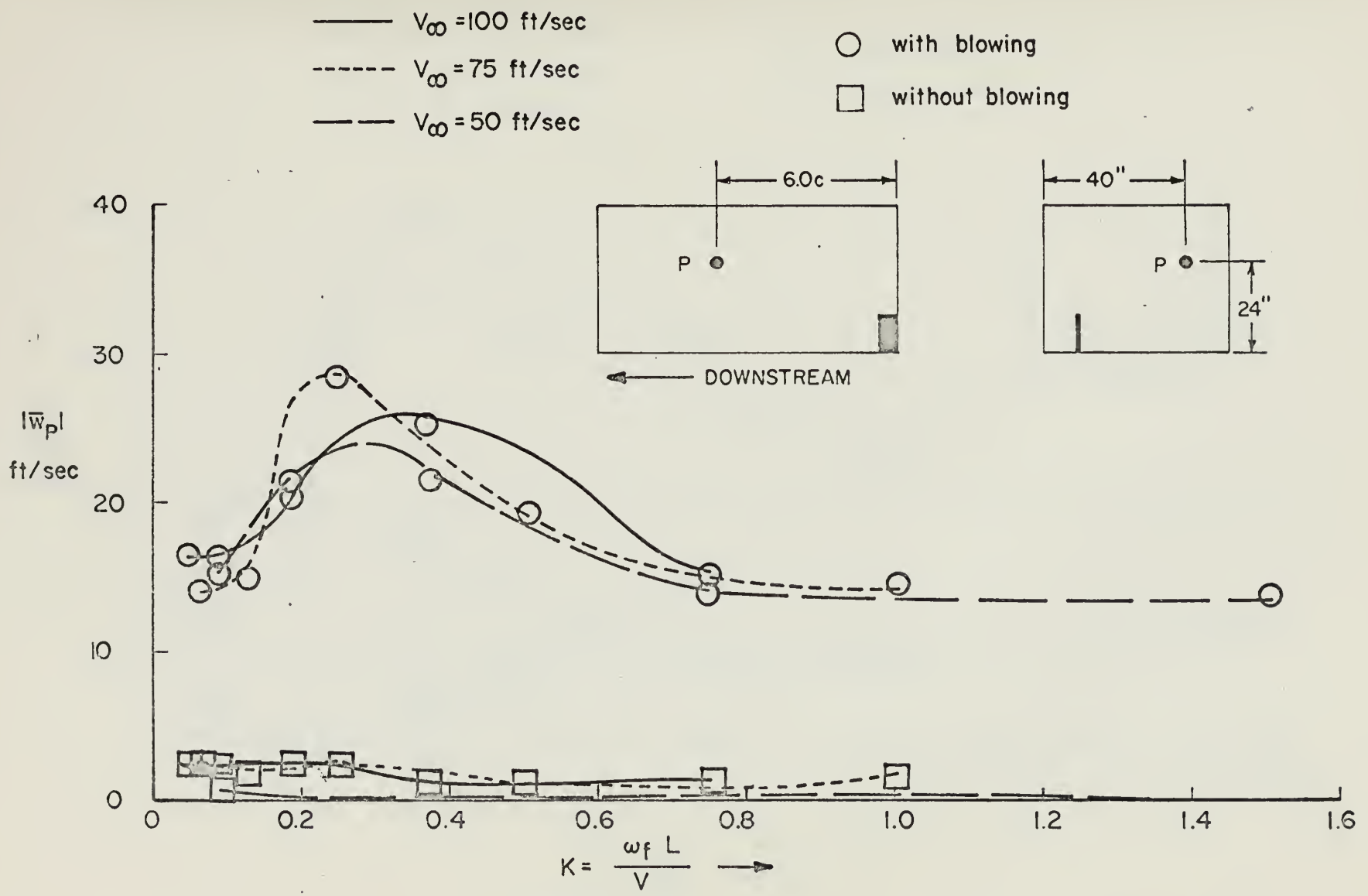

FIGURE 22.

STREAMWISE POSITION 6.0c, SECTIONAL POSITION 40"x12"

$\delta_f = \pm 60°$

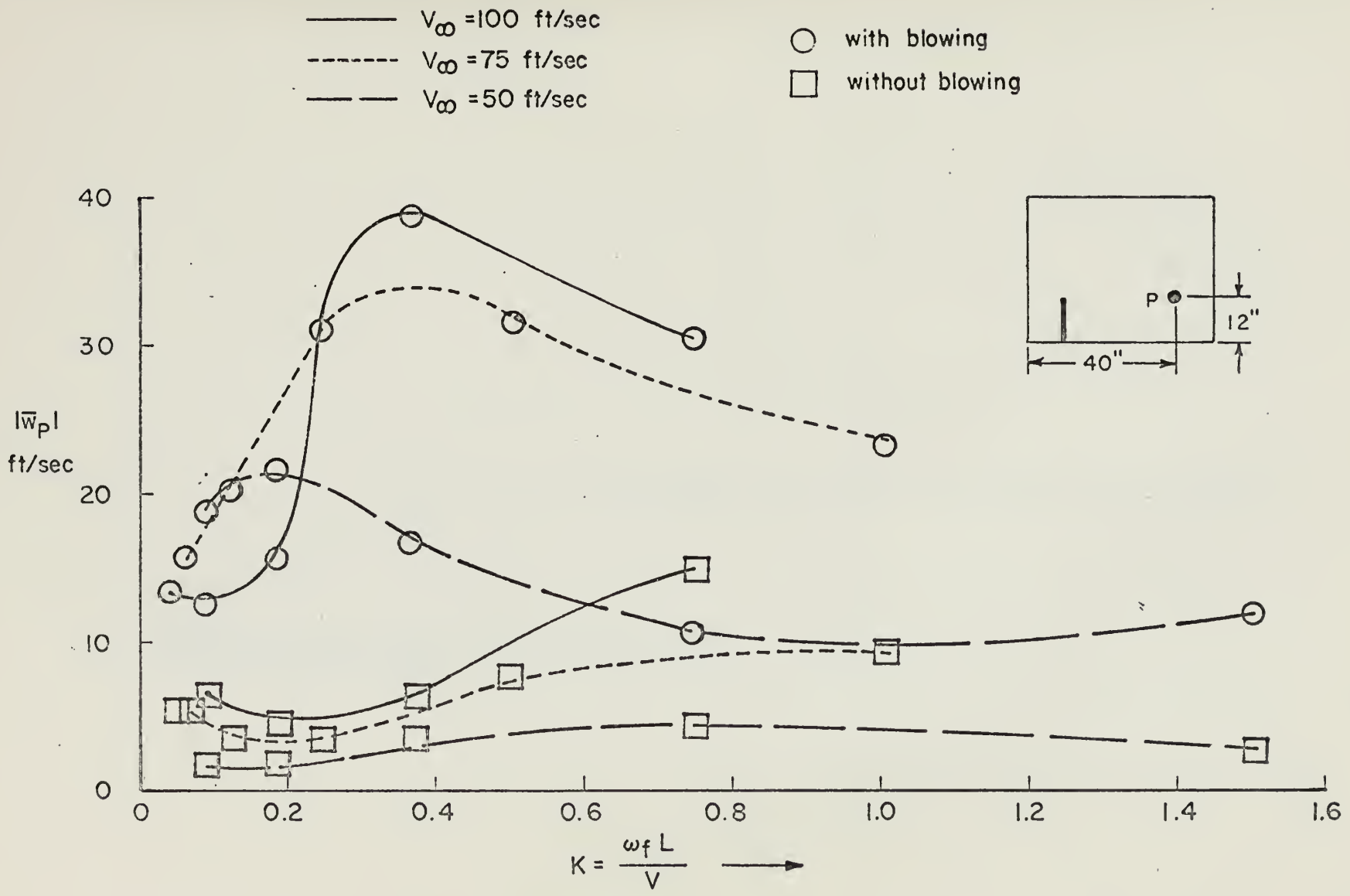

FIGURE 23.

STREAMWISE POSITION 2.0c, SECTIONAL POSITION 40" x 24"

$\delta_f = 0 \rightarrow +60°$ UNIDIRECTIONAL

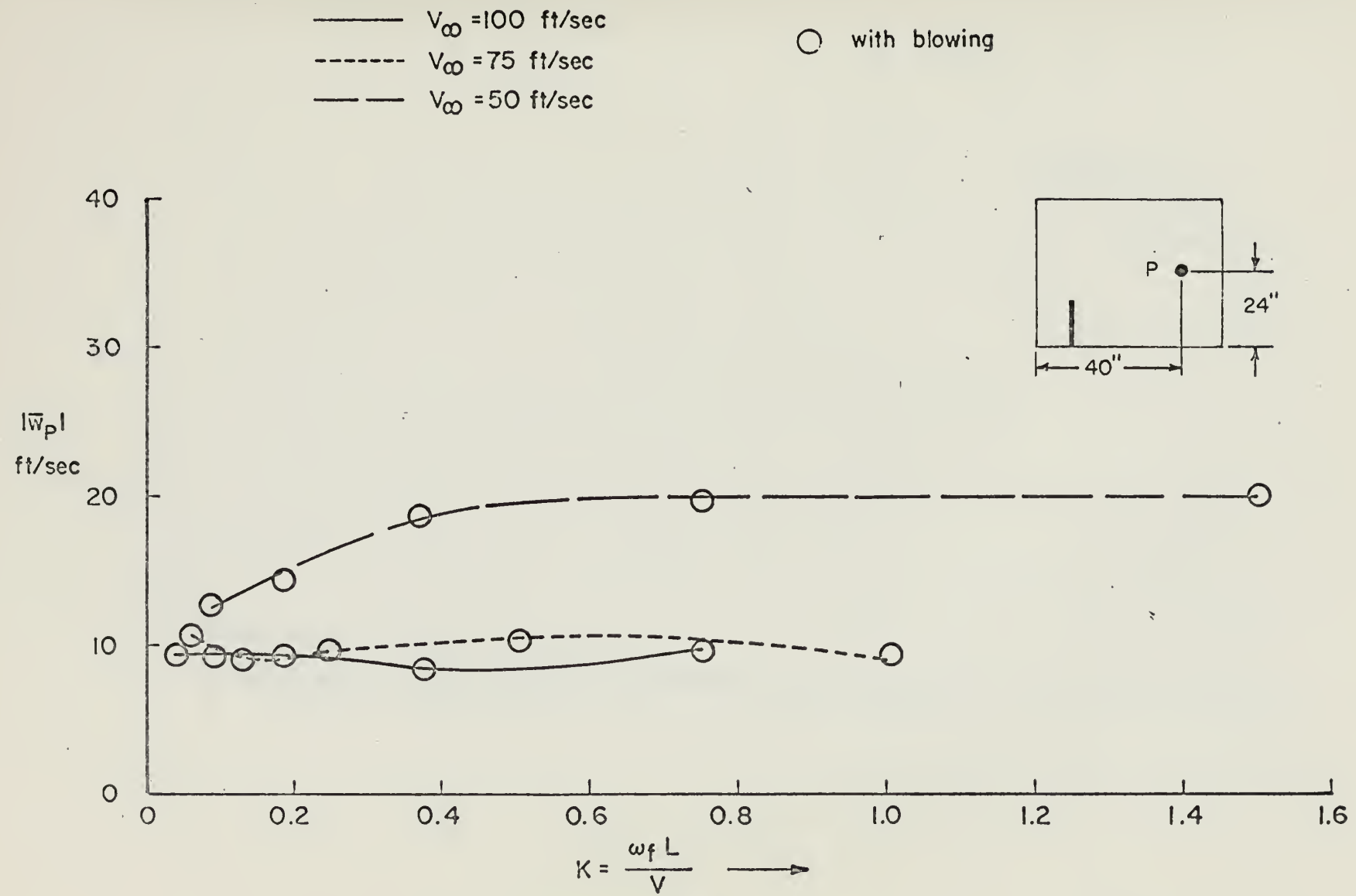

FIGURE 24.

STREAMWISE POSITION 2.0c, SECTIONAL POSITION 30" x 30"
$\delta_f = 0 \rightarrow +60°$ UNIDIRECTIONAL

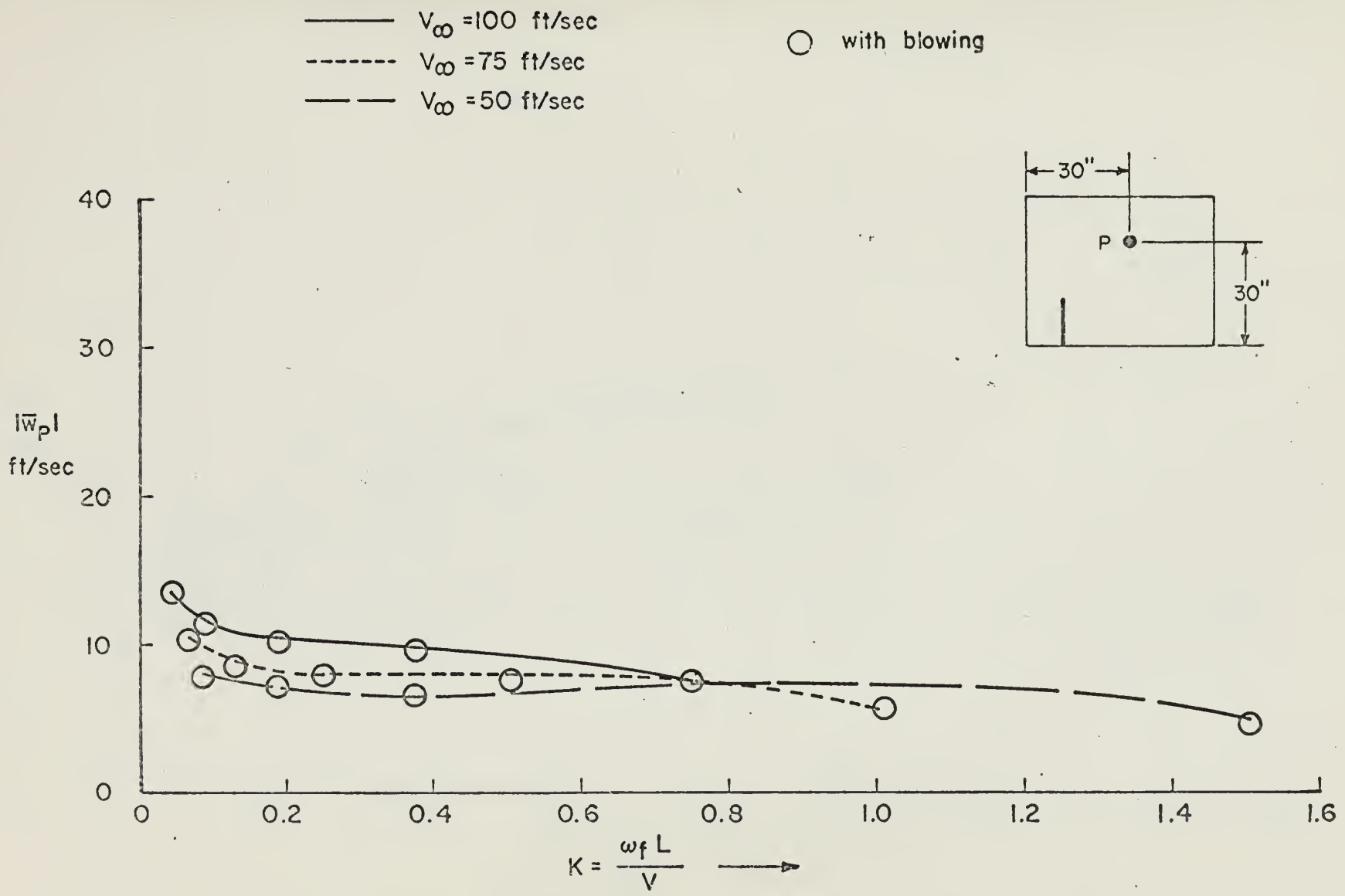

FIGURE 25.

STREAMWISE POSITION 6.0c, SECTIONAL POSITION 40" x 24"

δ_f = 0 → +60° UNIDIRECTIONAL

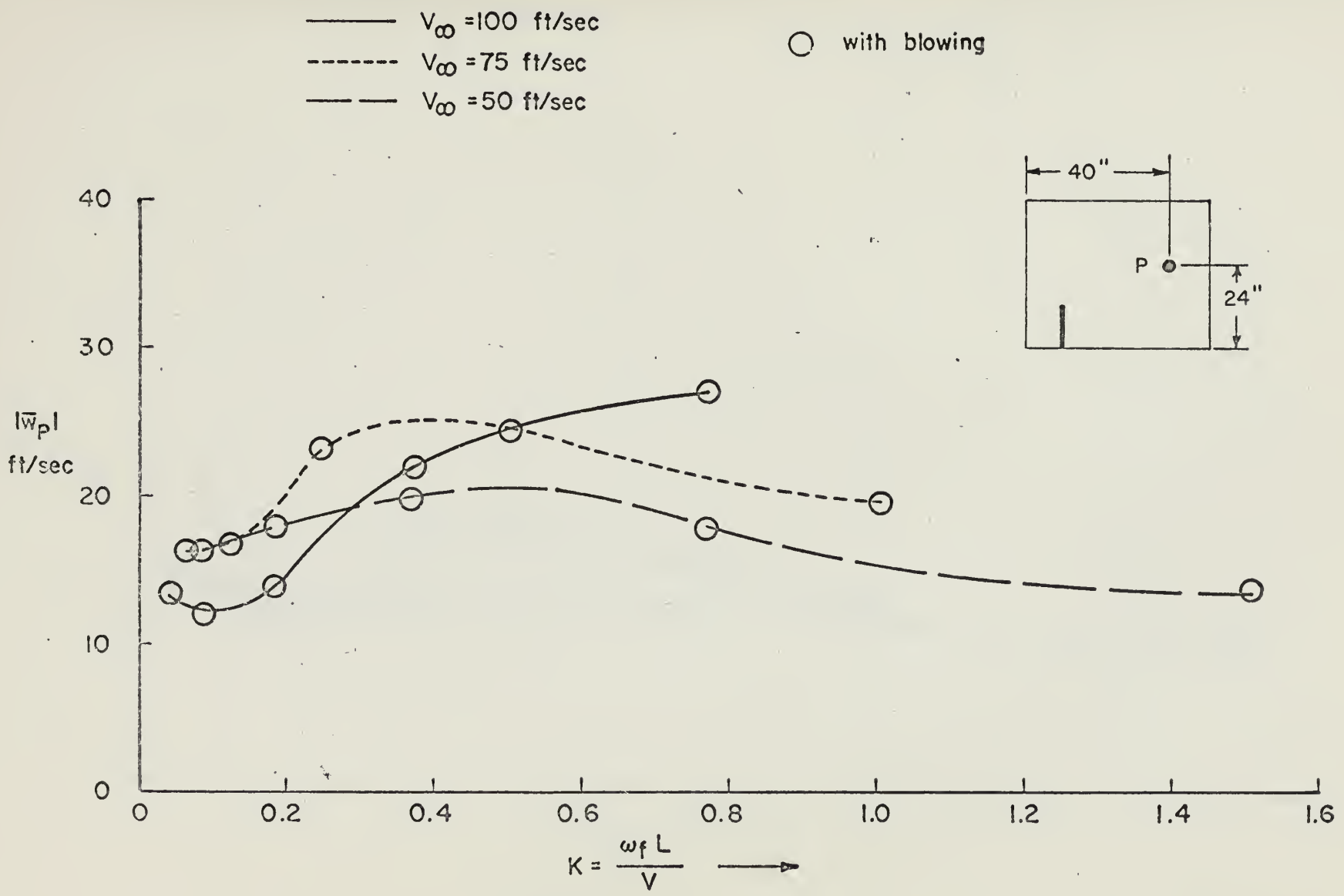

FIGURE 26.

STREAMWISE POSITION 6.0c, SECTIONAL POSITION 30" x 30"

$\delta_f = 0 \rightarrow +60°$ UNIDIRECTIONAL

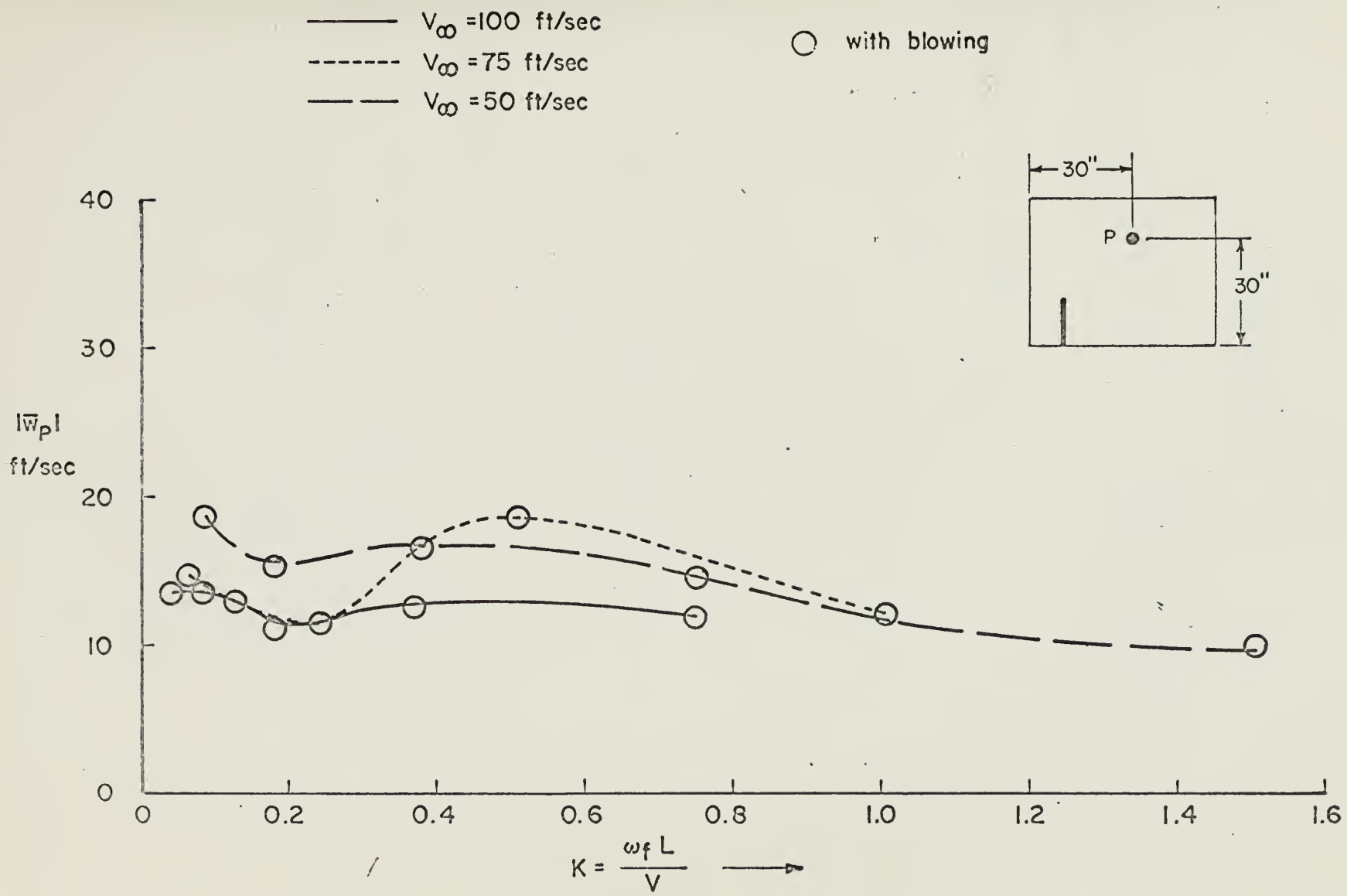

FIGURE 27.

NUMERICAL EXAMPLE

To compare the proposed theory of Appendix I with the actual experimental data, a typical set of parameters is chosen to be analyzed in the static regime.

The following are assumed:

(1) δ_{VANE} , such that

X = 6.0c downstream
Y = 30"
Z = 30"

(2) $\delta_F = 45°$, static in the positive direction

(3) V_∞ = 100 ft/sec with a choked

$$\therefore C_\mu = .84$$

From Table I:

(1) $C_L = 3.49$

(2) $\alpha_{i\infty} = 39.4°$

(3) Filament angle $(90° - \gamma) = 8.07°$

From the Biot-Savart Law

$$\omega_p = \frac{\Gamma(1+\cos\theta_A)}{4\pi h} \qquad (1)$$

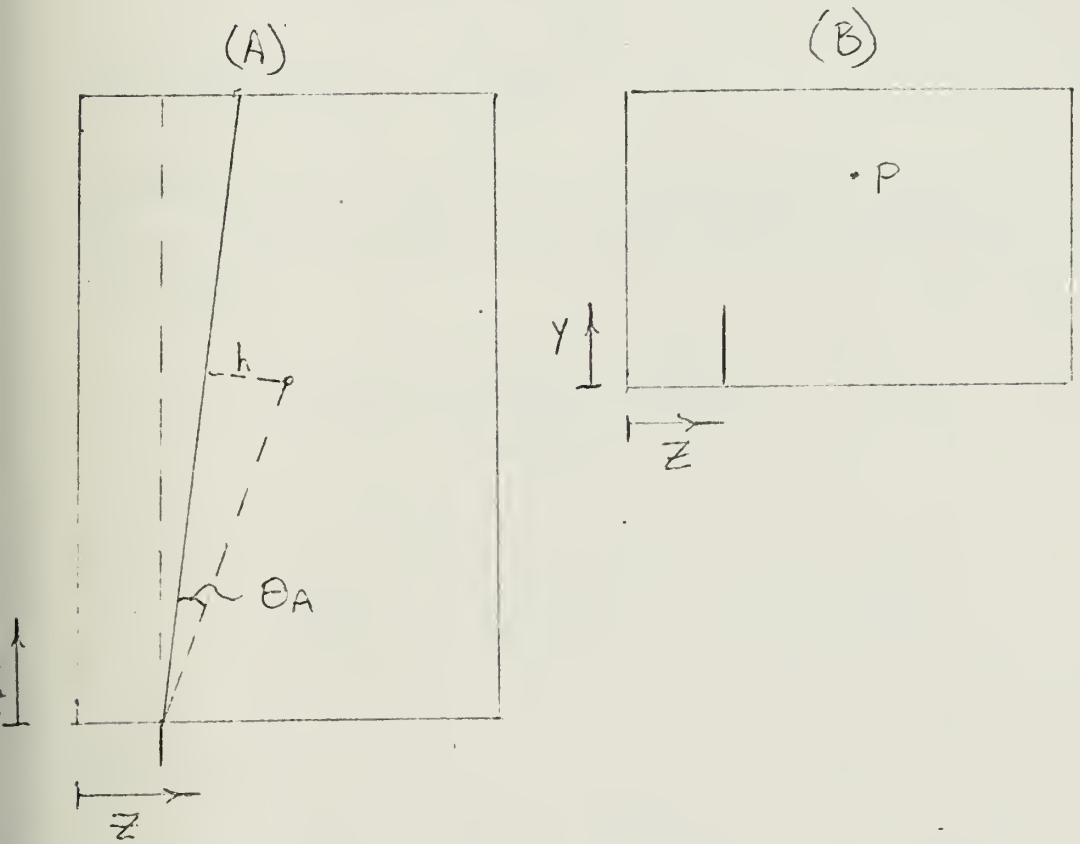

Figure 27 Downstream and Cross-Sectional Position of the Surveyed Datum Position.

The value of h when calculated from Figures A and B yields

$$h = 1.88 \text{ ft}$$

Also assuming this value of h, then

$$\sin \theta_A \approx \frac{h}{X} \tag{2}$$

Thus, the cos θ_A = .923

Substituting these values into (1) and assuming ω_∞ behind the flap along the jet sheet is constant, the induced velocity at point P is as follows:

$$\omega_P = \frac{\Gamma(1+\cos\theta_A)}{4\pi h} \tag{1}$$

or

$$\omega_P = \frac{C_L V_\infty \bar{c}}{8\pi} \left(\frac{1+\cos\theta_A}{h}\right) \tag{3}$$

and finally

$$\omega_P = 10.7 \text{ ft/sec}$$

This value represents a single vortex in free air. Now the experimental wind tunnel results can be seen in Figure 11, where the magnitude of induced velocity is

$$\omega_P = 10.3 \text{ ft/sec}$$

This correlation holds true within the range experimental error, for the great majority of surveyed points. This would lead one to believe that some parameters in the wind tunnel are possibly changing the wall effects and cancelling them. In Heyson's report (Reference 12) the affects of both open and closed wind tunnel tests sections are analyzed. The overall effects of these two are opposite in sign. It also makes reference to the possibility of cancelling any wall effects by introducing a slotted or porous tunnel section. Something in the tunnel, which is seemingly obscure at this time, is simulating this porous tunnel effect. Further study is necessary to discover the exact problems.

PROPOSED MODEL

The ideal gust disturbance would be a two-dimensional gust. It would seem reasonable that such a disturbance could be achieved by the use of superposition of vortices. This report proposes just such a system. Although previous research has generated different methods such as the Texas A&M pulsing jet for longitudinal gusts (Reference 27) and Giannini Controls Corporation oscillating wall jet gust simulator (Reference 6), the oscillating airfoil method used at NASA Langley (Reference 7) for generating a sinusoidally oscillating airstream seems best for a two-dimensional gust generator.

As Reference 7 indicates, many problems arose in generating high frequency gusts in an attempt to simulate high speed flight conditions. Appendix I demonstrates the inertial load problems that would indicate selection of a simple flap mechanism with blowing augmentation to produce similar, if not greater, gust magnitude capabilities.

Purely vertical or horizontal gusts can thus be generated by a superposition model. By oscillating the jet augmented-flaps either in phase or out of phase by 180°, these gusts can be produced. The vortex array should be patterned to generate as near a constant cross-sectional gust as possible. Thus, the gust seen by the model being tested will be nearly constant in a spanwise direction. As will be seen later, with the flaps oscillating out of phase by 180°, the most uniform gust will remain on the centerline while varying in magnitude and direction. However, when oscillated in phase, the filament movement will cause an unwanted shift in this most uniform gust position. The complex velocity potential is,

$$f(z) = -i\frac{\Gamma}{2\pi}\ln(z-a) \qquad (1)$$

for a single vortex, where

$$z = x + iy = r e^{i\theta} \tag{2}$$

a = location of the vortex in the plane.

Since $F(z) = -i \frac{\Gamma}{2\pi} \ln z$ at a = 0 (3)

by substitution of (2) into (3) we arrive at

$$F(z) = -i \frac{\Gamma}{2\pi} \ln (r e^{i\theta}) \tag{4}$$

or

$$F(z) = -i \frac{\Gamma}{2\pi} [\ln r + i\theta] \tag{5}$$

Now

$$F(z) = \phi + i\psi \tag{6}$$

By comparing (5) with (6) we see that

$$\phi + i\psi = \frac{\Gamma}{2\pi} \theta - i \frac{\Gamma}{2\pi} \ln r \tag{7}$$

Hence,

$$\phi = \frac{\Gamma}{2\pi} \theta \quad \text{AND} \quad \psi = -\frac{\Gamma}{2\pi} \ln r \tag{8}$$

Now

$$v_r = \frac{\partial \phi}{\partial r} = \frac{1}{r} \frac{\partial \psi}{\partial \theta} \tag{9}$$

and

$$v_\theta = \frac{1}{r} \frac{\partial \phi}{\partial \theta} = -\frac{\partial \psi}{\partial r} \tag{10}$$

Substituting we arrive at the radial velocity

$$v_r = 0 \tag{11}$$

and the tangential velocity

$$v_\theta = \frac{\Gamma}{2\pi r} \tag{12}$$

This equation illustrates the inverse proportionality between the radial distance and magnitude of the vortex-induced velocity.

Since the proposed system has an array of four vortices its velocity potential is assumed to be the following,

$$F(z) = -i\frac{\Gamma}{2\pi}\ln[z-(x_1+iy_1)] - i\frac{\Gamma}{2\pi}\ln[z-(x_1-iy_1)]$$
$$+i\frac{\Gamma}{2\pi}\ln[z+(x_1+iy_1)] + i\frac{\Gamma}{2\pi}\ln[z+(x_1-iy_1)] \tag{13}$$

The array would appear as in Figure 28.

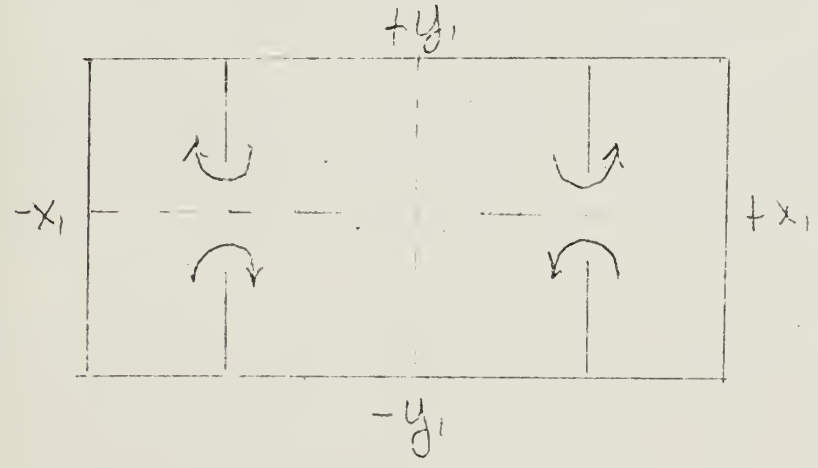

Figure 28

Such an array would produce a purely vertical oscillating gust. In producing a gust perpendicular to the flap chord, the dynamic movement of the vortex filaments at positions farther downstream will all be out of phase. However, even in a high frequency mode the lateral velocity components will all cancel in the central area of the tunnel. The position of the most uniform spanwise gust velocity will not move as a function flap deflection. This presents the best use of oscillating jet flap position, frequency and phase of oscillation, to date. If the jet flaps were mounted on the side walls of the tunnel a pure horizontal gust could be generated.

From the complex potential previously described can be derived the conjugate velocities in the x and y directions.

$$\frac{\partial F}{\partial z} = u - iv$$

Where u = velocity in x direction

v = velocity in y direction

By differentiating, the following exists

$$\frac{\partial F}{\partial z} = -i\frac{\Gamma}{2\pi}\left[\frac{(x-x_1)-i(y-y_1)}{(x-x_1)^2+(y-y_1)^2}\right] - i\frac{\Gamma}{2\pi}\left[\frac{(x-x_1)-i(y+y_1)}{(x-x)^2+(y+y_1)^2}\right]$$

$$+ i\frac{\Gamma}{2\pi}\left[\frac{(x+x_1)-i(y+y_1)}{(x+x_1)^2+(y+y_1)^2}\right] + i\frac{\Gamma}{2\pi}\left[\frac{(x+x_1)-i(y-y_1)}{(x+x_1)^2+(y-y_1)^2}\right] \quad (14)$$

In separating the real and imaginary parts such that

$$u = \frac{\Gamma}{2\pi}\left\{ -\frac{(y-y_1)}{(x-x_1)^2+(y-y_1)^2} - \frac{(y+y_1)}{(x-x_1)^2+(y+y_1)^2} + \frac{(y+y_1)}{(x+x_1)^2+(y+y_1)^2} + \frac{(y-y_1)}{(x+x_1)^2+(y-y_1)^2}\right\} \quad (15)$$

$$-v = \frac{\Gamma}{2\pi}\left\{ -\frac{(x-x_1)}{(x-x_1)^2+(y-y_1)^2} - \frac{(x-x_1)}{(x-x_1)^2+(y+y_1)^2} + \frac{(x+x_1)}{(x+x_1)^2+(y+y_1)^2} + \frac{x+x_1}{(x+x_1)^2+(y-y_1)^2}\right\} \quad (16)$$

Using these equations, the theoretical magnitude and direction of the induced velocity can be shown. The movement of the vortex filaments is involved in this analysis. The equivalent vortex positions at x = 6.0c were assumed. This provides a means of comparison for this case with the actual experimental value.

The dimensions of Figure 28 will be assumed since the experimental data will be of that configuration. With the gust generation devices mounted to the floor and roof of the tunnel, the flaps are synchronized 180° out of phase with the bordering flaps as shown in Figure 28. This will provide as even a vertical gust as possible. Figure 29 illustrates theoretically the magnitude and distortion of w which must be tolerated when testing under such a configuration. This distortion, for a 2-foot span model, is approximately 40% from mid-span to tip.

Figure 30, is the comparable experimental result due to superposition. Here again, spanwise distortion, in vertical w is important. It is approximately 40% over the same 2-foot span model.

Creating lateral gusts would seem at first, easily accomplished by changing the phase of the flap oscillations. Figure 32, is an illustration of this configuration. The generators in the array are all of the same phase. However, the filaments all moving in phase back and forth are ignored.

In Figure 32, experimental superposition shows that the center of the array of filaments as appears in Figure 31, will move a certain distance to the left as the filament particles move downstream. Hence, at maximum static deflection, at $x = 6.0c$ downstream, a very erratic pattern appears in the centerline position. This is intolerable when a relatively constant cross-sectional gust is required. In the production of these gusts, both lateral and vertical, combinations of parameters could possibly be found and programmed to induce a uniform gust flow over the entire span of the model. In addition, a half span model could be mounted to the tunnel floor with the previous vertical turbulence, thereby simulating a lateral gust. This,however, is left for future work.

THEORETICAL

DISPLACED FILAMENTS

C_L = 2.33

V_∞ = 100 ft/sec

δ_f = 30° STATIC

X = 6.0c

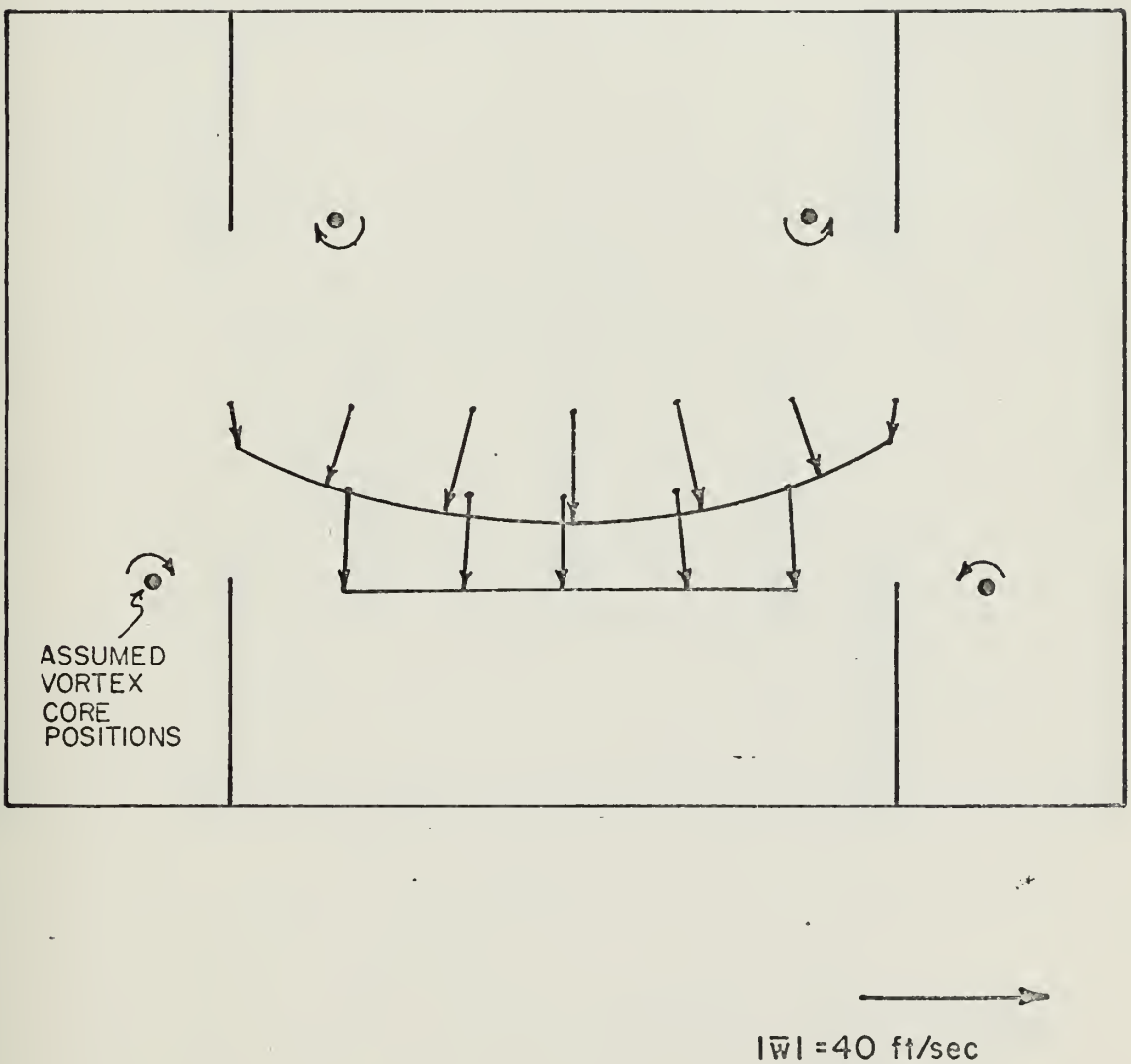

FIGURE 29. CENTER LINE GUST DISTRIBUTION ACROSS THE SECTION.

EXPERIMENTAL

DISPLACED FILAMENTS

$C_L = 2.33$

$V_\infty = 100$ ft/sec

$\delta_f = 30°$ STATIC

$X = 6.0c$

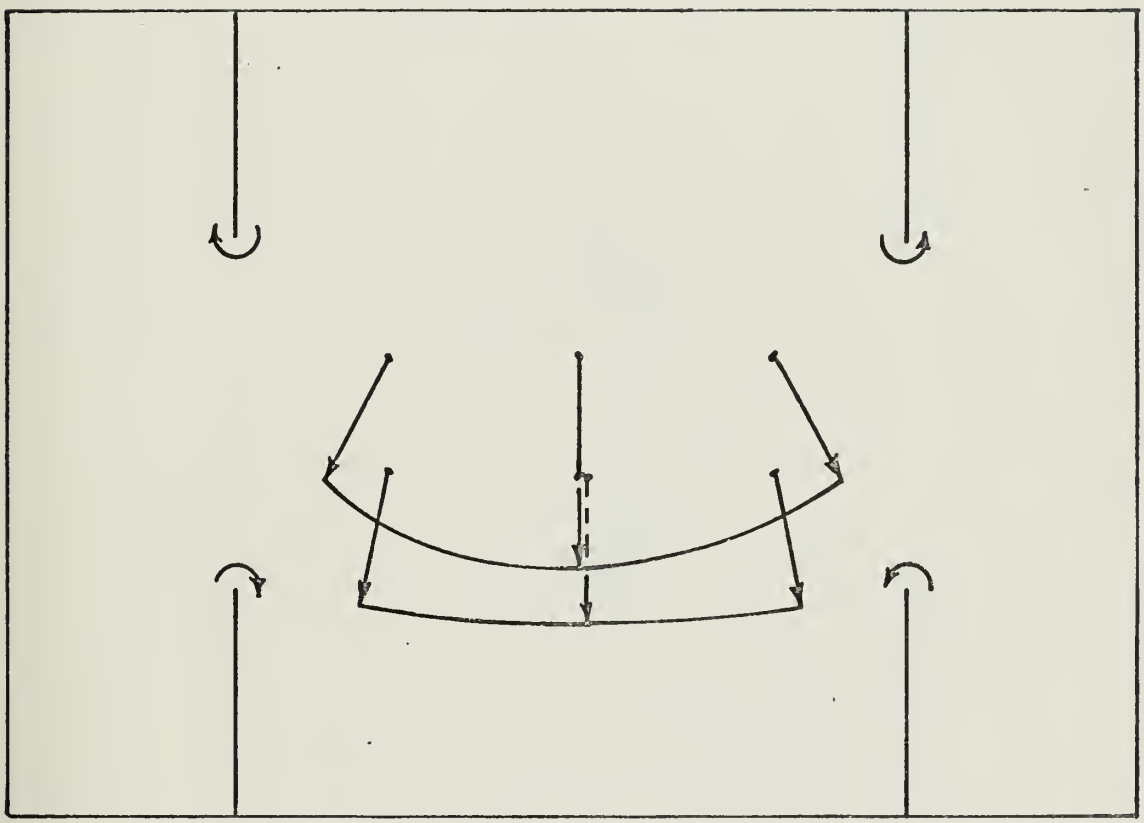

$|\bar{w}| = 40$ ft/sec

FIGURE 30.

THEORETICAL

C_L =2.33

V_∞ =100 ft/sec

δ_f = ± 30° STATIC

X = 6.0c

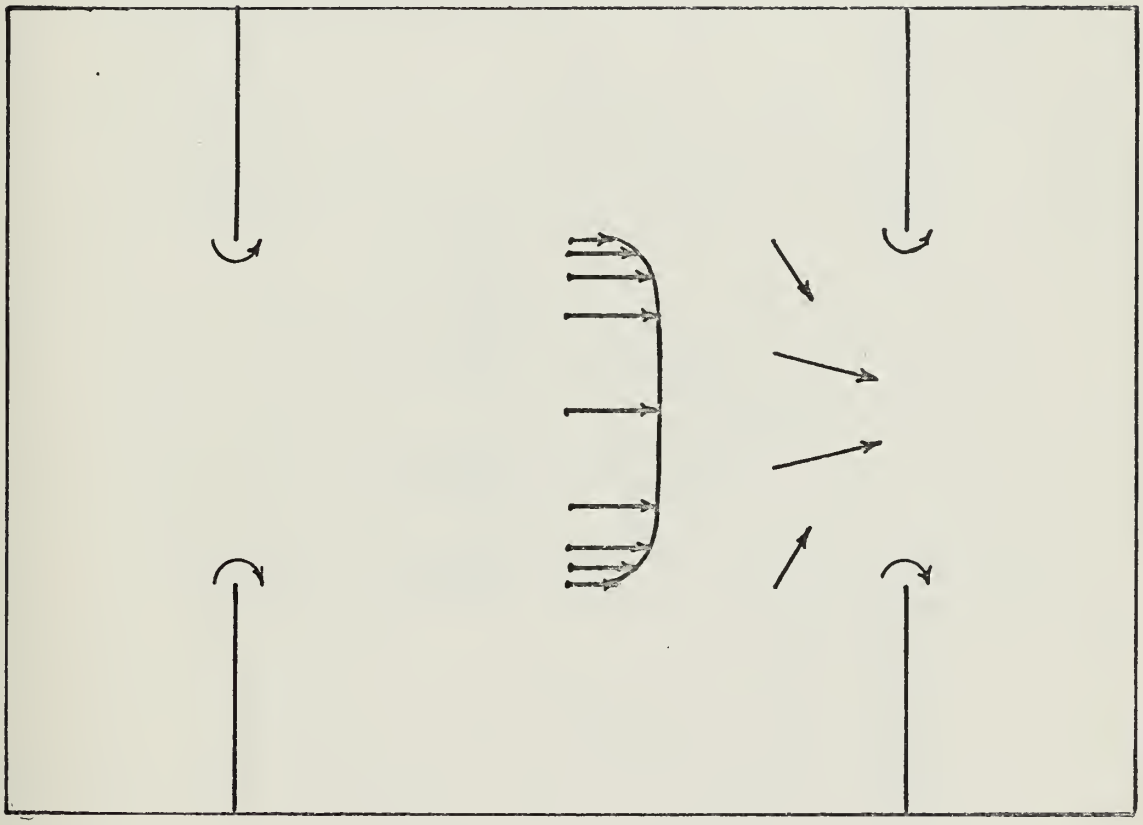

$|\bar{w}|$ =40 ft/sec

FIGURE 31.

EXPERIMENTAL

$C_L = 2.33$

$V_\infty = 100$ ft/sec

$\delta_f = \pm 30°$ STATIC

$X = 6.0c$

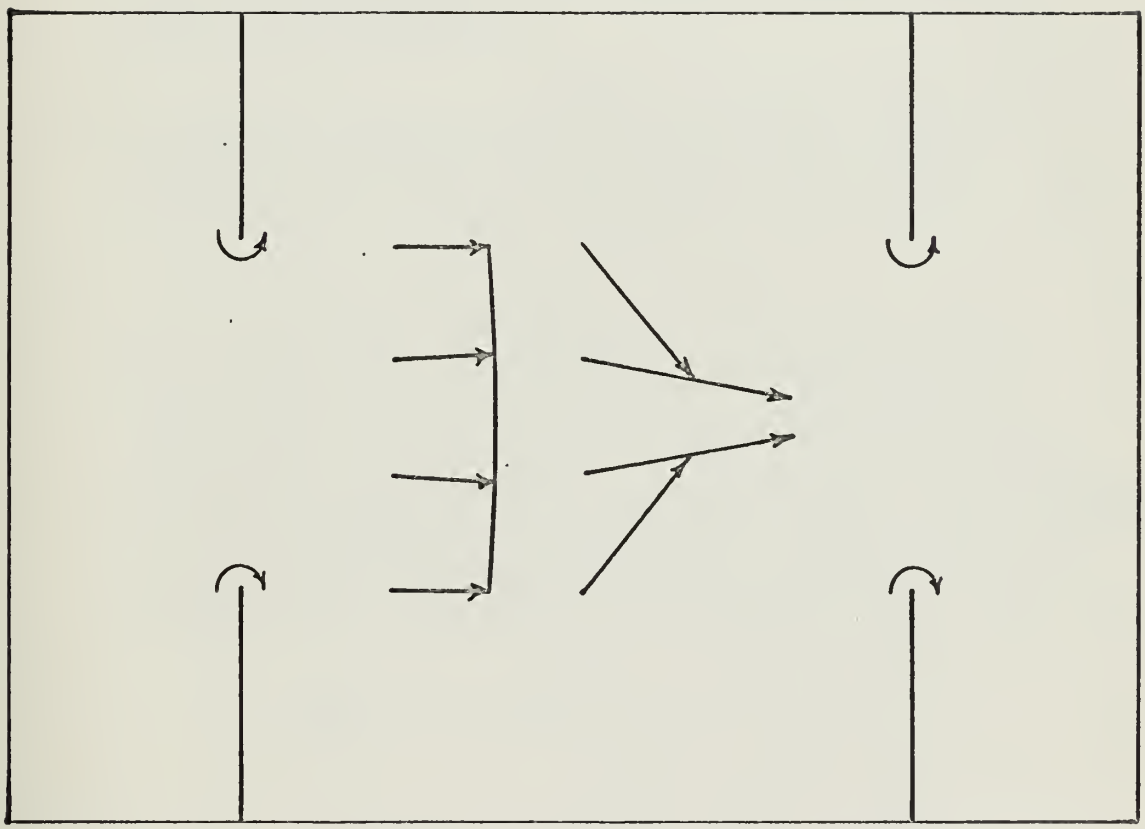

$|\bar{w}| = 20$ ft/sec

FIGURE 32.

CONCLUSIONS

There are some basic conclusions that can be drawn from the discussion and analysis of the experimental data and theoretical calculations as presented previously.

1) Since only the flap and not the entire airfoil is being oscillated, the inertial loads at high frequencies can be decreased considerably.

2) By properly programming the vortex generators, the array of airfoils can produce a uniform cross-sectional gust in the vertical or lateral directions.

3) In the dynamic case the flap was oscillated both bi-directionally and uni-directionally. Theoretically, the former should produce an oscillation in induced velocity symmetrically centered about zero. At very high frequencies the dynamic components tend to cancel themselves. Experimentally, this was substantiated. Theoretically, the latter should be centered about a finite value such that when $\omega_f \doteq \infty$,

$$\omega_p \doteq \tfrac{1}{2}\omega_{p_{STATIC}}$$

However, the experimental results in this series of tests did not fully agree. The experimental dynamic peak to peak value did not decrease symmetrically about the constant value. However, frequencies corresponding to Strouhal Numbers in excess of 1.5 must be observed and more data taken to substantiate this deviation from the theory.

4) Vortex filament movement is a factor in determining the value of the constant value of ω_p when $\omega_f \Rightarrow \infty$ With the present apparatus, the steady state value for the bi-directional oscillation will be displaced from the zero position. This, however, does not influence the fact that the time varying oscillation is cancelled as if the core position did not vary. Core movement in the uni-directional oscillation again simply biases the steady state value, but again, had no effect on the dynamic cancellation. The experimental data confirms these theoretical observations. Hence, in the production of a very high frequency, sinusoidal, time varying gusts, the vortex generator is of little use. However, the apparatus can be operable for a low to medium frequency band-width while taking into account the rapid magnitude decay at the upper band frequencies.

5) Attempts to account for the presence of the tunnel wall by image vortex systems indicate that little or no wall effects are necessarily accounted for in the calculation of ω_p. In the numerical example this fact was shown for an average test point where it can be seen that the test section actually simulates a porous section, and, theoretically, needs little or no tunnel wall correction. Further investigation is needed to discover the reasons for this trend.

REFERENCES

1. A. J. Alexander, J. Williams: "Wind-Tunnel Experiments on a Rectangular-Wing Jet-Flap Model of Aspect-Ratio", ARC 22,947, June 1961.

2. A. Anscombe, J. Williams: "Some Comments on High-Lift Testing in Wind-Tunnels With Particular Reference to Jet-Blowing Models", Advisory Group for Aeronautical Research and Development, Report No. 63, August 1956.

3. Dynasciences Corporation: Proposal for the Turbulence Generating System for Installation in the 16-Foot Transonic Wind-Tunnel, Report No. DCP-215, May 26, 1966. (Unpublished)

4. J. H. Dwinnell: Principles of Aerodynamics , McGraw-Hill Book Co.,Inc. New York, Toronto, London, 1949.

5. J. C. Erickson: "A Theory for Unsteady Motions of Jet-Flapped Thin Airfoils", Cornell University Graduate School of Aerospace Engineering, September 1962.

6. Giannini Corporation: A Feasibility Study of a Turbulence Generation System, Proposal No. ARD-01-062, May 25, 1966. (Unpublished)

7. J. Gilman, R. M. Bennett: "A Wind-Tunnel Technique for Measuring Frequency-Response Functions for Gust Load Analyses", Journal of Aircraft, Vol. 3, No. 6, Nov-Dec 1966.

8. D. Graham: "Automatic Control and the Lateral Oscillatory Motion", Cornell Aero Lab Report No. TB514-F-1, April 1949.

9. J. E. Hackett, M. R. Evans: "Vortex Wakes Behind High-Lift Wings", AIAA Report No. 69-740.

10. D. C. Hazen, R. F. Lehnert: "Smoke Flow Studies Conducted at Princeton University", Princeton Report No. 290.

11. D. C. Hazen, F. C. Karins: "A Preliminary Study of the Rate of Growth and Decay of Blowing-Jet-Induced Circulation on Two-Dimensional Profiles", U. S. Army Ordnance, Frankford Arsenal, Report No. 632, December 1962.

12. H. H. Heyson: "Linearized Theory of Wind-Tunnel Jet Boundary Corrections and Ground Effect for VTOL-STOL Aircraft", NASA TR R-124, 1962.

13. H. H. Heyson: "Wings, Wakes, Wind-Tunnels, and Wall Effects", Langley Research Center Working Paper (LWP No. 341), Dec. 15, 1966.

14. M. P. Knowlton: "A Theoretical Investigation on the Determination of Lift Coefficients in Two-Dimensional Smoke-Tunnels", Princeton Report No. 289, March 1955.

15. G. K. Korbacher: "Performance, Operation and Use of Low Aspect Ratio Jet-Flapped Wings", UTIAS No. 97, May, 1964.

16. P. B. S. Lisserman: "Aerodynamic Characteristics of Jet-Flapped Airfoils in Ground Effect", VRC Report No. 18, December 31, 1964.

17. E. C. Maskell, S. B. Gates: "Preliminary Analysis for a Jet-Flap System in Two-Dimensional Inviscid Flow", C.P. No. 359, ARC TR No. 17,949, 1957, Ministry of Supply.

18. E. C. Maskell, D. A. Spence: " A Theory of the Jet Flap in Three Dimensions", Royal Society of London Proceedings, Vol. A 251, June 9, 1959, PD 407-425.

19. E. C. Maskell: "The Interference on a Three-Dimensional Jet-Flap Wing in a Closed Wind Tunnel", ARC R&M No. 3219, 1961, Ministry of Aviation.

20. B. W. McCormick, Jr.: Aerodynamics of V/STOL Flight , Academic Press, New York, London, 1967.

21. B. W. McCormick, J. L. Tangler, H. G. Sherrieb: "Structure of Trailing Vortices", Journal of Aircraft, Vol. 5, No.3, May-June, 1968.

22. C. F. Reid, C. G. Wrestler: "An Investigation of a Device to Oscillate a Wind Tunnel Airstream", NASA TND-739, April 1961.

23. A. J. Ross: "The Theoretical Evaluation of the Downwash Behind Jet-Flapped Wings", ARC R&M No. 3719, 1961, Ministry of Aviation.

24. W. R. Sears: "Some Aspects of Non-Stationary Airfoil Theory and its Practical Application", Journal of the Aeronautical Sciences, Vol. 8, No. 3, January, 1941.

25. D. A. Spence: "The Lift Coefficient of a Thin, Jet-Flapped Wing", Royal Society of London Proceedings, Vol. A 238, 1957, pp. 46-48.

26. J. R. Spretter, A. H. Sacks: "The Rolling Up of the Trailing Vortex Sheet and its Effect on the Downwash Behind Wings", Condensed from a paper at Aerodynamics Session, Eighteenth Annual Meeting, I.A.S., New York, January 23-26, 1950.

27. R. E. Thomas, B. T. Morland: "Gust Simulation in a Wind-Tunnel", Space Technology Report 67-52, July 1967, Texas A&M University.

28. R. D. Vogler, T. R. Turner: "Wind-Tunnel Investigation at Low Speeds to Determine Flow-Field Characteristics and Ground Influence on a Model With Jet-Augmented Flaps", NACA TN 4116, September 1957.

29. J. W. Westmore and J. P. Reeder: "Aircraft Vortex Wakes in Relation to Terminal Operation", NASA TND 1777, April 1963.

30. J. Williams, S. F. J. Butler, M. N. Wood: "The Aerodynamics of the Jet-Flap", ARC R&M No. 3304, 1963, Ministry of Aviation.

31. Sq.Ldr. L. C. Woods: "Some Contributions to Jet-Flap Theory and to the Theory of Source-Flow From Aerofoils", C. P. No. 388, ARC TR No. (16,452; 17,563; 18,980), 1958, Ministry of Supply.

32. Y. A. Yoler: "A Lifting Line Theory of the Jet Flapped Wing", Boeing Scientific Research Laboratories, DI-82-0042, January 1960, Flight Sciences Laboratory Report No. 24.

APPENDIX I

JET FLAP ANALYSIS

Important aerodynamic parameters of the jet flap were fixed due to the problem itself. First, an airfoil of a symmetrical cross section was desirable to accommodate the changes in circulation throughout a $-\delta_F$ to $+\delta_F$ range which would in turn produce symmetrical gusts. The NACA 0012 section was chosen for convenience because templates with a nine inch chord were already in existence, thus simplifying construction.

Once the chord was fixed, the flap size had to be determined. Preliminary two dimensional work, described in Appendix II, was done in the Princeton 2" X 36" smoke tunnel to arrive at a possible C_L for the 3-D model. Knowlton, in Reference 14, discussed methods of determining ΔC_L for a 2-D airfoil section by measuring the streamline deflection of an upstream position.

Various tunnel dynamic pressures, flap deflections, and C_μ's were observed with varying flap chord ratio. The tests were conducted at 30-50 ft/sec. Thus, the data were for the range of Reynold's Numbers $3\times10^5 < R_e < 4.5\times10^5$ and, hence, this regime corresponds very well with the 3-D model.

VORTEX FILAMENT

From 3-D elementary airfoil theory without blowing argumentation,

$$L = C_L q S \tag{I-1}$$

or substituting for a constant chord model,

$$L = C_L \left(\tfrac{1}{2}\rho V_\infty^2\right) b\bar{c} \tag{I-1a}$$

From the simple circulation theory of lift and the Kutta Joukowski theorem,

$$L/b = \rho V_\infty \Gamma \tag{I-2}$$

such that lift per unit span is equal to the product of air density, free stream velocity, and circulation.

By equating (1a) and (2) we arrive at

$$C_L \left(\tfrac{1}{2}\rho V_\infty^2\right) b\bar{c} = b\rho V_\infty \Gamma \tag{I-3}$$

Eliminating terms by dividing through we arrive at a value for circulation as a function of C_L, V_∞, and $\bar{c}$.
Hence, from (3)

$$\Gamma = \frac{C_L V_\infty \bar{c}}{2} \tag{I-4}$$

Since

$$C_L = f(\alpha, \delta_F) \quad \text{at } C_\mu = 0 \tag{I-5}$$

in that C_L is a function of angle of attack and flap deflection angle with no blowing augmentation, we realize that when the angle of attack is zero then lift coefficient depends only on flap deflection or

$$C_L = f(\delta_F) \qquad \text{at } \alpha = 0 \tag{I-5a}$$

For the model used in these experiments, the flapchord is nearly half the total chord. Let us assume that the change in angle of zero lift is approximated by half the δ_F, or the change in angle of zero lift is,

$$\alpha'_e \doteq \frac{\delta_F}{2} \qquad \text{for } \alpha = 0 \tag{I-6}$$

Since, for any non-augmented airfoil, $C_{L_{\alpha_e}}$ is a constant,

then,

$$\Gamma = \frac{C_{L_{\alpha_F}} \delta_F V_\infty \bar{c}}{2} \qquad \text{(I-7)}$$

Thus, for an unaugmented, plain-flapped airfoil at $\alpha = 0$

$$\Gamma \sim \delta_F, V_\infty \qquad \text{(I-8)}$$

until the flap deflection reaches a value of twice the stalling angle of attack, or when

$$\delta_F \geq 2\alpha_{STALL} \qquad \text{(I-8a)}$$

The average induced angle of attack, with a fully attached flow is dependent only on δ_F. Thus,

$$\frac{w_{i\infty}}{V_\infty} \sim \delta_F \qquad \text{(I-9)}$$

In the case of the blown flap augmentation (Reference 19), the lift coefficient is a function of both δ_F and V_∞, where

$$C_L = g(\delta_F, C_\mu) \qquad \text{(I-10)}$$

due to the introduction of C_μ into the analytic determination of C_L in Reference 20.

Hence, circulation for the blown flap is proportional to the product of V_∞ and C_L, with the latter a function of both δ_F and C_μ. Thus, for this case

$$\Gamma = g(\delta_F, C_\mu) \cdot V_\infty \qquad \text{(I-11)}$$

Now by definition

$$C_\mu = \frac{\dot{m}_j V_j}{q S} \qquad \text{(I-12)}$$

in that the product of the mass flow rate of jet air and its local slot velocity is nondimensionalized by the mass momentum over the wing. Thus, C_μ is in fact, a lift coefficient in addition to the C_L or circulation lift coefficient. V_j is constant throughout the present experiments; hence, C_μ is dependent only on V_∞.

As in Reference 25, the increment in lift is by reaction to the vertical component of the jet momentum and the increases in wing circulation lift from the introduction of asymmetry to the airfoil by the jet and the energy injected into the boundary layer to retard separation. Both increases in lift will be assumed to add a component of to the trailing vortex shed from the tip of the 3-D wing.

JET SHEET

From thin airfoil theory, the jet must first be considered in inviscid flow. Figure 33 gives an illustration of the problem.

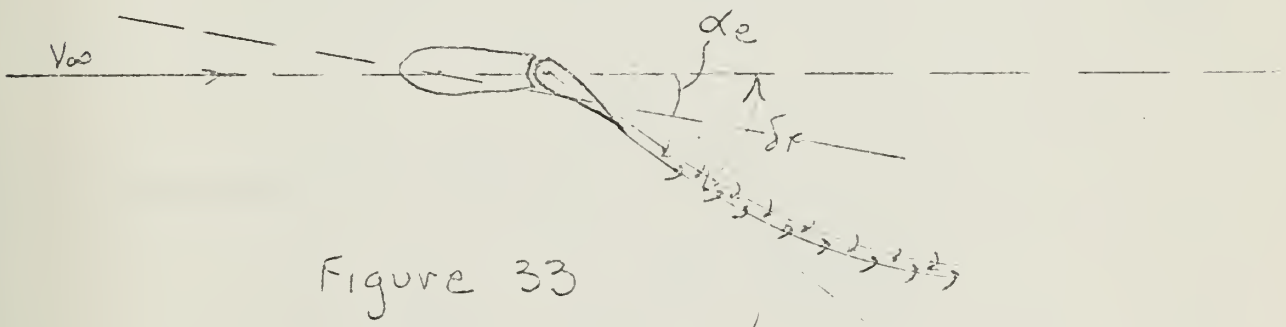

Figure 33

The high velocity air jet is issued from the leading edge of the flap, leaving the flap surface at the δ_F angle. Both the flow inside the jet and surrounding the jet are irrotational. Total head pressure is greater in the jet than in the free stream. Figure 34 illustrates a segment of the jet downstream.

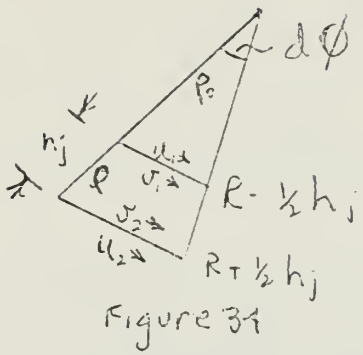

Figure 34

Since the flow has a discontinuous velocity gradient, we can consider the jet surrounded by two opposite signed vortices each proportional to the strength of the local flow external to the jet.

Again from Reference 25, the pressure at the boundaries is continuous, i.e. total head is constant across the boundaries. From Bernoulli's equations,

$$P_1 + \tfrac{1}{2}\rho_0 u_1^2 = P_2 + \tfrac{1}{2}\rho_0 u_2^2 \qquad \text{(I-13)}$$

$$P_1 + \tfrac{1}{2}\rho v_1^2 = P_2 + \tfrac{1}{2}\rho v_2^2 \qquad \text{(I-14)}$$

Since irrotational flow is concerned

$$v_1\left(R - \tfrac{1}{2}h_j\right) = v_2\left(R + \tfrac{1}{2}h_j\right) \qquad \text{(I-15)}$$

By involving mean velocities in the discussion and rearranging algebraically we can arrive at the conclusion that

$$P_1 - P_2 = -\frac{\rho V_j^2 h_j}{R} \qquad \text{(I-16)}$$

where

$$V_j = \tfrac{1}{2}(U_1 + U_2) . \qquad \text{(I-17)}$$

Again this assumes that the jet extends to infinity and thrust is totally recovered.

The pressure differential described in(I-16)is due to the difference in the elemental strength of the upper and lower boundary vortices. By integrating the two into one vortex by assuming

$$h_j \doteq 0 \qquad \text{(I-18)}$$

we will arrive at a vortex sheet with a strength equal to the difference in strength of the previous two, located at the centerline of the jet. Thus,

$$\gamma_j\, ds = \gamma_1\, ds_1 + \gamma_2\, ds_2 \qquad \text{(I-19)}$$

Following Spence's progression in theory, the strength of the vortex jet sheet per unit span is

$$\gamma_j \simeq \left(\frac{V_\infty}{R}\right)\left(\frac{\dot{m}_j}{\rho V_\infty^2 \bar{c}} - h_j\right) \qquad \text{(I-20)}$$

But since $h_j \to 0$ from(I-18)and $\dot{m}_j$ must remain constant, then V_j must approach ∞ as

$$\gamma_j \simeq \left(\frac{V_\infty}{R}\right)\left(\frac{\dot{m}_j}{\rho_0 V_\infty^2 \bar{c}}\right) \qquad \text{(I-21)}$$

and the pressure differential per unit span can be assumed from (I-16) to be

$$P_2 - P_1 = \frac{\dot{m} j}{R} \qquad \text{(I-22)}$$

Now the total lift is the sum of circulation lift and momentum lift

$$L = \rho V_\infty \left[\Gamma_c + \Gamma_j \right] \qquad \text{(I-23)}$$

Where Γ_c is the corrected circulation lift for the blowing augmented flap, and

$$\Gamma_j = \int_1^\infty \gamma_j \, ds \qquad \text{(I-24)}$$

Since

$$\gamma_j = \frac{V_\infty}{2R} C_\mu \qquad \text{(I-25)}$$

Then the following thin airfoil approximations are made for small δ_F and α.

1) the vortex distribution representing the jet is located from $1 < X < \infty$ along the real axis;

2) $\gamma_j(x) = -\frac{1}{2} V_\infty C_\mu y''(x)$
where y (x) is deflection of the jet below the horizontal line;

3) and $\gamma_c(x) = V_\infty f(x)$ for $0 < X < 1$
as in Figure 35

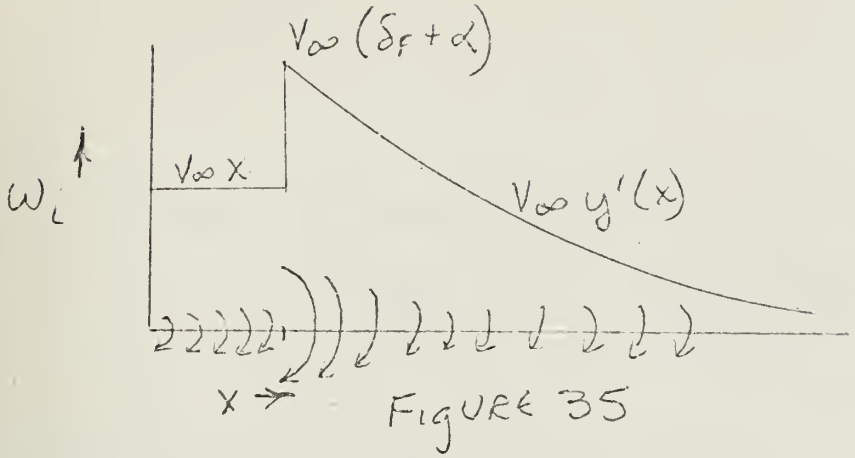

FIGURE 35

where

$$\gamma(x) = V_\infty f(x) - \tfrac{1}{2} V_\infty C_\mu y''(x) \qquad \text{(I-25a)}$$

By following through with integration of(I-25a), taking the function to its limits, and solving for C_L, a total of the force components will give values of

$$\frac{\partial C_L}{\partial \delta_f} = 3.54 C_\mu^{1/2} + .325 C_\mu + .156 C_\mu^{3/2} \qquad \text{(I-26)}$$

and

$$\frac{\partial C_L}{\partial \alpha} = 2\pi + 1.152 C_\mu^{1/2} + 1.106 C_\mu + .051 C_\mu^{3/2} \qquad \text{(I-27)}$$

With further refinements Spence's equations are displayed in McCormick (Reference 20) as follows:

$$\frac{\partial C_L}{\partial \delta_f} = \left[4\pi C_\mu (1 + .151 C_\mu^{1/2} + .139 C_\mu\right]^{1/2} \qquad \text{(I-28)}$$

and

$$\frac{\partial C_L}{\partial \alpha} = \left[2\pi (1 + .15 C_\mu^{1/2} + .219 C_\mu)\right] \qquad \text{(I-29)}$$

These equations hold true for $C_t/c = 0$, however, the graphical plot in Reference 20 was used for actual interpolation between the above two equations.

For total C_L the following is true:

$$C_L = \left(\frac{\partial C_L}{\partial \delta_F}\right)\delta_F + \left(\frac{\partial C_L}{\partial \alpha}\right)\alpha \quad . \tag{I-30}$$

Since the present flap chord is in the region of

$$0 < c_F/c < 1.0$$

an interpolation was necessary, and a numerical C_L was obtained. Table I lists the numerical values for all experimental regimes calculated using McCormick's interpolation. Also the actual value of α_i is listed for varying values of C_μ and δ_F. Numerically, here it can be seen that C_μ (or V_∞) has little effect on the average downwash angle at infinity; but that it is nearly linearly dependent on δ_F.

Thus $$\frac{\partial \alpha_{i\infty}}{\partial V_\infty} \doteq 0 \tag{I-31}$$

while $$\frac{\partial \alpha_{i\infty}}{\partial \delta_F} \neq 0 \tag{I-32}$$

with a fairly constant positive value. This in turn shows that the position of the vortex filament downstream, as shown in Figure 36, is not a function of V_∞ but only of δ_F. Also this leads to the conclusion that h and $\cos \theta_A$ are independent of V_∞.

For analytic purposes assume the value of $\frac{\partial C_L}{\partial \alpha}$ given in (29) to be correct.

Thus,

$$C_L = \alpha_e \left(\frac{\partial C_l}{\partial \alpha}\right) \tag{I-33}$$

where $\alpha'_e \cong \frac{\delta_F}{2}$ from (6)

TABLE I

V_∞ (ft/sec) →	50	75	100	
C_μ →	3.33	1.50	.84	
δ_F				
30°	3.4	2.62	2.33	C_L
45°	5.1	3.8	3.49	
60°	6.8	5.07	4.66	
30°	25.7	26.2	26.3	$\alpha_{i\infty}$
45°	38.6	37.9	39.4	
60°	51.5	50.6	52.6	
30°	5.3	5.37	5.4	$.41\,\alpha_i$
45°	7.9	7.8	8.1	
60°	10.6	10.4	10.8	

ASSUMPTIONS:

(1) $C_L = F\left[\left(\frac{\partial C_L}{\partial \delta_F}\right)\frac{\delta_F}{57.3}\left(1+t/c\right)\right] - t/c\, C_\mu \frac{\delta_F}{57.3}$

(2) $\alpha_{i\infty} = \frac{2C_L}{\pi AR + 2C_\mu}$

(3) $.41\,\alpha_i = \frac{.41\,C_L}{\pi AR + 2C_\mu}$

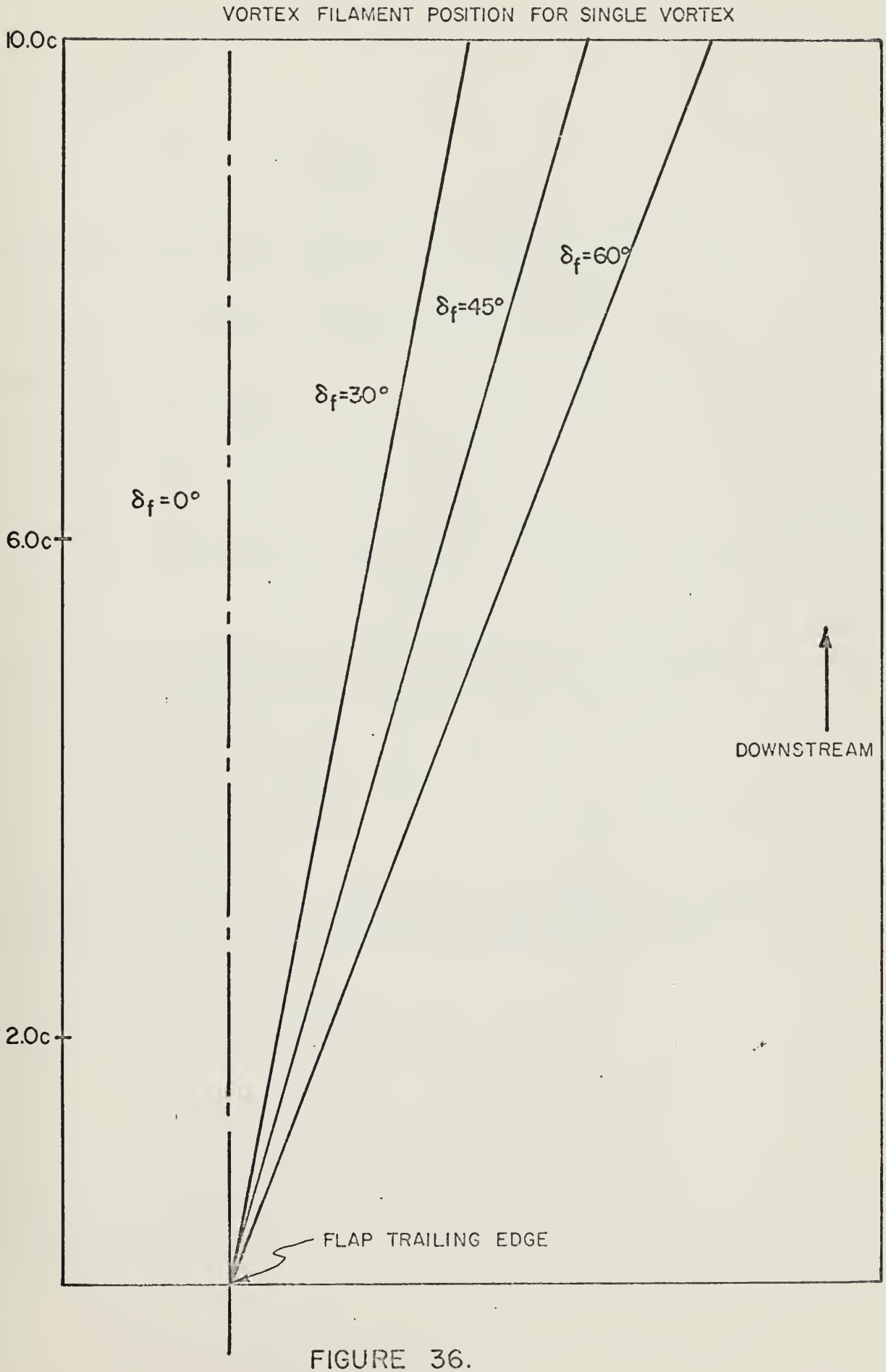
VORTEX FILAMENT POSITION FOR SINGLE VORTEX
10.0c
6.0c
2.0c
$\delta_f = 0°$
$\delta_f = 30°$
$\delta_f = 45°$
$\delta_f = 60°$
DOWNSTREAM
FLAP TRAILING EDGE

FIGURE 36.

Since from (4)

$$\Gamma = \frac{C_L V_\infty \bar{C}}{2} \qquad \text{(I-34)}$$

Then substituting (29) and (33) into (34) we get

$$\Gamma = \delta_F \left[C_1 + \frac{C_2}{V_\infty} + \frac{C_3}{V_\infty^2} \right] \frac{V_\infty \bar{C}''}{4} \qquad \text{(I-35)}$$

where

$$C_1 = 2\pi$$
$$C_2 = 2\pi (.151) \left(\frac{h_i V_i}{\bar{C}} \right)^{1/2}$$
$$C_3 = 2\pi (.219) \left(\frac{h_i V_i}{\bar{C}} \right) \qquad \text{(I-35a)}$$

From the law of Biot and Savart, the induced velocity anywhere in the system due to the circulation in a single trailing vortex is,

$$\partial w_p = \frac{\Gamma}{4\pi h^2} \sin\theta \, dl \qquad \text{(I-36)}$$

From Dwinnell (Reference 4), in the steady flap condition, the total induced flow at a point "P" due to the entire trailing vortex is

$$w_p = \int \partial w_p \qquad \text{(I-37)}$$

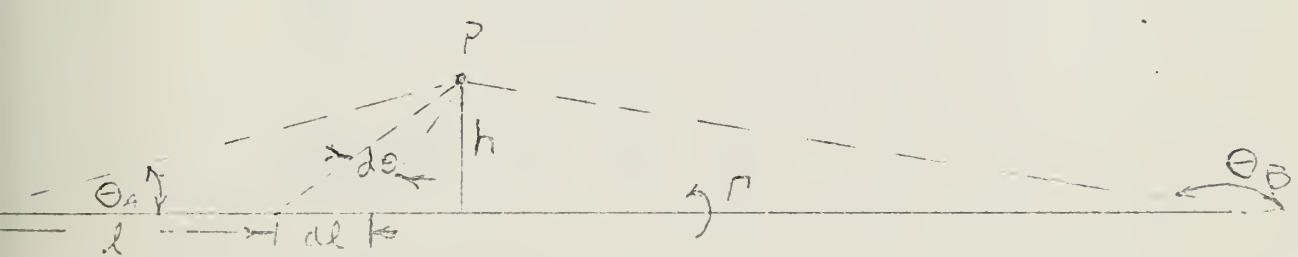

Figure 37

Expressing r and dl in terms of θ and $d\theta$

$$\omega_P = \frac{\Gamma}{4\pi} \int_{\theta_A}^{\theta_B} \frac{\sin\theta}{h} d\theta \tag{I-38}$$

After integrating (38) the following results;

$$\omega_P = \frac{\Gamma}{4\pi h} (\cos\theta_A - \cos\theta_B) \tag{I-39}$$

For an infinite vortex

$$\omega_P = \frac{\Gamma}{2\pi h} \tag{I-40}$$

and for a semi-infinite vortex,

$$\omega_P = \frac{\Gamma}{4\pi h} \tag{I-41}$$

In the present experimentation the value of induced flow at a point P will always be in the region

$$\frac{\Gamma}{4\pi h} < \omega_P < \frac{\Gamma}{2\pi h} \tag{I-42}$$

for the static case.

Since $\theta_B \rightarrow 180^\circ$

Then $\cos\theta_B \rightarrow -1$

Hence from (25)

$$\omega_p = \frac{\Gamma}{4\pi h}\left(1+\cos\Theta_A\right) \tag{I-43}$$

Now assuming a constant spanwise downwash distribution in the work of Spreiter and Sacks (Reference 26), we know that the trailing vortex core will flow in the direction of the flap deflection with a velocity of approximately

$$V_{CORE} = .41 \tan \alpha_i \cdot V_\infty \tag{I-44}$$

or as in Reference 18

$$V_{CORE} = .41 \tan\left(\frac{C_L}{\pi AR + 2C_\mu}\right) \cdot V_\infty \tag{I-45}$$

Thus,

$$\frac{V_{CORE}}{V_\infty} \simeq (.41)\frac{C_L}{\pi AR + 2C_\mu} \tag{I-46}$$

Then by substituting (I-29) and (I-35a) into (I-46) we arrive at

$$\frac{V_{CORE}}{V_\infty} = .41\,\delta_F \frac{\left[c_1 + \frac{c_2}{V_\infty} + \frac{c_3}{V_\infty^2}\right]}{\pi AR + \frac{4h}{\bar{c}}\left(\frac{V_j}{V_\infty}\right)^2} \tag{I-47}$$

Transposing (I-47) we arrive at

$$\frac{V_{CORE}}{V_\infty} = .41\,\delta_F \frac{\left[C_1 V_\infty^2 + C_2 V_\infty + C_3\right]}{\pi AR\, V_\infty^2 + 4\frac{h_j}{\bar{c}} V_j^2} \qquad \text{(I-48)}$$

Assuming

$$\pi AR\, V_\infty^2 \gg 4\frac{h_j}{\bar{c}} V_j^2 \qquad \text{(I-49)}$$

and

$$C_1 V_\infty^2 \gg C_2 V_\infty \qquad \text{(I-50)}$$

we can readily see that the value of $\frac{V_{CORE}}{V_\infty}$ is independent of velocity and is dependent only on δ_F. This theoretical analysis corroborates the previous hypothesis that V_∞ has no affect on either λ or $\cos\epsilon_x$.

From (I-35) $$\Gamma = \delta_F \left[C_1 + \frac{C_2}{V_\infty} + \frac{C_3}{V_\infty^2}\right] V_\infty \frac{\bar{c}}{4}$$

Thus, the partial of circulation with respect to V_∞ approaches the value given as follows:

$$\frac{\partial \Gamma}{\partial V_\infty} = \delta_F \frac{\bar{c}}{4}\left[C_1 - \frac{C_3}{V_\infty^2}\right] \qquad \text{(I-51)}$$

For velocities decreasing from 100 ft/sec to 50 ft/sec

$$\frac{C_3}{V_\infty^2} \rightarrow C_1 \tag{I-52}$$

Hence, the partial derivative is a positive number, or

$$\frac{\partial \Gamma}{\partial V_\infty} \equiv + \tag{I-53}$$

A typical plot is shown in Figure 38, for Γ as a function of V_∞. The actual value, though positive, has a small value and hence the affect of V_∞ on Γ is very small.

Previously, it has been proven that

$$\frac{\partial h}{\partial V_\infty} \doteq \frac{\partial \cos\theta_A}{\partial V_\infty} \doteq 0 \tag{I-54}$$

This too is obvious from the plot of $\frac{V_{core}}{V_\infty}$ as a function of V_∞ in Figure 38.

From (I-43) it was shown that

$$\bar{\omega_p} = \frac{\Gamma}{4\pi h}\left(1+\cos\theta_A\right) \tag{I-55}$$

Assuming (I-53) is true and substituting (I-54) into (I-55) it is obvious that $\bar{\omega_p}$ is a function of V_∞ but is influenced very weakly by a change in V_∞. Thus,

$$\frac{\partial \bar{\omega_p}}{\partial V_\infty} \equiv +$$

and is approaching a constant at high V_∞.

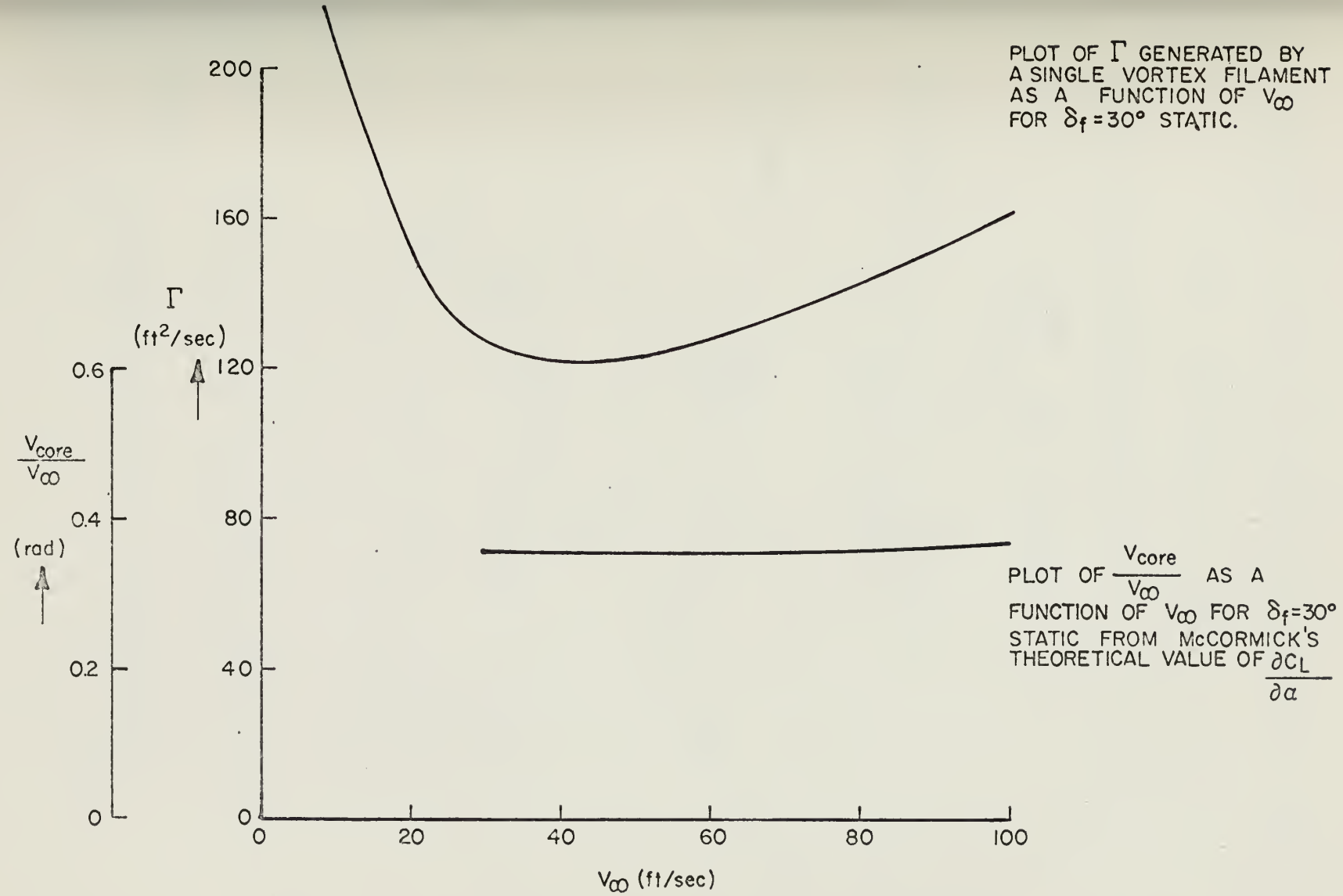
PLOT OF Γ GENERATED BY A SINGLE VORTEX FILAMENT AS A FUNCTION OF V_∞ FOR $\delta_f = 30°$ STATIC.
PLOT OF $\frac{V_{core}}{V_\infty}$ AS A FUNCTION OF V_∞ FOR $\delta_f = 30°$ STATIC FROM McCORMICK'S THEORETICAL VALUE OF $\frac{\partial C_L}{\partial \alpha}$
Γ (ft²/sec)
$\frac{V_{core}}{V_\infty}$ (rad)
200
160
120
80
40
0
0.6
0.4
0.2
0
0
20
40
60
80
100
V_∞ (ft/sec)

FIGURE 38.

Next, the influence of δ_F on w_p can be investigated. Again from (I-55) we know that

$$w_p = f(\Gamma, h, \cos\theta_A) \tag{I-56}$$

Readily, we can see from that (I-35) that

$$\frac{\partial \Gamma}{\partial \delta_F} \equiv \text{constant} \tag{I-57}$$

Geometrically, the value of h can be described as

$$h = \sqrt{H^2 + W^2} \tag{I-58}$$

from Figure 39,

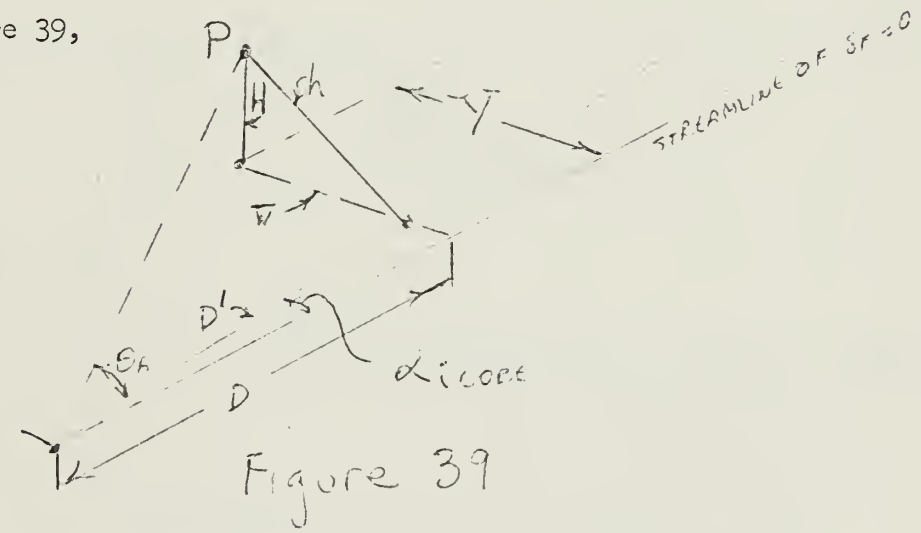

Figure 39

Now,

$$W = Y - D \sin \alpha_{i\,CORE} \tag{I-59}$$

or

$$W^2 = Y^2 - 2YD \sin \alpha_{i\,CORE} + D^2 \sin^2 \alpha_{i\,CORE} \tag{I-60}$$

Finally,

$$h = \sqrt{H^2 + Y^2 - 2YD \sin \alpha_{i\,CORE} + D^2 \sin^2 \alpha_{i\,CORE}} \tag{I-61}$$

Now the $\cos\theta_A$ is directly related to h in that

$$\cos\theta_A = \frac{D'}{\sqrt{D'^2 + h^2}} \tag{I-62}$$

Since $D' = D/\cos\alpha_{i\,CORE}$, (I-63)

then from (I-62), $\cos\theta_A = \dfrac{D/\cos\alpha_{i\,CORE}}{\sqrt{(D/\cos\alpha_{i\,CORE})^2 + h^2}}$ (I-64)

or

$$\cos\theta_A = \frac{D/\cos\alpha_{i\,CORE}}{\sqrt{(D/\cos\alpha_{i\,CORE})^2 + H^2 + \bar{Y}^2 - 2\bar{Y}D\sin\alpha_{i\,CORE} + D^2\sin^2\alpha_{i\,CORE}}} \tag{I-65}$$

Assuming small angles throughout

$$\cos\alpha_{i\,CORE} \to 1$$
$$\sin\alpha_{i\,CORE} \to \alpha_{i\,CORE} \tag{I-66}$$

Hence from (I-65)

$$\cos\theta_A \cong \frac{D}{\sqrt{D^2 + H^2 + \bar{Y}^2 - 2\bar{Y}D\alpha_{i\,CORE} + D^2\alpha_{i\,CORE}^2}} \tag{I-67}$$

Also from (I-61)

$$h \cong \sqrt{H^2 + \bar{Y}^2 - 2\bar{Y}D\alpha_{i\,CORE} + D^2\alpha_{i\,CORE}^2} \tag{I-68}$$

Now recalling from (I-46) that

$$\alpha_{i\,CORE} \cong .41\left[\frac{C_L}{\pi AR + 2C_{\mu_\alpha}}\right] \tag{I-69}$$

We know that the derivative of C_μ with respect to δ_F is

$$\frac{\partial C_\mu}{\partial \delta_F} = 0 \tag{I-70}$$

Thus, δ_F has no effect on C_L. Now recalling (I-29) it is known that with all other parameters remaining constant

$$\frac{\partial C_L}{\partial \delta_F} = \text{CONSTANT}_A \tag{I-71}$$

Hence, from chain rule differentiation, the results are,

$$\frac{\partial \alpha_{i\,CORE}}{\partial \delta_F} = \frac{\partial \alpha_{i\,CORE}}{\partial C_L} \cdot \frac{\partial C_L}{\partial \delta_F} \tag{I-72}$$

From (I-69)

$$\frac{\partial \alpha_{i\,CORE}}{\partial C_L} = \text{CONSTANT}_B \tag{I-73}$$

So by substituting (I-71) and (I-73) into (I-72) the result is obvious.

$$\frac{\partial \alpha_{i\,CORE}}{\partial \delta_F} = \text{CONSTANT}_C \tag{I-74}$$

Hence, $\alpha_{i\,CORE}$ is linearly proportional to δ_F

From both (I-67) and (I-68)

$$2\gamma D\,\alpha_{i,CORE} > D^2 \alpha_{i,CORE}^2 \tag{I-75}$$

Hence,

$$\frac{\partial \cos\theta_A}{\partial \delta_F} \equiv + \tag{I-76}$$

And

$$\frac{\partial h}{\partial \delta_F} \equiv - \tag{I-77}$$

Both values in (I-76) and (I-77) are not constant.

Incorporating (I-57), (I-76) and (I-77) into (I-43) we realize that

$$\frac{\partial \omega_p}{\partial \delta_F} \equiv + \qquad \text{(I-78)}$$

This is contributed to by all three variables defined in (I-56).

From the previous study we conclude that for the standard flapped airfoil without blowing augmentation that $\omega_{i\infty} = f(\delta_F, V_\infty)$ whereas in the blown flap case it is $\omega_p \doteq f(\delta_F, V_\infty{}^n)$

In the regime studied, $n<1$. At higher velocities it approaches

$$\omega_p \doteq f(\delta_F, V_\infty) \quad \text{For} \quad n=1$$

In summary it can be said that there are two variables of importance in the present study. They are δ_F and V_∞. All other parameters involved in the generation of induced velocities at remote points downstream are also functions of δ_F and V_∞. And, from the previous discussion it would seem that δ_F is the more important parameter in the final magnitude of generated turbulence.

THEORETICAL DISCUSSION OF DYNAMIC INTERFERENCE

As discussed in Reference 24, the forces on a flapped airfoil are a function of its frequency of flap deflection and its aerodynamic properties. The magnitude of induced velocities varies as in Figure 40, a vector diagram following the Theodorsen function in magnitude and phase changes.

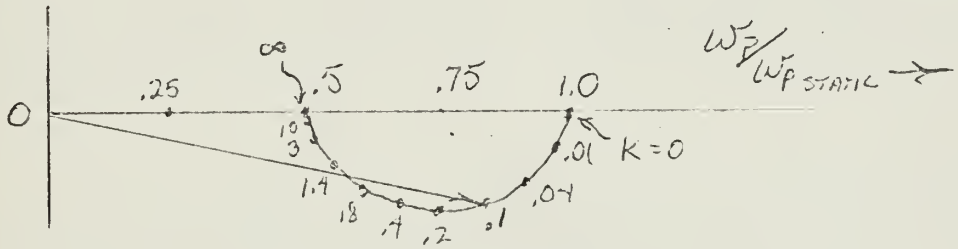

Figure 40

As can be seen, the phase lags, and the magnitude decreases with increasing reduced frequency, K. In this discussion

$$K = \frac{\omega_f \bar{c}}{V_\infty} \qquad \text{(I-79)}$$

In the experimental work the reduced frequencies vary from

$$0 \leq K \leq 1.5 \qquad \text{(I-80)}$$

Obviously, with such high values of K, the magnitude is decreased by nearly half, for the unidirectionally oscillated flap.

Two unsteady effects have a significant bearing on the forces and moments on the wing. "Virtual mass" and "wake effect" are the component parts that vary the forces and moments on the wing/flap with increased K.

The virtual mass effect has no influence on the strength of the shed vortex. It does, however, increase the load on the motor which oscillates the flap. By incorporating a motor with a large output, this problem is of no consequence.

The wake effect is a 3-D effect as opposed to the 2-D virtual mass problem. Although it can be shown mathematically, that the flow-induced by a flap oscillation through a plus and minus δ_F would theoretically cancel itself out at very high ω_δ, the sinusoidal oscillation was attempted for a first run. The final value would be zero as opposed to the case shown in Figure 43, in which the flap is oscillated in one direction only; in this case, ω_p would have a constant value when $\omega_\delta \to \infty$.

For the symmetrically oscillating case the magnitude did begin to decrease when higher frequencies were encountered. However, it is obvious that the theory will be altered when the movement of the vortex core is taken into account such that at $\omega_\delta \doteq \infty$, the actual ω_p was still greater than zero, although only a fraction of the static or quasi static value. Figure 41, illustrates the wake effect for symmetrical oscillation.

The law of Biot-Savart gives the incremental induced velocity at "P" in terms of circulation strength, Γ; distance from the vortex core, h; and the difference in the cosines of the angles to the ends of the segment. At high frequencies, both positive and negatively signed vortex circulation components affect the induced velocity at P. Therefore, the actual magnitude in the positive direction is less than that of the static or low frequency case. Figure 42 shows the static case in which the

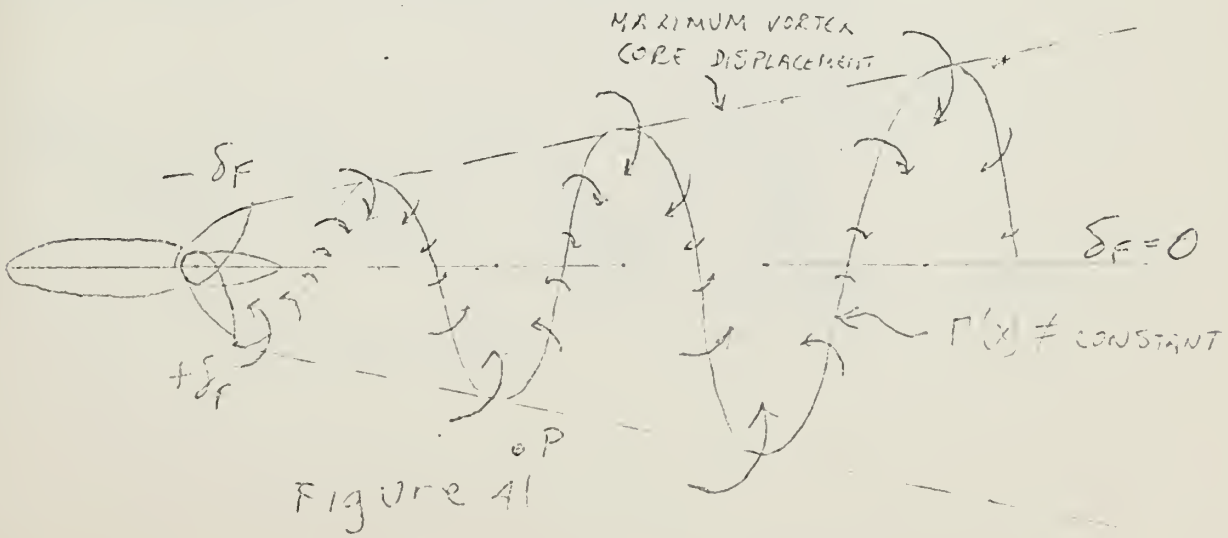

Figure 41

circulation is assumed constant to infinity and that there is no dynamic cancellation.

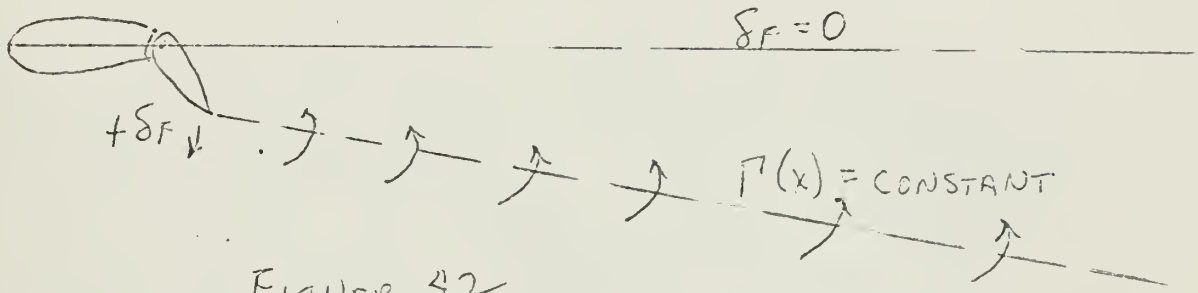

Figure 42

By oscillating the flap in one direction, the only real affect on the sinusoidal frequency response is to input a bias such that as $\omega_s \Rightarrow \infty$ the ω_f value approaches zero. Hence, assuming at present that the vortex core position is constant, the oscillatory component of the induced velocity will symmetrically decrease about the mean value of

$$\omega_p = \tfrac{1}{2}\omega_{p\,\text{STATIC}} \tag{I-79}$$

until at $\omega_f = \infty$, ω_f will actually equal this constant value and the oscillatory gust will no longer be present.

Figure 43 illustrates the typical core motion and accompanying circulation strength for a deflection in a single direction.

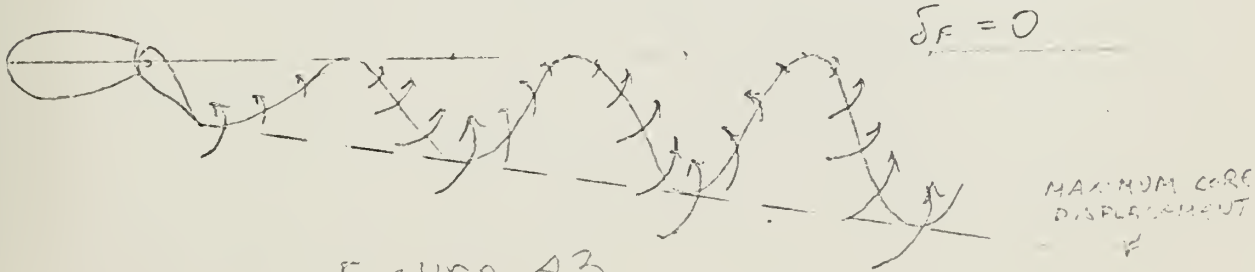

Figure 43

Since the vortex core does cross the plane of symmetry it is obvious that the bias will change and that the value at $\omega_f = \infty$ will be

$$\tfrac{1}{2}\omega_{P_{STATIC}} < \omega_P|_{\omega_f=\infty} < \omega_{P_{STATIC}} \qquad \text{(I-80)}$$

The sensor dynamics had little or no affect on the output data since the experimental oscillation bandwidth of the present discussion was far below the natural frequency of the sensor. As described in Appendix IV, $\zeta = .7$ for the sensor. These frequency and damping characteristics assure fidelity in the measurement of the induced velocities. For experimentation at much higher frequencies (i.e.; $\omega_f > 40$ hz) sensors with correspondingly higher natural frequency must be substituted for the present vanes.

APPENDIX II

INITIAL EXPERIMENTAL WORK IN TWO DIMENSIONS

Experimental trends in C_L generation for the blown flap were arrived at through a comparison to an analytic and experimental study of a simple airfoil section with known aerodynamic properties. Some characteristics of the blown flap model had to be preserved. First, the slot position was investigated. From a physical point of view, the slot must be directed to produce an increase in boundary layer energy in the streamwise direction. This re-energization of the boundary layer will tend to maintain attached flow over the flap and thus from supercirculation addition, increase C_L. Again, as previously analyzed, the vector component of momentum also adds to the C_L. The slot is chosen at the flap hinge point since it is there that separation would be likely to occur and it must operate bi-directionally. Since, in all cases, the forward stagnation point will always occur exactly at the leading edge for $\delta_F = 0$ and $C_\mu = 0$, except for very large C_L's, leading edge blowing is not necessary. Slot area was designed at a width capable of being choked at the required flow rate by the Schramm compressor.

The chord of the airfoil and flap are important in lift and circulation development. To correlate the 2-D experiments with those of Hazen and Knowlton (References 10 and 14), the overall chord was chosen to be 16 inches over the tunnel velocity range, the Re's agree well in both 2-D and 3-D cases in concern. The flap size is of great importance since the airfoil will always have an initial $\alpha = 0$; hence, the larger the deflected area, the larger the circulation produced. The flap size, however, must also be considered from an actuation load viewpoint. Thus, the required circulation must be weighed against the required input power to oscillate the flap at high frequency. A basic .45c flap seemed a reasonable initial compromise.

The tradeoff of deflection angle for inertia of the flap was also a basic concern. Although very high flap deflection angles could produce high C_L, it is also a fact that the blown air produces dynamic loads which increase with δ_f and add to the already large inertial loads at high frequencies. Previous experimentation by Korbacher (Reference 15) with jet flap blowing has lead to a group of optimal parameters for a similar model. In his work, Korbacher optimizes the lift and drag. In the present study, the drag is of little importance since it is circulation only that produces shed vortices. Thus, as large a deflection as possible would be the optimum. Actuation mechanics again limit the range of operations. Flap deflection greater than 60° would be difficult to oscillate with the present equipment; hence, $\delta_f = \pm 60°$ was taken as the maximum with variable connecting arm positions available for ±45° and ±30°.

2-D Smoke Tunnel Testing

The 2-D smoke tunnel experimentation was used as a means of observing trends in C_L production due to variations in flap chord, δ_f and C_μ. The plot on Figure 47 gives some idea as to the results of these tests. Knowlton, in Reference 14, describes a method of calculation of C_L by streamline deflection upstream. In the present study a simple comparison was made between the jet flapped models and the 2-D symmetric airfoil with assumed C_{L_α} = .1/deg.

Having made this assumption, the 2-D symmetric airfoil without blowing was given increments of α. Observing the streamline deflection at a point K upstream

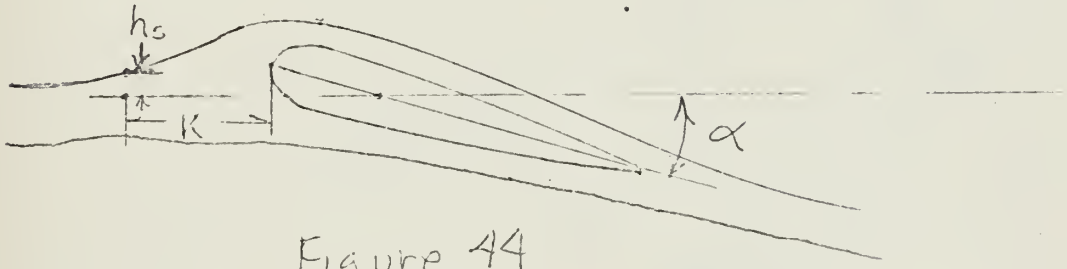

Figure 44

of the leading edge in Figure 44. Thus a graph of α versus h_s and hence, C_L versus h_s was arrived at for the perfect 2-D, infinite airfoil.

The assumptions made to this point are:

(1) infinite AR

(2) $\delta_F = 0$

(3) $C_\mu = 0$

(4) varying α

(5) tunnel velocity $(V_\infty) \doteq$ 50 ft/sec

The results of these observations appear on Figure 45. The C_L versus h_s has a constant slope. Thus, this curve can be used to determine C_L for other configurations at $\alpha = 0$ but with $C_\mu \neq 0$ and $\delta_F \neq 0$.

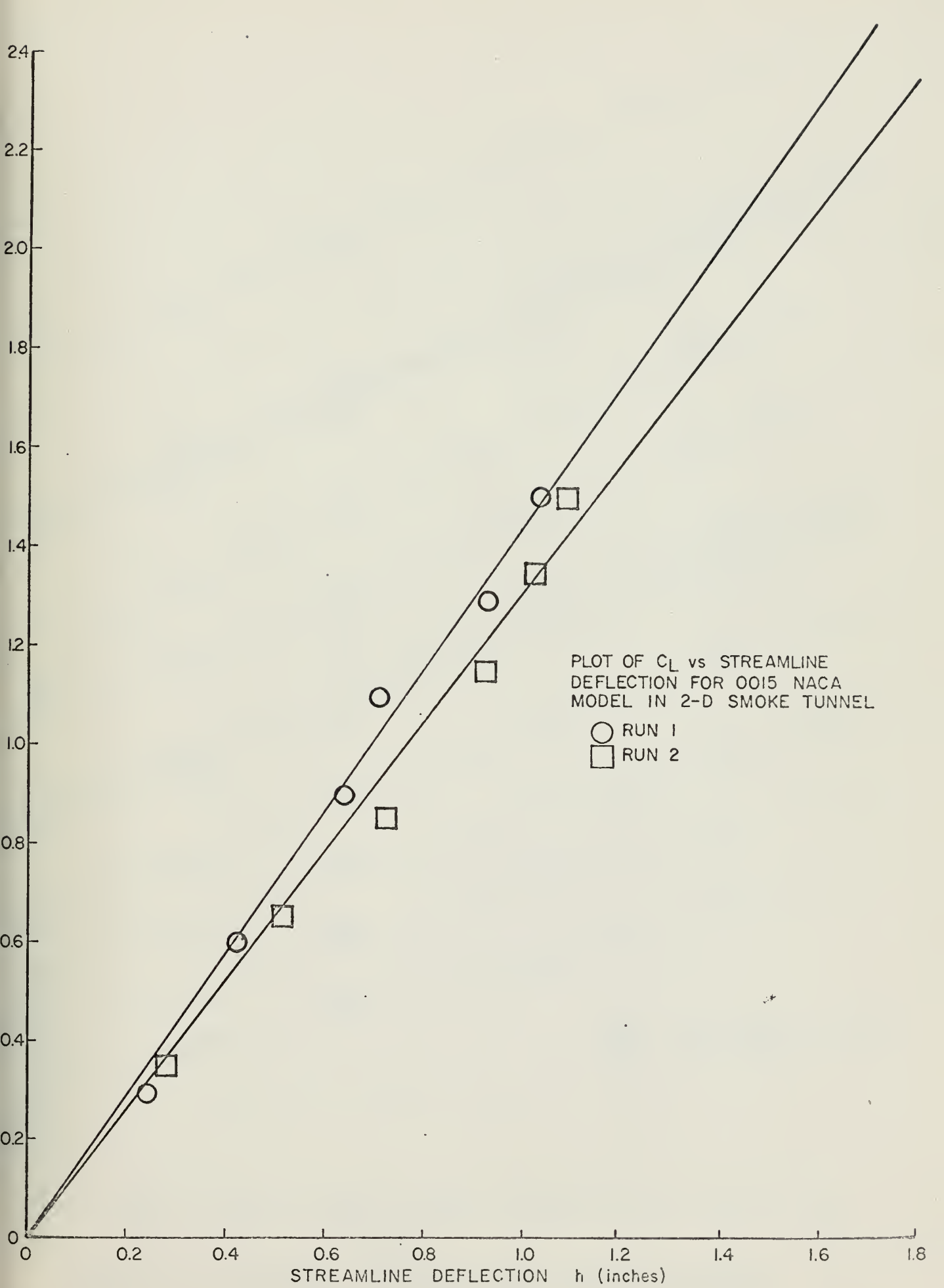
2.4
2.2
2.0
1.8
1.6
1.4
1.2
1.0
0.8
0.6
0.4
0.2
0
0
0.2
0.4
0.6
0.8
1.0
1.2
1.4
1.6
1.8
STREAMLINE DEFLECTION h (inches)
PLOT OF C_L vs STREAMLINE DEFLECTION FOR 0015 NACA MODEL IN 2-D SMOKE TUNNEL
RUN 1
RUN 2

FIGURE 45.

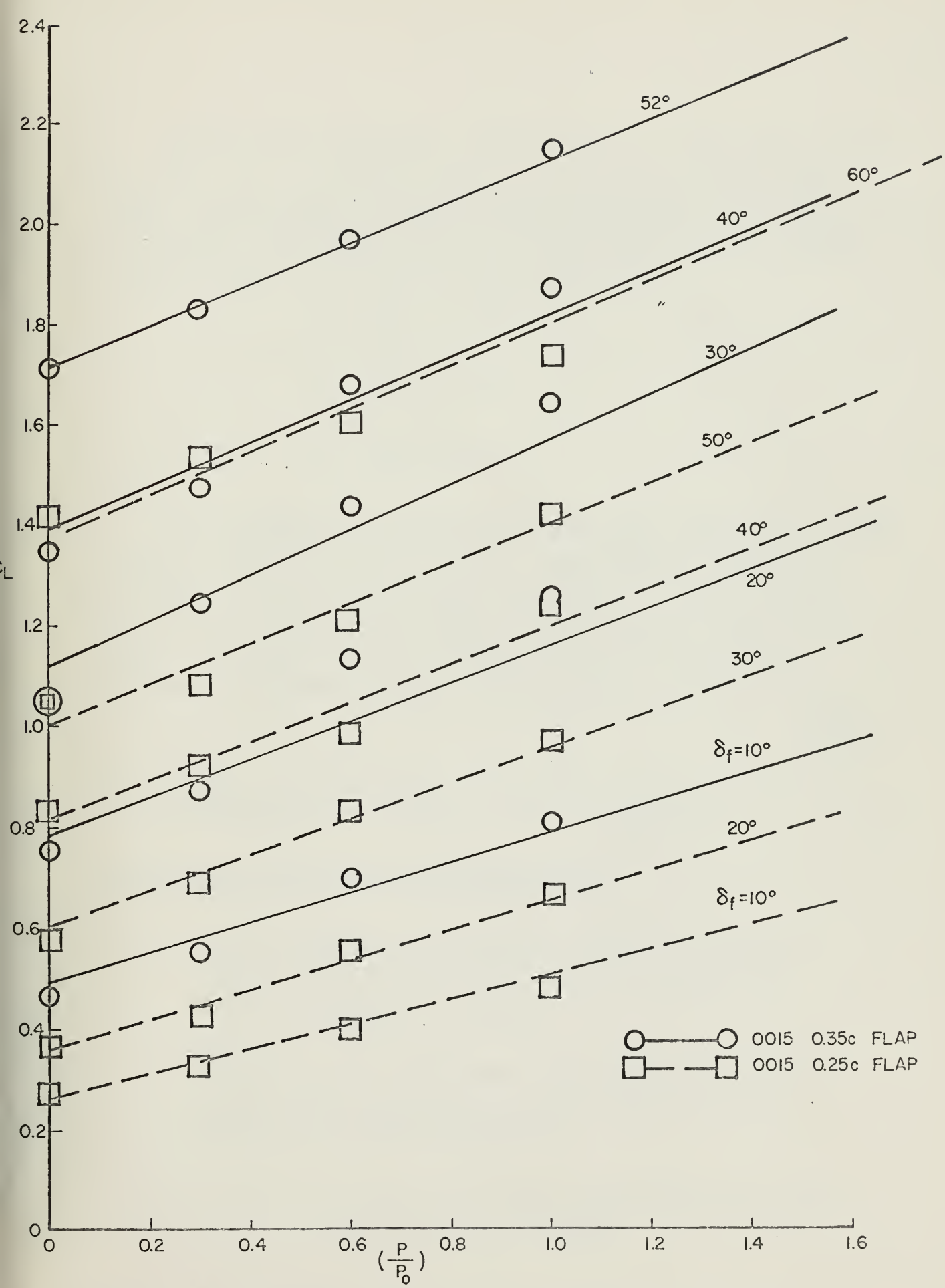

FIGURE 43. BLOWING AUGMENTATION POWER SETTING.

Results of this comparative analysis appear in Figure 46 for various C_μ and δ_f at C_f = .25c and then .35c. As can be seen, the overall trend illustrates that the various partial derivatives in C_L production are all positive. From these conclusions and knowledge of dynamic inertial load difficulties, the following values were chosen:

(1) $C_f/C = .45$

(2) $\delta_f = \pm 60^\circ$

(3) CHOKED FLOW

Vortex generation was attempted at NASA Langley (References 7 and 22) in the low speed wind tunnel facility. High frequency oscillation of the entire airfoil seemed mechanically unfeasible. By decreasing the size of the oscillating area to just the flap aided with blowing, the large Γ is possible without the tremendous inertia loads at high frequency. As discussed previously from Figure 46, the values of $\partial C_L / \partial C_f/C$ and $\partial C_L / \partial C_\mu$ are obviously high. With C_f/C increased to .45c and C_μ to a choked condition, the entire C_L will increase greatly.

CONCLUSIONS OF 2-D SMOKE TUNNEL EXPERIMENTATION

1) A basic symmetrical airfoil with a .45c flap will give an adequate tradeoff between ΔC_L and the aerodynamic and inertial load effects at high ω_f.

2) Choked flow at the blowing slot will give an even emission of high velocity air across the span of the model while producing the largest possible ΔC_L.

3) $\delta_f = \pm 60^\circ$ will be the optimal tradeoff deflection between ΔC_L and mechanical driving problems.

4) From the graphs (Figure 46) previously presented of experimental C_L production, partial derivatives can be assumed as follows:

$$\partial C_L / \partial \delta_F \doteq 2 \text{ /rad}$$

and

$$\partial C_L / \partial P/P_c \doteq .4$$

APPENDIX III

SCALING

In wind tunnel testing, scaling of parameters is very important in the simulation of real atmospheric situations. Of major importance in producing acceptable turbulence in a 3-D tunnel is the frequency of the sinusoidal gusts being generated with respect to the tunnel speed. Reduced frequency, $K \equiv \frac{\omega \lambda}{V_\infty}$ is a nondimensional parameter that expresses this relationship and represents a grouping of the important dimensional characteristics.

To begin, we first hypothesize a full scale aircraft and a model size. If we assume a gust wave length equal to the overall length of the aircraft we would have typically

$$\lambda_{a/c} = 50 \text{ ft.} \tag{III-1}$$

and

$$\lambda_{MOD} = 2 \text{ ft.} \tag{III-2}$$

Next the range of K possible for the wind tunnel can be calculated.

$$K_{MOD} = \frac{2\pi \omega_{MOD} l_{MOD}}{V_{MOD}} \tag{III-3}$$

Here

$$l_{MOD} = \lambda_{MOD} = 2 \text{ ft.} \tag{III-4}$$

with

$$50 \text{ ft/sec} \leq V_{MOD} \leq 100 \text{ ft/sec} \tag{III-5}$$

and

$$0 \leq \omega_{MOD} \leq 16 \text{ hz} \tag{III-6}$$

the possible range of K is

$$0 \leq K \leq 4.02 \tag{III-7}$$

Assuming

$$V_{A/C} = 600 \text{ ft/sec} \tag{III-8}$$

and

$$\ell_{A/C} = \lambda_{A/C} = 50 \text{ ft.} \tag{III-9}$$

and since

$$K_{MOD} \doteq K_{A/C} \tag{III-10}$$

for a correct simulation,

$$\omega_{A/C} = \frac{K_{MOD} V_{A/C}}{2\pi \ell_{A/C}} = K_{MOD}(1.91) \text{ hz} \tag{III-11}$$

or

$$0 \leq \omega_{A/C} \leq 7.68 \text{ hz} \tag{III-12}$$

The high frequency simulation is of interest for the study of structural and aeroelastic problems, whereas the low frequencies may be of interest in simulating pilot-control inter-relationships in the stability and control region of aerodynamic study.

APPENDIX IV

VANE DYNAMICS

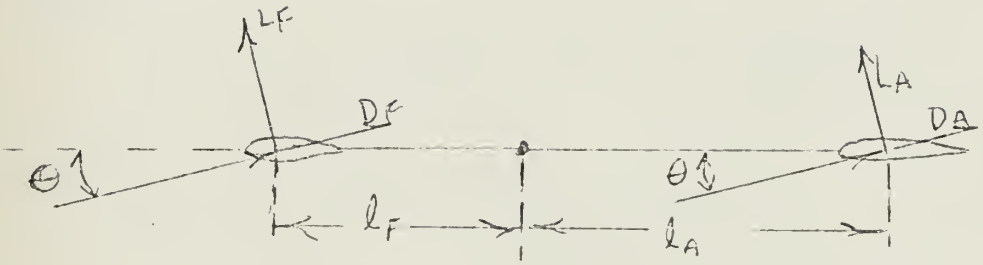

Figure 48

The dynamics of the vanes are very important to accurate measurements in both magnitude and frequency. Graham (Reference 8) undertook to hypothesize the dynamics of just such a vane with optimal dynamic characteristics.

Vanes, connecting arm, and potentiometers are the essential parts to the angle measuring system. All contribute to the overall moment of inertia of the system and thereby affect the natural frequency and damping in the simulated second order system.

Such a system can be described with the basic equation of motion,

$$I\ddot{\theta} + 2\zeta\omega_n\dot{\theta} + \omega_n^2\theta = 0 \qquad \text{(IV-1)}$$

This equation describes the summation of torques due to angular acceleration, angular velocity and angular position.

First, the torque tending to bring the vane to zero angle of attack is

$$\tau = (L_A\cos\theta + D_A\sin\theta)l_A - (L_F\cos\theta + D_F\sin\theta)l_F \qquad \text{(IV-2)}$$

This equation is the summation of the products of lift and moment arms for both fore and aft lifting surfaces.

For small angles

$$\cos\theta \approx 1$$
$$\sin\theta \approx \theta \qquad \text{(IV-2a)}$$

Hence,

$$\tau = [L_A + D_A\theta]\, l_A - [L_F + D_F\theta]\, l_F \qquad \text{(IV-3)}$$

The surface area of both vanes is identical so

$$\tau = [L_A + D_A\theta]\,[l_A - l_F] \qquad \text{(IV-4)}$$

Now

$$L = C_{L\alpha}\, q\, S\, \alpha \qquad \text{(IV-5)}$$

$$D = [C_{D\alpha}\alpha + C_{D0}]\, q\, S \qquad \text{(IV-6)}$$

In both cases

$$\alpha \doteq \theta \qquad \text{(IV-6a)}$$

Thereby

$$L = C_{L\alpha}\, q\, S_V\, \theta \qquad \text{(IV-7)}$$

$$D = [C_{D\alpha}\theta + C_{D0}]\, q\, S_V \qquad \text{(IV-8)}$$

Substituting in the torque equation

$$\tau = \{[C_{L\alpha}\theta]\, q S_V + [C_{D\alpha}\theta^2 + C_{D0}\theta]\, q S_V\}\,[l_A - l_F]$$

or

$$\tau = [C_{L\alpha}\theta + C_{D\alpha}\theta^2 + C_{D0}\theta]\, q S_V\,[l_A - l_F] \qquad \text{(IV-9)}$$

Differentiating with respect to θ yields

$$\frac{d\tau}{d\theta} = \left[C_{L\alpha} + 2C_{D_q}\theta + C_{D_0}\right] q S_V \left[\ell_A - \ell_F\right] \qquad \text{(IV-10)}$$

For small angles of attack

$$C_{D\alpha} \doteq 0$$

and C_{D_0} is approximated by $C_{D_{MIN}}$

Thus

$$\frac{d\tau}{d\theta} \doteq \left[C_{L\alpha} + C_{D_{MIN}}\right] q S_V \left[\ell_A - \ell_F\right] \qquad \text{(IV-11)}$$

Next, the torques proportional to angular velocity are important. As angular velocity occurs a damping opposing the motion is developed from the change in velocity perpendicular to the free stream.

$$\Delta\alpha = \frac{\ell\dot{\theta}}{V_\infty}$$

Thus,

$$\tau = \left[C_{L\alpha}\frac{\ell_A\dot{\theta}}{V_\infty} + C_{D_{min}}\left\{\theta + \dot{\theta}\frac{\ell_A}{V_\infty}\right\}\right] q S_V \ell_A$$

$$+ \left[C_{L\alpha}\frac{\ell_F\dot{\theta}}{V_\infty} + C_{D_{min}}\left\{\theta + \dot{\theta}\frac{\ell_F}{V_\infty}\right\}\right] q S_V \ell_F \qquad \text{(IV-12)}$$

Differentiating with respect to $\dot{\theta}$ we see

$$\frac{d\tau}{d\dot{\theta}} = \left[C_{L\alpha}\frac{\ell_A}{V_\infty} + C_{D_{min}}\frac{\ell_A}{V_\infty}\right] q S_V \ell_A$$

$$+ \left[C_{L\alpha}\frac{\ell_F}{V_\infty} + C_{D_{min}}\frac{\ell_F}{V_\infty}\right] q S_V \ell_F \qquad \text{(IV-13)}$$

Collecting terms yields

$$\frac{d\lambda}{d\dot{\theta}} = \left[C_{L\alpha} + C_{D_{min}}\right] \frac{q S_v}{V_\infty} \left[l_A^2 + l_F^2\right] \qquad \text{(IV-14)}$$

Substituting (IV-14) and (IV-11) into (IV-1) we arrive at the characteristic equation of motion for this second order, mass-spring-damper type system.

$$I\ddot{\theta} + \frac{d\lambda}{d\dot{\theta}}\dot{\theta} + \frac{d\lambda}{d\theta}\theta = 0 \qquad \text{(IV-15)}$$

or

$$I\ddot{\theta} + \left[C_{L\alpha} + C_{D_{min}}\right] \frac{q S_v}{V_\infty} \left[l_A^2 + l_F^2\right]\dot{\theta} + \left[C_{L\alpha} + C_{D_{min}}\right] q S_v \left[l_A - l_F\right]\theta = 0 \qquad \text{(IV-16)}$$

By comparing coefficients of (IV-16) and (IV-1) we see that

$$\omega_n^2 = \left[C_{L\alpha} + C_{D_{min}}\right] \frac{q S_v}{I} \left[l_A - l_F\right] \qquad \text{(IV-17)}$$

and

$$2\zeta\omega_n = \left[C_{L\alpha} + C_{D_{min}}\right] \frac{q S_v}{V_\infty I} \left[l_A^2 + l_F^2\right] \qquad \text{(IV-18)}$$

For the experimental model being used and the dimensions of the vanes, the following dimensional characteristics apply:

$I = .858 \times 10^{-6}$ slug ft^2
$C_{L\alpha} = 2.8$ /rad
$C_{D_{min}} = .007$
$S_v = .010$ ft^2
$l_A = .25$ ft
$l_F = .125$ ft

Solving equation (IV-17)

$$\omega_n \doteq 35 \text{ Hz}$$

and

$$\zeta \doteq .7$$

The following vane system is therefore critically damped with a natural frequency of 35 hz as indicated.

Experimental tests were made and the vanes react exactly as the theory would predict. Figure 49 is an example of the vane reaction to a step input.

It can be concluded that since the ω_n of the vanes is far above that of the actual testing frequencies and since the vanes are critically damped, no overshoot will occur even at high frequencies and measurement accuracy in the dynamic case is commensurate with that in the static case.

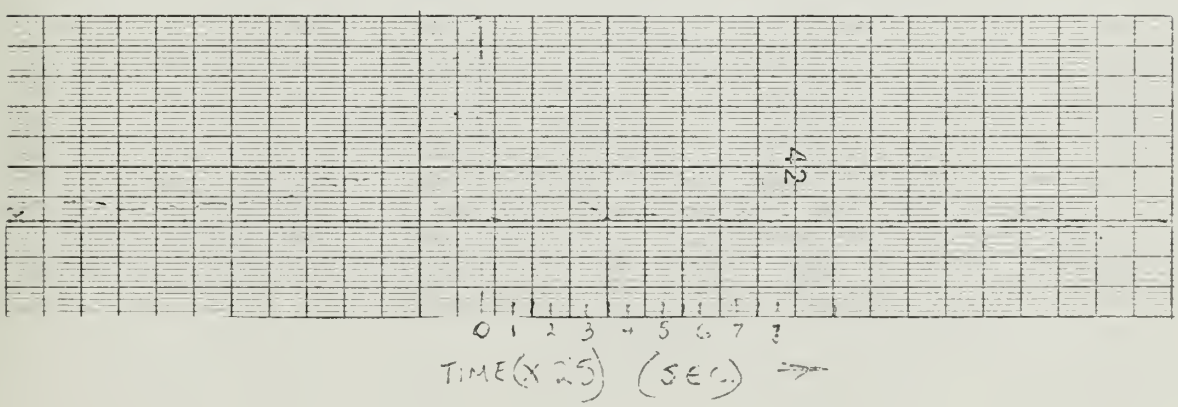

Figure 49

Gaylord
SHELF BINDER
Syracuse, N. Y.
Stockton, Calif.

8 MAR 71 S1048

8 MAR 71 123431
Thesis
U33 Umbarger
Wind tunnel gust
simulation.

Thesis 123431
U33 Umbarger
Wind tunnel gust
simulation.

thesis33
Wind tunnel gust simulation
3 2768 001 88935 5
DUDLEY KNOX LIBRARY